

**REPORT  
71**



# **GEOLOGICAL EVOLUTION OF THE PALAEOPROTEROZOIC TALBOT TERRANE AND ADJACENT MESO- AND NEO- PROTEROZOIC SUCCESSIONS PATERSON OROGEN WESTERN AUSTRALIA**

**by A. H. Hickman and L. Bagas**



**GEOLOGICAL SURVEY OF WESTERN AUSTRALIA  
DEPARTMENT OF MINERALS AND ENERGY**



**GEOLOGICAL SURVEY OF WESTERN AUSTRALIA**

**REPORT 71**

**GEOLOGICAL EVOLUTION  
OF THE PALAEOPROTEROZOIC  
TALBOT TERRANE, AND ADJACENT  
MESO- AND NEOPROTEROZOIC  
SUCCESSIONS, PATERSON OROGEN,  
WESTERN AUSTRALIA**

by  
**A. H. Hickman and L. Bagas**

**Perth 1999**

**MINISTER FOR MINES**  
**The Hon. Norman Moore, MLC**

**DIRECTOR GENERAL**  
**L. C. Ranford**

**DIRECTOR, GEOLOGICAL SURVEY OF WESTERN AUSTRALIA**  
**David Blight**

**Copy editor: I. R. Nowak**

**REFERENCE**

**The recommended reference for this publication is:**

HICKMAN, A. H., and BAGAS, L., 1999, Geological evolution of the Palaeoproterozoic Talbot Terrane, and adjacent Meso- and Neoproterozoic successions, Paterson Orogen, Western Australia: Western Australia Geological Survey, Report 71, 91p.

**National Library of Australia**  
**Cataloguing-in-publication entry**

Hickman, A. H. (Arthur Hugh), 1947–  
Geological evolution of the Palaeoproterozoic Talbot Terrane, and adjacent Meso- and Neoproterozoic successions,  
Paterson Orogen, Western Australia

Bibliography.  
ISBN 0 7309 6648 8

1. Geology, Stratigraphic — Proterozoic.
2. Orogeny — Western Australia.
3. Geology, Stratigraphic — Western Australia.
  - I. Bagas, L. (Leon).
  - II. Geological Survey of Western Australia.
  - II. Title. (Series: Report (Geological Survey of Western Australia); 71).

551.71509941

ISSN 0508-4741

Printed by Lamb Print, Perth, Western Australia

**Cover photograph:**

**Banded paragneiss of the c. 1800 Ma Butler Creek Formation in the southwest bank of the Rooney Creek (AMG 326096). Quartzite (white), psammitic gneiss, and semipelitic schist (dark grey) are interlayered at 5–30 cm intervals. These rocks represent metamorphosed and tectonically attenuated beds of sandstone, wacke, and silty shale.**

## Contents

Abstract .....	1
Introduction .....	1
Summary of geology .....	2
Palaeo- to early Neoproterozoic geology .....	2
Rudall Complex .....	6
Stratigraphic overview .....	6
Orthogneiss .....	11
Yeneena Supergroup and Tarcunyah Group .....	13
Dolerite dykes, quartz veins, and gossan .....	14
Structure .....	14
Pre-Yeneena Supergroup deformation .....	15
Yapungku Orogeny .....	15
D <sub>1</sub> structures .....	15
D <sub>2</sub> structures .....	16
Post-Yeneena Supergroup deformation .....	19
Miles Orogeny .....	19
D <sub>3</sub> structures .....	19
D <sub>4</sub> structures .....	19
Paterson Orogeny .....	21
D <sub>6</sub> structures .....	21
Metamorphism .....	21
Previous work .....	21
Metamorphism in the Talbot Terrane .....	22
Metasomatism .....	22
Metamorphism of the Throssell Group .....	24
Summary of metamorphism .....	24
Geochronology .....	24
Tectonic evolution .....	26
Rudall Complex .....	27
Regional setting .....	27
Evidence from the Talbot Terrane .....	28
Throssell and Tarcunyah Groups .....	29
Regional setting .....	29
Evidence from the Throssell and Tarcunyah Groups .....	29
Late granitoids .....	30
Metallogenic implications .....	30
Mineral resources .....	31
Geochemical investigation .....	31
Gold .....	31
Uranium (and associated gold, copper, lead, and zinc) .....	31
Copper, lead, and zinc .....	35
Platinum-group elements (PGE) .....	35
Other metals (molybdenum, tungsten, tin, bismuth, and vanadium) .....	35
Diamonds .....	36
Barite .....	36
Mineral potential .....	36
Acknowledgments .....	39
References .....	40

## Appendix

1. Analytical data from the RUDALL 1:100 000 sheet .....	42
--	----

## Figures

1. Regional setting of the Talbot Terrane, and the regional distribution of the Yeneena Supergroup and the Tarcunyah Group .....	3
2. Simplified geological map of the Talbot Terrane on the RUDALL 1:100 000 map, showing stratigraphy and major structures .....	4
3. Diagrammatic map of the geology (orthogneiss omitted) of the Talbot Terrane on part of the RUDALL 1:100 000 map, distinguishing $D_2$ from $D_4$ structures, and showing zones of peridotite .....	5
4. Major tectono-stratigraphic units of the Talbot Terrane on the RUDALL 1:100 000 map .....	7
5. Generalized stratigraphic columns through the stratigraphic succession of the Rudall Complex in the Talbot Terrane .....	9
6. $S_2$ -foliated augen orthogneiss ( <i>ERga</i> ) .....	12
7. $S_2$ in augen orthogneiss ( <i>ERga</i> ) folded by $F_4$ folds .....	12
8. $S_2$ in augen orthogneiss ( <i>ERga</i> ), folded and crenulated by $F_4$ folds .....	13
9. Minor structures on RUDALL: $F_2$ axes .....	16
10. Minor structures on RUDALL: $F_4$ axes and $S_4$ .....	17
11. Stereographic projections plotting $S_2$ foliations to estimate the pre-Throssell Group orientation of $S_2$ in the Poynton and Rooney Domains .....	18
12. Diagrammatic cross section through Rudall River, showing major $D_2$ and $D_4$ structures .....	20
13. Prograde metamorphic minerals of the Rudall Complex .....	23
14. Strike-slip faulting and deposition during the early stages of Yeneena Basin development, RUDALL–BROADHURST area .....	30
15. Locations of prospects, mineral occurrences, and mineral anomalies on the RUDALL 1:100 000 map .....	32
16. Economic geology of the Talbot Terrane, and the Throssell and Tarcunyah Groups on the RUDALL 1:100 000 map .....	33
17. Summary of main zones of known and interpreted mineral potential on the RUDALL 1:100 000 map .....	34

## Tables

1. Summary of tectono-stratigraphic domains in the Talbot Terrane .....	8
2. Stratigraphy of the sedimentary succession of the Talbot Terrane .....	10
3. Summary of deformation episodes affecting the Talbot Terrane, and the Throssell and Tarcunyah Groups .....	15
4. Geochronological results for the Paterson Orogen .....	25
5. Geochronological data relevant to the evolution of the Paterson Orogen .....	27
6. Summary of Proterozoic tectonic evolution on RUDALL, with theoretical metallogenic implications .....	37

# Geological evolution of the Palaeoproterozoic Talbot Terrane, and adjacent Meso- and Neoproterozoic successions, Paterson Orogen, Western Australia

by

A. H. Hickman and L. Bagas

## Abstract

Recent mapping of the RUDALL 1:100 000 sheet has provided considerably more-detailed geological data than were previously available from the reconnaissance mapping carried out by the Geological Survey of Western Australia in 1975–76. The new information has led to major reinterpretations of stratigraphy, structure, tectonic evolution, and mineral potential in the central (Talbot Terrane) part of the Palaeoproterozoic Rudall Complex in the Paterson Orogen.

The Palaeoproterozoic Talbot Terrane of the western part of the Rudall Complex contains a foreland basin-type clastic succession deposited east of the Archaean Pilbara Craton. The Pilbara Craton collided with a continental plate moving from the northeast, around 1760 Ma. As a result, the sedimentary succession was thrust and overfolded from the northeast and east, metamorphosed to amphibolite facies, and extensively intruded by sheets of granite–granodiorite.

The Meso- to Neoproterozoic Throssell Group of the Yeneena Supergroup, which unconformably overlies the Talbot Terrane, is a sandstone–shale–carbonate assemblage that was deposited by 900 Ma. The group was deposited in a northwesterly trending basin system, with terrigenous supply from the southwest. Transpressional upright folding and high-angle thrusting between about 900 and 700 Ma resulted in the main northwest-trending fold system ( $D_4$ ) of the Miles Orogeny.

Gold, base metal, and uranium mineralization within and adjacent to the Talbot Terrane is chiefly syn- to post-Throssell Group in age and occurs on, or in close proximity to, northwesterly to north-northwesterly striking  $D_4$  faults.

**KEYWORDS:** Paterson Orogen, Rudall Complex, Talbot Terrane, Yeneena Supergroup, Throssell Group, stratigraphy, structure, metamorphism, tectonic evolution, mineralization, mineral potential

## Introduction

Mapping of the RUDALL\* 1:100 000 sheet area during 1991 and 1992 by the Geological Survey of Western Australia (GSWA) provided information on the geology, tectonic evolution, and mineral potential of a well-exposed section of the Paterson Orogen (Hickman and Bagas, 1998).

The Paterson Orogen is a northwesterly trending orogenic belt of multiply folded and metamorphosed sedimentary and igneous rocks of Proterozoic age. The orogen can be subdivided into the Palaeoproterozoic

Rudall Complex (Williams, 1990) and the unconformably overlying Meso- to Neoproterozoic Yeneena Supergroup (Throssell and Lamil Groups), and Neoproterozoic Tarcunyah Group (Williams and Bagas, in press).

The Rudall Complex consists of a broad imbricate zone of northeasterly and easterly dipping thrust sheets with crosscutting relationships that indicate progressively younger thrusts towards the east. Some of the thrusts are major faults separating distinct tectono-stratigraphic terranes known as the Talbot, Connaughton, and Tabletop Terranes (Bagas and Smithies, 1998). This report will concentrate on the Talbot Terrane. Smithies and Bagas (1997) and Bagas and Smithies (1998) describe the Connaughton and Tabletop Terranes to the east.

---

\* Capitalized names refer to standard 1:100 000 map sheets

The Talbot Terrane comprises a metamorphosed succession of siliciclastic rocks in the western part of the Rudall Complex that occupies the central part of the northwestern Paterson Orogen in northwestern Western Australia, and is situated between the Great Sandy Desert and Little Sandy Desert (Fig. 1). The orogen extends southeastward and includes the Mesoproterozoic Musgrave Complex of central Australia (Williams and Myers, 1990).

Until recently, the limited understanding of the geology of the orogen relied on reconnaissance studies (Chin et al., 1980) and limited geochronological data (Chin and de Laeter, 1981). Subsequent studies have highlighted complexities both typical and atypical of Proterozoic orogenic belts (Clarke, 1991; Hickman and Clarke, 1994; Bagas et al., 1995; Smithies and Bagas, 1997; Bagas, 1998; Bagas and Smithies, 1998; Hickman and Bagas, 1998).

This Report provides a detailed account of the Palaeoproterozoic geology (Talbot Terrane) of the area, and the geology of the unconformably overlying Meso- to Neoproterozoic (Throssell Group) and Neoproterozoic (Tarcunyah Group). The Report does not describe in any detail the younger Neoproterozoic Savory Group or the Phanerozoic units in the region. These units are described in Hickman and Bagas (1998), which should be read with this Report.

## Summary of geology

The Paterson Orogen is a northwest-trending belt of folded and metamorphosed Proterozoic igneous and sedimentary rocks that lies in the central part of Western Australia, and extends southeast to the Musgrave Complex (Williams and Myers, 1990). Within the study area there are three major subdivisions of the orogen — the Palaeoproterozoic Rudall Complex, Meso- to Neoproterozoic Throssell Group of the Yeneena Supergroup, and the Neoproterozoic Tarcunyah Group of the greater Officer Basin (Fig. 1).

The Rudall Complex was subjected to a Palaeoproterozoic orogenic event, and the unconformably overlying Throssell and Tarcunyah Groups were deformed by Mesoproterozoic to Neoproterozoic orogenies.

The Rudall Complex is composed of gneiss, schist, and quartzite, which represent a range of igneous and sedimentary rocks deformed and metamorphosed during at least two pre-Throssell Group orogenic episodes. This report (see **Tectonic evolution**) interprets these events in terms of northeast–southwest plate collisions that resulted in the formation of fold-thrust belts, and partial melting. Orthogneiss constitutes about 50% of the Rudall Complex and was derived by metamorphism of a range of granitoid protoliths. The main protolith was porphyritic granite to monzogranite that intruded the sedimentary succession between about 1787 and 1765 Ma (see **Geochronology**). An earlier suite, forming part of a complex lithologically layered orthogneiss, crystallized at about 2015 Ma (see

**Geochronology**). Available geochronology is inadequate to provide firm time constraints for the evolution of the Rudall Complex, but the  $D_1$ – $M_1$  collision probably occurred between 2015 and 1787 Ma, and  $D_2$ – $M_2$  occurred either during or after the period 1787–1765 Ma. Both these deformation events have been included in the Yapungku Orogeny (Bagas and Smithies, 1997; Bagas and Smithies, 1998).

The Yeneena Supergroup, as recently defined by Bagas et al. (1995), consists of the Throssell and Lamil Groups, but the latter is not present in the vicinity of the Talbot Terrane.

The Throssell Group is a sandstone–shale–carbonate succession, representing a range of depositional environments from fluvial–deltaic to shelf. The age of the group is between 1250 and 900 Ma (see **Geochronology**), and initial deposition probably commenced in a strike-slip basin system, which later evolved into a northeast-deepening shelf environment responsible for the Lamil Group in the Telfer area.

The Tarcunyah Group is c. 800 Ma in age (Bagas et al., 1995), and represents deltaic to shallow-shelf sedimentation along the eastern margin of the Pilbara Craton. No  $D_4$  structures have been identified in the Tarcunyah Group (Williams and Bagas, in prep.a,b), which indicates that deposition of the group followed tectonic closure of the Throssell Group basin.

Deformation of the Rudall Complex and Throssell Group during  $D_4$  resulted in the formation of tight to isoclinal, upright, southeast-trending folds, and associated brittle–ductile faults and shear zones; metamorphism was greenschist facies.

The  $D_6$  deformation, which also affects the Tarcunyah Group, involved a combination of upright folding, thrusting, and dextral strike-slip movements along a northwest-trending zone from the McKay Range on RUDALL to eastern THROSSELL (Williams and Bagas, prep.a), and further north to the eastern margin of the Gregory Range. East of this zone,  $D_6$  effects appear to be minor, and are mainly confined to dextral strike-slip reactivation of  $D_4$  faults and the formation of some new minor faults.

## Palaeo- to early Neoproterozoic geology

This Report describes the Palaeo- to early Neoproterozoic geology of the Talbot Terrane (Rudall Complex), and adjacent formations of the Yeneena Supergroup and the Tarcunyah Group. The Neoproterozoic Savory Group is described elsewhere ((Hickman and Bagas, 1998). Figure 2 presents a simplified map of the Proterozoic geology on RUDALL, and Figure 3 (which omits orthogneiss) diagrammatically clarifies the regional distribution of sedimentary formations of the Rudall Complex.

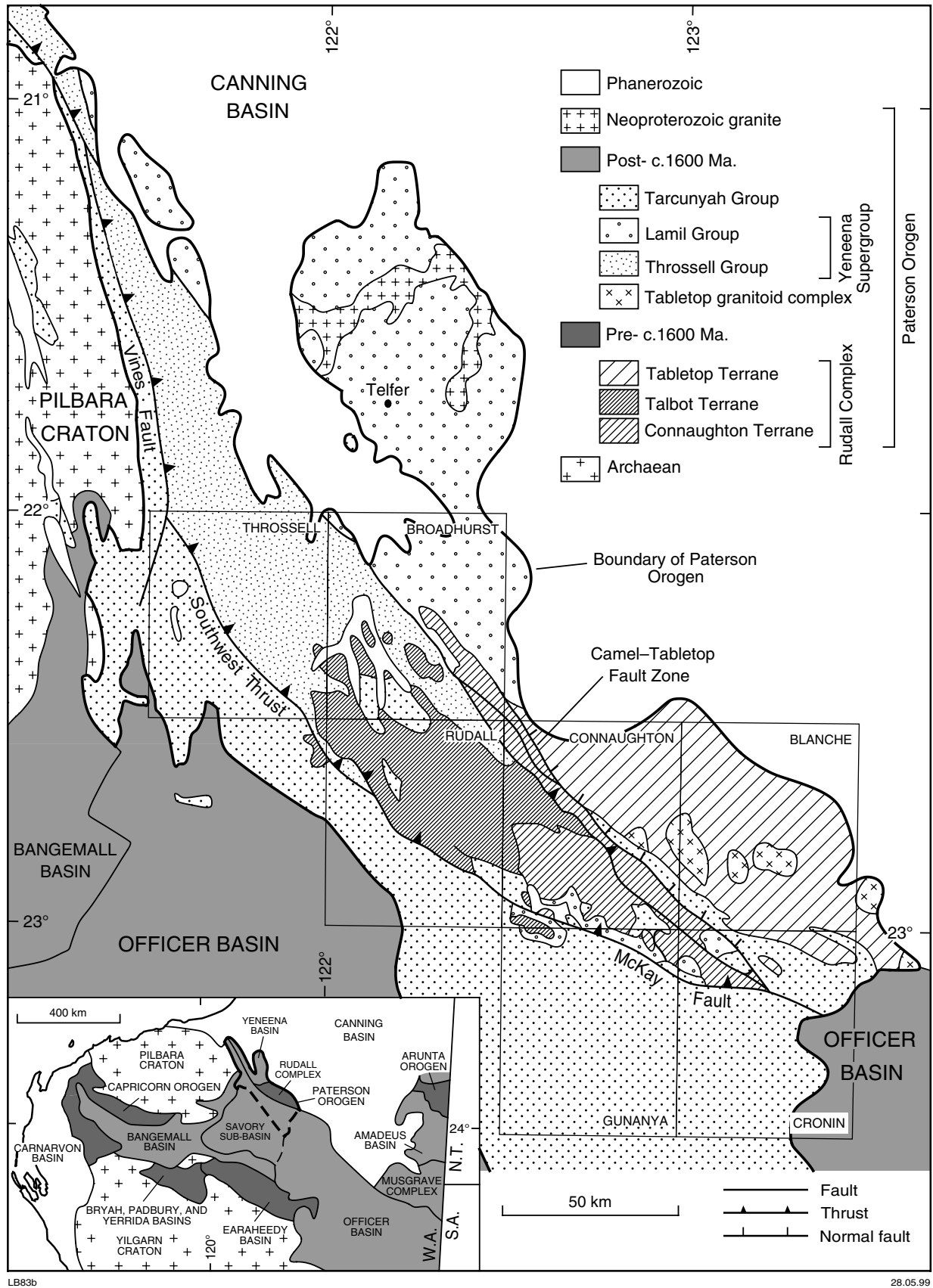
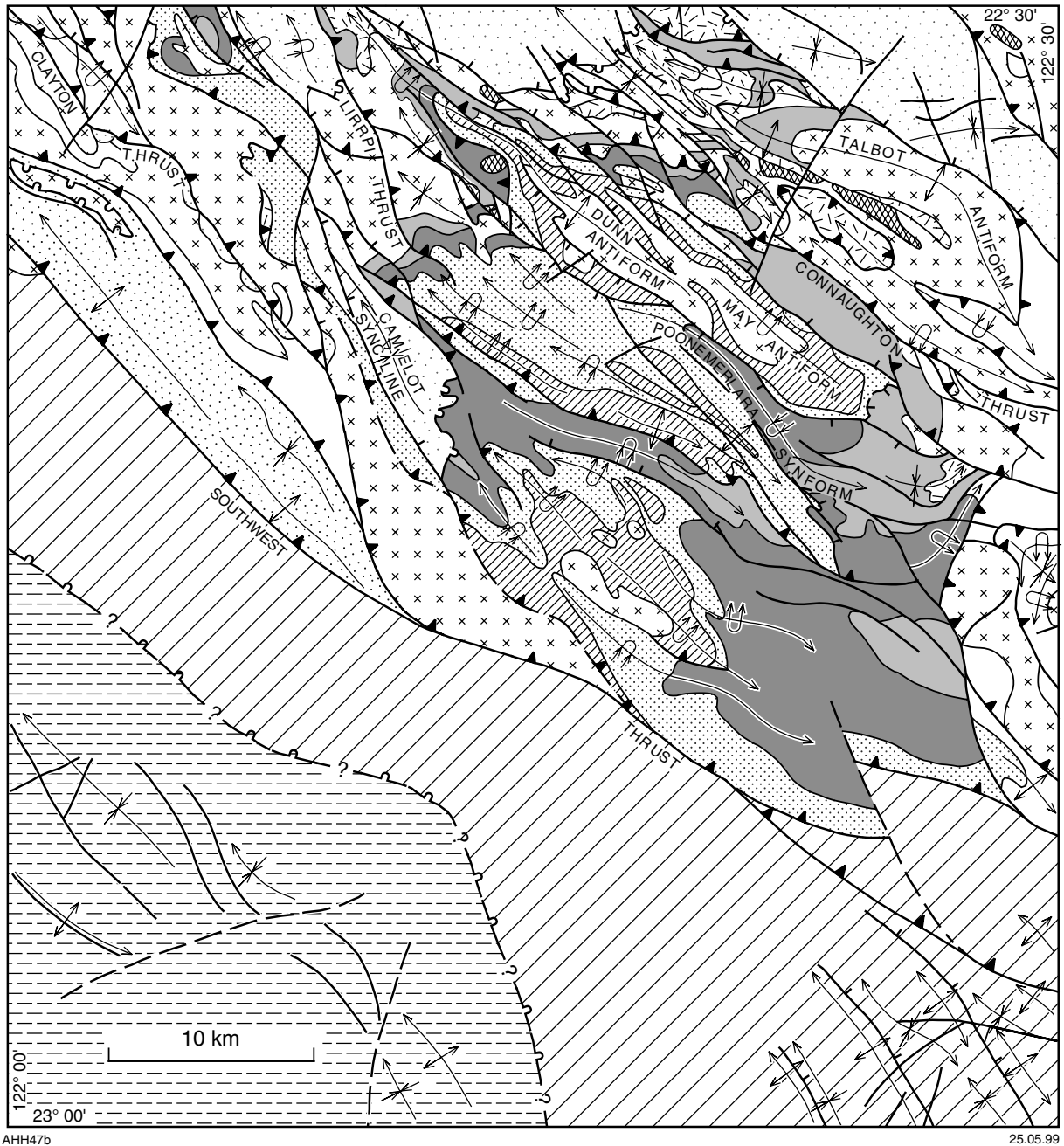


Figure 1. Regional setting of the Talbot Terrane, and the regional distribution of the Yeneena Supergroup and the Tarcunyah Group





AHH47b

25.05.99

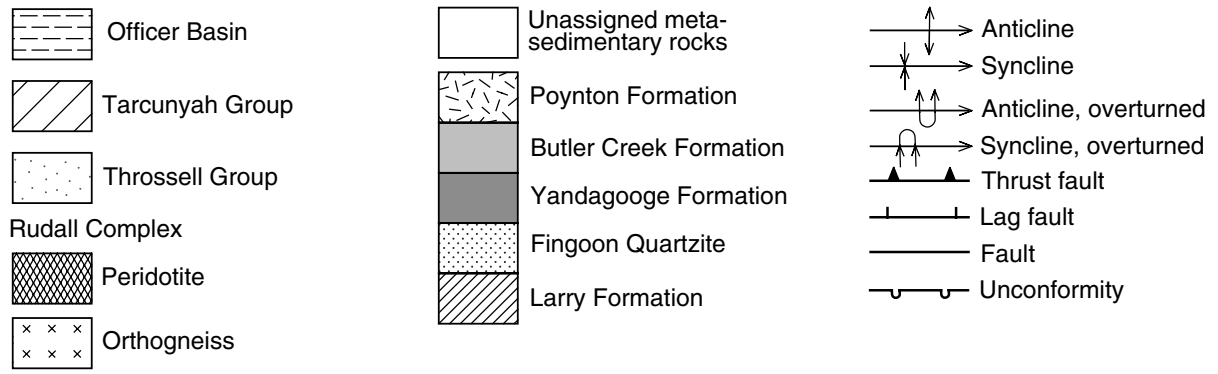


Figure 2. Simplified geological map of the Talbot Terrane on the RUDALL 1:100 000 map, showing stratigraphy and major structures. See Figures 3 and 4 for the location of the Talbot and Connaughton Terranes

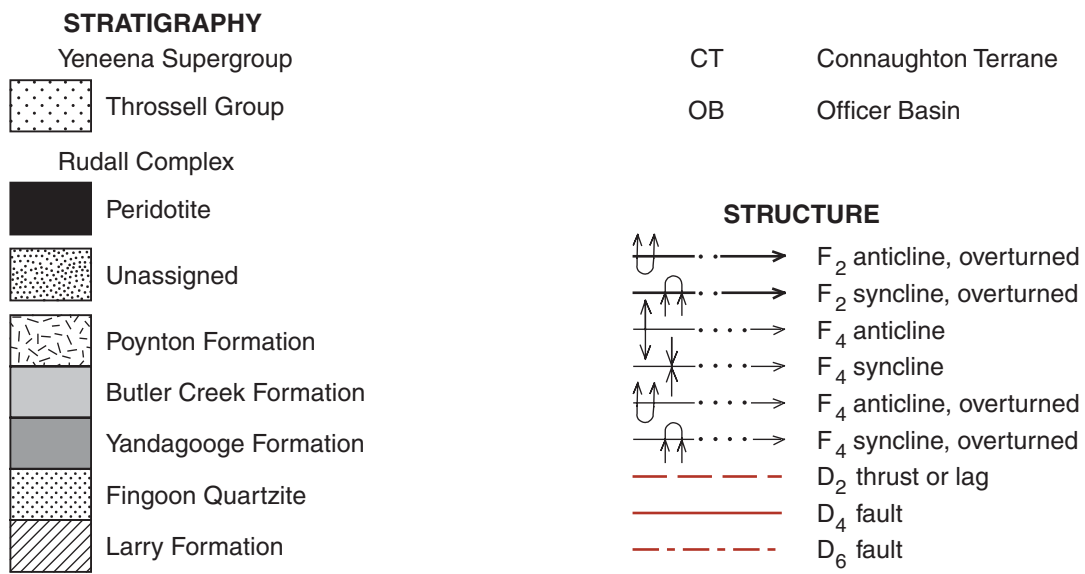
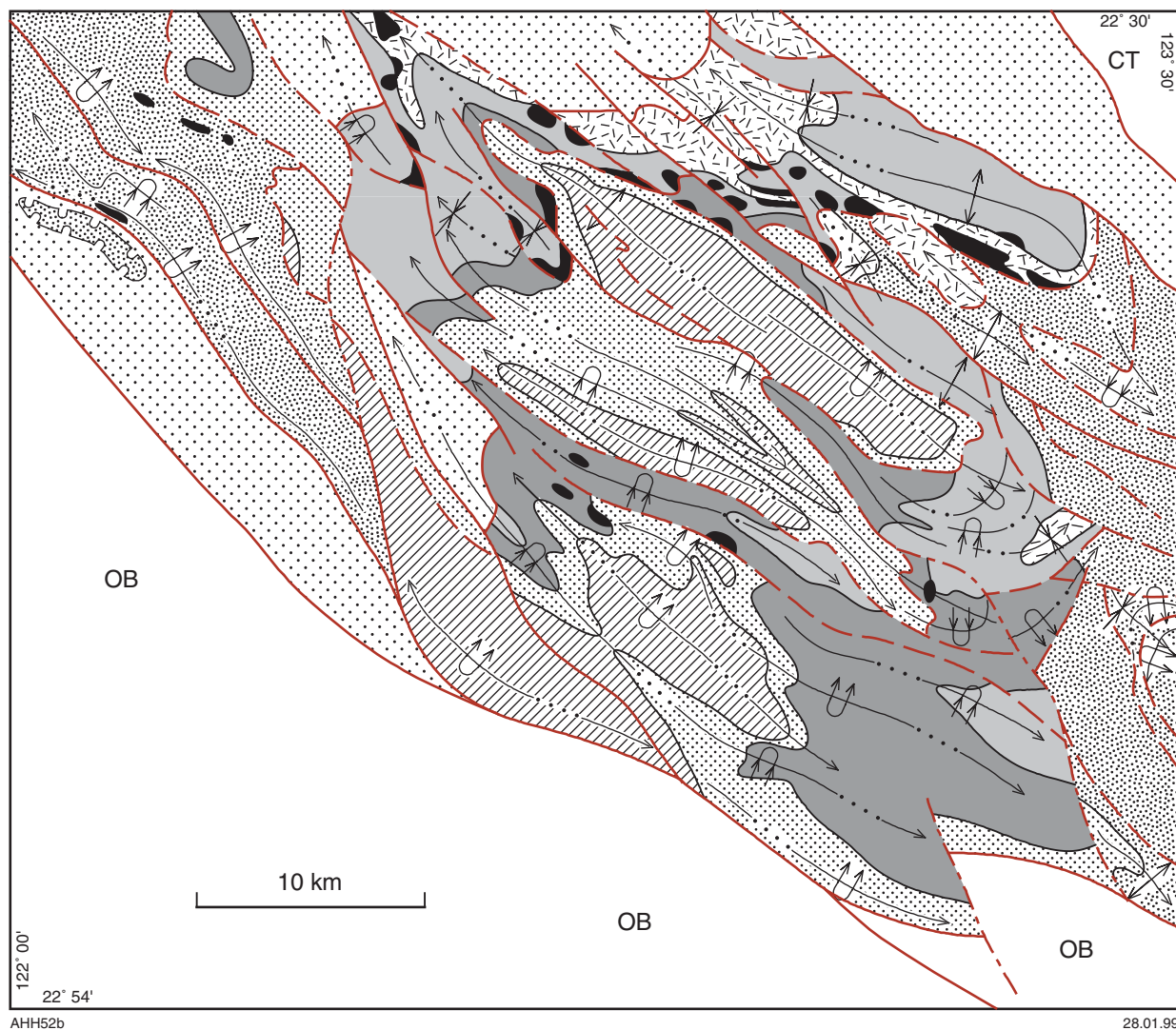


Figure 3. Diagrammatic map of the geology (orthogneiss omitted) of the Talbot Terrane on part of the RUDALL 1:100 000 map, distinguishing D<sub>2</sub> from D<sub>4</sub> structures, and emphasizing zones of peridotite

## Rudall Complex

The Talbot Terrane consists of an arenaceous and pelitic succession (now paragneiss) intruded by pre- to syn-orogenic granitoids (now orthogneiss). The terrane is tectonically divided into ten crustal segments referred to as 'tectono-stratigraphic domains' (Fig. 4). The boundaries of these domains are principally major  $D_2$  faults, but  $D_4$  faults and the unconformity at the base of the Throssell Group also form some boundaries. Each domain has a distinctive assemblage of structures and lithostratigraphic units (Table 1) due to lateral transposition and variable rotation of adjacent segments. Thus, geometrical structural analysis of minor early structures is generally impossible (variable rotation) across domain boundaries, and differences between stratigraphic successions of adjacent domains reflect juxtaposition of sedimentary sequences more widely separated during deposition.

Figure 5 presents lithological columns for eleven areas, and relates these local successions to a possible regional stratigraphic succession. However, the stratigraphy of the Poynton, and Rooney Domains may not be related to that of the Fingoon, Warturnkurru and Butler Domains. In particular, a major fault separates the Poynton Domain from the Fingoon and Butler Domains precluding confident stratigraphic correlations between those areas. No stratigraphic succession has been established in the tectonically fragmented Clayton Domain, and the stratigraphic positions of some paragneiss units are therefore left unassigned. Hickman and Bagas (1998) have described these units. In addition, the successions of the Lalapa, Martu, and Parnngurr Domains are not correlated with the stratigraphic succession in central RUDALL.

For a detailed lithological description of the five formations see Hickman and Bagas (1998).

### Stratigraphic overview

The regional distribution of the five defined formations in the Talbot Terrane is illustrated by Figure 3. Principal stratigraphic and lithological features of the succession, including derivation of name, type area and distribution, are summarized in Table 2.

Granitoid intrusion and tectonism fragment the succession, and metamorphism has destroyed most primary fabrics such as sedimentary structures. Lithological layering and rare graded bedding are the only recognizable sedimentary features, with the result that local younging directions cannot be directly determined. The regional extent of the relatively uniform lithological successions, and the nature of vertical facies changes, are consistent with the interpreted way-up. However, the relative ages of the successions of the Poynton Domain and the Fingoon–Warturnkurru Domains are uncertain (Hickman and Bagas, 1998).

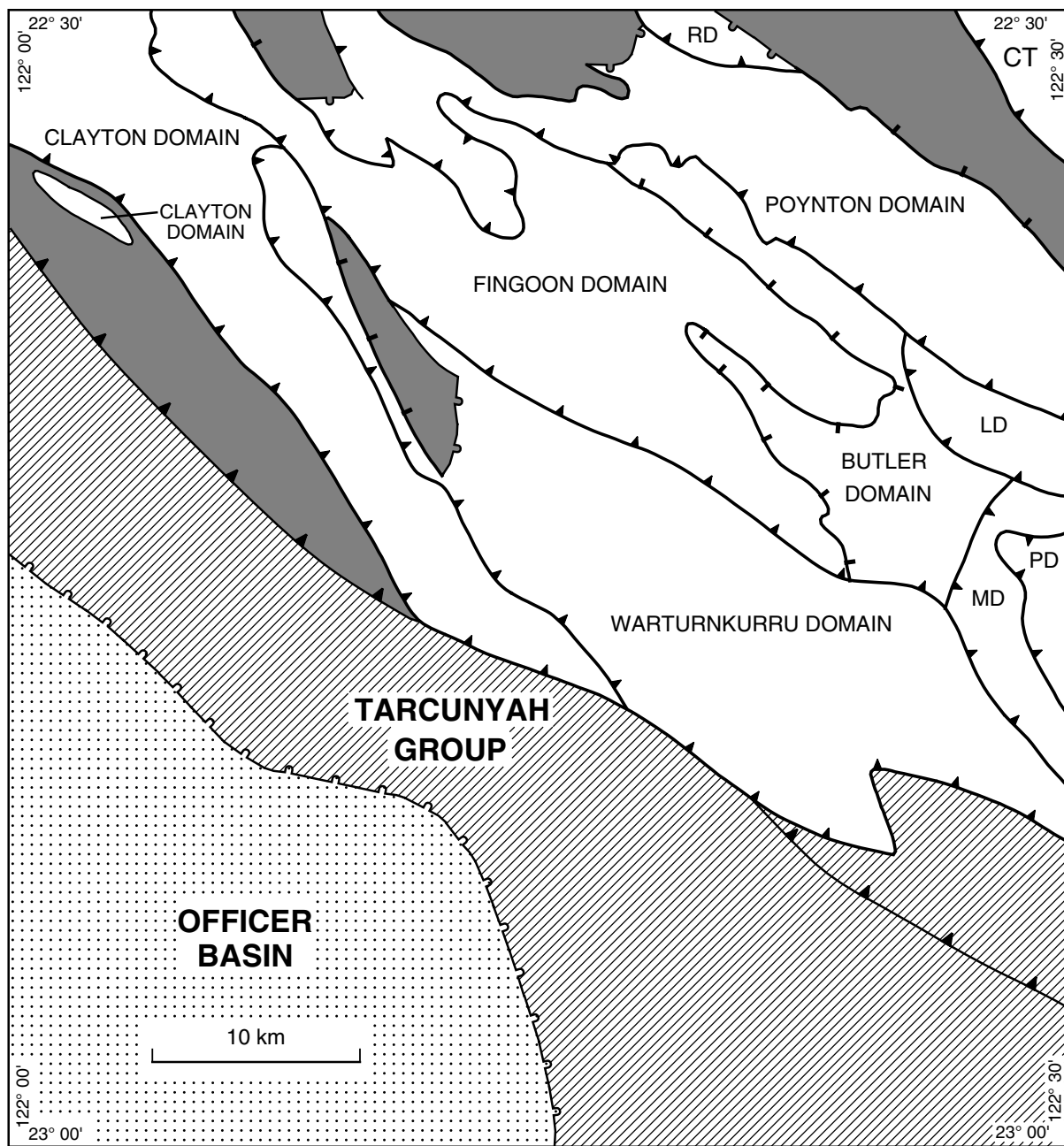
The stratigraphic subdivision of the Talbot Terrane is lithostratigraphic, and based on regional continuity of successions. No unconformities are recognized within the

succession, and contacts with orthogneiss are either tectonic or intrusive. The stratigraphic succession has been extensively fragmented by thrust faults of  $D_2$  and  $D_4$  generations, and the various tectono-stratigraphic domains contain distinct stratigraphic packages (Table 1). Correlation across domain boundaries is partly tentative, and no correlations have been made into the complexly disrupted stratigraphy of the Clayton Domain, or into the Lalapa, Martu, and Parnngurr Domains of eastern RUDALL.

Uncertainties in lithostratigraphic correlations between certain domains may only be resolved by acquiring more geochronological data. New isotopic evidence indicates that the depositional age of the Fingoon Quartzite in the Fingoon Domain is younger than  $1790 \pm 10$  Ma (U–Pb data on clastic zircons, Nelson, 1995). Field observations suggest that the stratigraphically or structurally younger Yandagooge and Butler Creek Formations of the Poynton Domain were intruded by granitoids ranging in age between 1787 and 1765 Ma (zircon U–Pb data, Nelson, 1995). These data appear to establish that the augen orthogneiss (*ERga*)\* and the sedimentary formations are of closely similar age, implying that both are genetically related to the same orogeny. Alternatively, it could be argued that the Fingoon Quartzite might be significantly younger (it is not known to be intruded by *ERga* granitoids that now form augen orthogneiss), and that the Fingoon Quartzite–Yandagooge Formation contact might be tectonic rather than stratigraphic. The field evidence of a transitional contact does not support this latter possibility, but lack of conclusive way-up criteria precludes firm conclusions. Generalized stratigraphic sections, from the Warturnkurru, Fingoon, Butler, and Poynton Domains are shown in Figure 5.

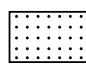
The depositional environments responsible for the succession are discussed under **Tectonic evolution**, but some preliminary observations are appropriate at this stage. The lithostratigraphic succession of the Rudall Complex appears to broadly define an orogenic cycle commencing with a mixed sandstone–mudstone (Larry Formation) to quartzite (Fingoon Quartzite) assemblage in the lowest part of the succession. The overlying Yandagooge Formation and Butler Creek Formation are composed of pelite, and rare carbonate rocks and turbidite, and a thick quartzite (Poynton Formation) completes the upper part of the cycle. The type of depositional system responsible for this succession cannot be directly determined owing to non-preservation of its eastern section, and because of destruction of important sedimentological criteria (e.g. facies relationships and sedimentary structures). However, by analogy with modern environments, the lithological character of the sedimentary assemblage indicates either intracratonic or continental margin deposition. Later in this Report (**Tectonic evolution**), additional geological evidence is used to favour deltaic–shelf to moderately deep-water deposition on a rifted continental margin. The continental landmass, which lay to the southwest and west of the shelf, was the southeastern part of the Pilbara Craton.


\* Rock codes refer to map accompanying Hickman and Bagas (1998).



AHH43b

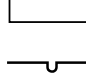
25.05.99


 Officer Basin units above Tarcunyah Group


 Tarcunyah Group

 Throssell Group

 Rudall Complex

 Unconformity

 Thrust fault

 Lag fault

Abbreviations:

Talbot Terrane

PD Parngurr Domain

MD Martu Domain

RD Rooney Domain

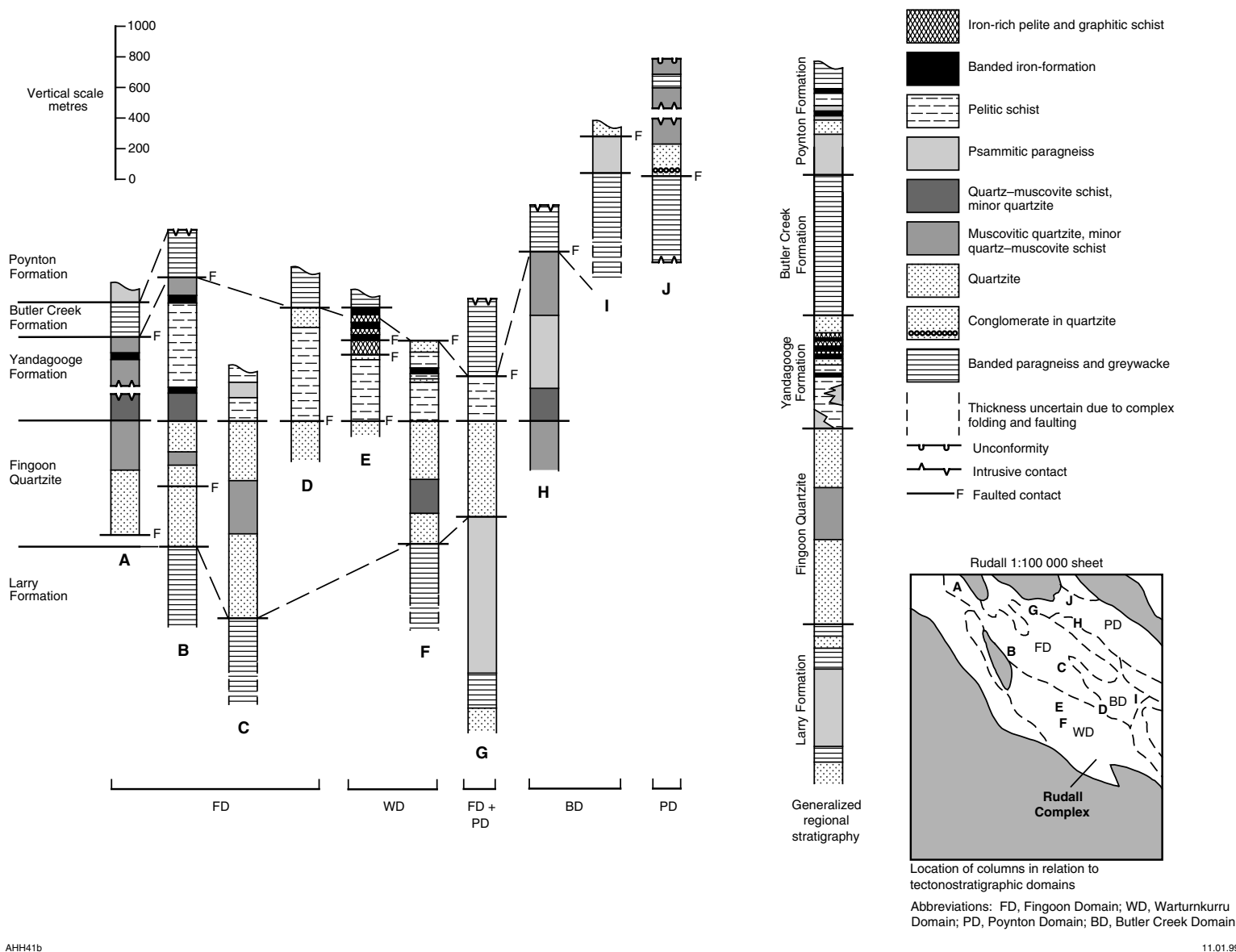
LD Lalapa Domain

CT Connaughton Terrane

Figure 4. Major tectono-stratigraphic units of the Talbot Terrane on the RUDALL 1:100 000 map

**Table 1. Summary of tectono-stratigraphic domains in the Talbot Terrane**

<i>Domain</i>	<i>Rock units</i>	<i>Structural characteristics</i>
<b>Rooney</b>	Psammitic gneiss, quartz–muscovite schist, and quartzite (assemblage correlated with Poynton Formation), and banded paragneiss (correlated with Butler Creek Formation). Minor sheets of <i>ERga</i> and local layers of amphibolite	Pervasive D <sub>2</sub> shearing and isoclinal folding have obliterated stratigraphic and intrusive relationships within this domain. S <sub>2</sub> now dips SSW, but prior to D <sub>2</sub> its inclination was probably low towards the north-northeast. Post-D <sub>2</sub> pegmatite veins occur locally
<b>Poynton</b>	The Poynton Formation and banded paragneiss correlated with the Butler Creek Formation are each intruded by thick sheets of <i>ERga</i> . <i>ERu</i> is common along, and close to, the SSW boundary of the domain	Mappable, large-scale folds in this domain are almost entirely D <sub>4</sub> structures, but these everywhere deform S <sub>2</sub> and tight to isoclinal F <sub>2</sub> folds. F <sub>2</sub> axes now generally plunge west WNW or ESE, and prior to D <sub>4</sub> would have had low plunges in these same directions. D <sub>4</sub> of the thrust contact with the Fingoon Domain establishes that its original dip was low, north-northeasterly. Likewise, low-angle D <sub>2</sub> thrusts, refolded by F <sub>4</sub> folds, occur in the eastern part of the domain
<b>Butler</b>	Domain is mainly composed of Butler Creek Formation, which stratigraphically overlies the Yandagooge Formation. Arenites that correlate with the Poynton Formation form a small outcrop in the east. Minor <i>ERga</i> intrusions	The relatively incompetent rock types of this domain have been complexly folded, first by F <sub>2</sub> isoclinal and later by upright F <sub>4</sub> folds. Minor F <sub>2</sub> folds exhibit no prevailing orientation due to refolding by F <sub>4</sub> folds, but are probably related to a major F <sub>2</sub> syncline close to the lag-faulted boundary with the Fingoon Domain. F <sub>4</sub> folds plunge SE, except in the Rudall River area where plunge is NW.
<b>Lalapa</b>	Unassigned metasedimentary rocks and orthogneiss	This domain is an imbricated wedge between the Poynton, Butler, and Martu Domains. Major F <sub>2</sub> isoclinal trends SE. The arcuate SW boundary fault transects earlier structures in the Butler Domain. Relative importance of D <sub>2</sub> and D <sub>4</sub> faulting is uncertain
<b>Martu</b>	Dominantly orthogneiss, except in the north where paragneiss may be correlated with the Butler Creek Formation. Schist and arenite in the south may be correlated with the Yandagooge and Poynton Formations	F <sub>2</sub> isoclinal shows no prevailing plunge due to F <sub>4</sub> refolding. The western boundary of domain is partly concealed, but appears to be an arcuate thrust
<b>Parnngurr</b>	Unassigned metasedimentary rocks with minor orthogneiss	Major N-trending F <sub>2</sub> isoclinal are refolded by a SE-plunging F <sub>4</sub> synform. Domain is thrust onto the Martu Domain, and this D <sub>2</sub> fault is also folded by the F <sub>4</sub> fold
<b>Fingoon</b>	Fingoon Quartzite, Larry Formation, and orthogneiss with Yandagooge and Butler Creek Formations in the NW	Domain contains major F <sub>2</sub> recumbent folds intensely deformed by upright F <sub>4</sub> folds and F <sub>4</sub> faults. F <sub>4</sub> folds plunge NW in the northwest and NW and SE in the southeast due to the existence of a major NE-trending antiform (probably post-D <sub>2</sub> and pre-D <sub>4</sub> ). Domain is thrust SW onto Warturkurru Domain, and the original D <sub>2</sub> age of this fault is established by F <sub>4</sub> folding in the northwest. However, it was reactivated during D <sub>4</sub>
<b>Warturkurru</b>	All formations except the Poynton Formation. Minor orthogneiss	Major folds are upright, tight-open F <sub>4</sub> structures except for an inferred F <sub>2</sub> syncline adjacent to the NE boundary with the Fingoon Domain. Major F <sub>4</sub> fold plunges change from NW to SE across the NE-trending antiform (see Fingoon Domain above), but the axis of this fold has been sinistrally displaced by D <sub>4</sub> movement along the Gap Thrust (Figs 2 and 14)
<b>Clayton</b>	Dominantly lithologically layered orthogneiss ( <i>ERgx</i> ) and K-feldspar orthogneiss ( <i>ERga</i> ), with subordinate slices and xenoliths of unassigned metasedimentary units, metagabbro, and ultramafic rock	Most are of D <sub>4</sub> and D <sub>6</sub> age, but pre-D <sub>4</sub> structural complexity indicates D <sub>2</sub> imbrication. Orthogneiss ( <i>ERgx</i> ) contains S <sub>1</sub> foliation that is folded by isoclinal F <sub>2</sub> folds. F <sub>4</sub> folds change plunge from NW to SE, possibly due to ESE-trending D <sub>6</sub> transpressional folds. Isoclinal, fault-bounded wedges of Coolbro Sandstone are an unusual feature of this domain



AHH41b

11.01.99

Figure 5. Generalized stratigraphic columns through the stratigraphic succession of the Rudall Complex in the Talbot Terrane. The inset is a simplified version of Figure 4, showing the location of the generalized sections

Table 2. Stratigraphy of the sedimentary succession of the Talbot Terrane

Unit, symbol, maximum thickness	Name derivation; type area; distribution	Lithology and succession	Relationships <sup>(a)</sup>
<b>Poynton Formation</b> <i>Pro</i> 1000 m	Poynton Creek (AMG330051); Poynton Creek, around AMG 330070; northeastern and northern parts of the Talbot Terrane—almost entirely restricted to the Poynton Domain	At Poynton Creek basal quartzite ( <i>Proq</i> ) passes upward into interlayered psammitic gneiss, quartzite and quartz–muscovite schist ( <i>Prom</i> ). The upper part of the formation is dominantly quartz–feldspar–muscovite gneiss with minor semi-pelitic schist ( <i>Pros</i> ) and local biotite–plagioclase–quartz schist ( <i>Prot</i> ). Banded iron-formation ( <i>Proi</i> ) occurs in tectonic contact with the Butler Creek Formation at Rooney Creek	Unconformably overlain by the Coolbro Sandstone (Yeneena Supergroup), and pervasively intruded by porphyritic granitoid protoliths ( <i>Prga</i> )
<b>Butler Creek Formation</b> <i>Rrc</i> >1000 m	Butler Creek (AMG 400961); Butler Creek, around AMG 400900; eastern part of the Talbot Terrane, north of the Rudall River, and northwest of Fingoon Range	Generally a monotonous succession of banded paragneiss containing thin layers of quartz–feldspar(–biotite) gneiss, quartz–biotite schist, and minor amphibole–chlorite schist. Thicker units of micaceous psammitic gneiss ( <i>Rrcs</i> ), banded iron-formation ( <i>Rrci</i> ), and muscovitic quartzite ( <i>Rrcq</i> ) are locally distinguished. Psammitic units are mainly developed north of Rudall River	Conformity or disconformity Pervasively interlayered with <i>Prga</i> and includes tectonic zones of intricately interleaved paragneiss and orthogneiss. North of Rudall River and north-west of Fingoon Range, lenticular serpentinite ( <i>Rru</i> ) bodies are present
<b>Cassandra Member</b> <i>Rryp</i> of the Yandagooge Formation <230 m	Cassandra mineral prospect (AMG 323853); around AMG 287895 to AMG 291902; around headwaters of Larry Creek on RUDALL	Iron-rich graphitic, pelitic schist, BIF and chert. BIF units ( <i>Rrypi</i> ) are locally sufficiently thick to be mapped separately. Rock types of the member include ferruginous quartz–feldspar–biotite schist, andalusite (–staurolite)–graphite–garnet–quartz–biotite schist, graphite–sericite–biotite schist, and quartz–amphibole(–grunerite)–pyrite–graphite schist (associated with BIF and chert). BIF contains magnetite, quartz, and cummingtonite–grunerite	Conformable contact Member in upper part of Yandagooge Formation
<b>Yandagooge Formation</b> <i>Rry</i> 1500 m	Yandagooge Creek (AMG 053310); NW Fingoon Range, around AMG 175005; SW BROADHURST (3353) and in the Fingoon Range area, RUDALL	Dominantly a pelitic to semipelitic assemblage of quartz–muscovite schist with hematitic biotite schist and thin intercalations of muscovitic quartzite. Features of the succession are a basal transitional assemblage of psammitic quartz–feldspar–muscovite gneiss, quartz–muscovite schist and inter-layered subordinate quartzite units ( <i>Rrys</i> ), an uppermost unit of muscovitic quartzite ( <i>Rryq</i> ), and units of BIF or pyritic graphitic schist ( <i>Rryi</i> ). Local variations are a more arenaceous development of muscovite–feldspar–quartz gneiss ( <i>Rrya</i> ), mainly north of Rudall River, an iron-rich pelitic unit (Cassandra Member, <i>Rryp</i> ) in the SW Fingoon Range, and a pelite–carbonate–chert association in the upper part of the formation around the Tracy uranium deposit (on BROADHURST)	Extensively intruded by porphyritic granitoid protoliths of <i>Prga</i> in N RUDALL, but not intruded in the Wartunkurru Domain and the southern part of the Fingoon Domain. Locally contains lenticular serpentinite ( <i>Rru</i> ) bodies. Transitionally overlies the Fingoon Quartzite
<b>Fingoon Quartzite</b> <i>Rrf</i> 1500 m	Fingoon Range, central RUDALL; around AMG 244932–248938 and AMG 289945–296955; Fingoon Range, NW RUDALL and SW BROADHURST	Dominantly massive or layered quartzite, but including quartz–muscovite schist with minor micaceous quartzite ( <i>Rrfm</i> ), muscovitic quartzite with intercalations of quartz–muscovite schist ( <i>Rrfq</i> ), and local quartz–feldspar–muscovite schist ( <i>Rrfs</i> ). Pelitic and semipelitic components are most common towards the top of the formation. Pebbly beds locally occur near the base of the formation	Conformable contact Boundary contacts with orthogneiss insome areas

Table 2. (continued)

Unit, symbol, maximum thickness	Name derivation; type area; distribution	Lithology and succession	Relationships <sup>(a)</sup>
			<i>Conformable contact</i>
<b>Larry Formation</b> <i>LRW</i> >1000 m	Larry Creek (AMG 288914); around AMG 236854–250870, and AMG 288914; Fingoon Range area, RUDALL	Quartz–feldspar–mica paragneiss containing quartz–mica schist and minor muscovitic quartzite is the dominant rock type. Psammitic gneiss and muscovitic quartzite ( <i>LRwa</i> ) occur close to the overlying Fingoon Quartzite. Pebbly beds occur locally near the top of the formation	Lowest formation of the succession. Base not exposed. Transitional contact with Fingoon Quartzite

NOTES: (a) excluding tectonic contacts

The Larry Formation, Fingoon Quartzite, and Yandagooge Formation are chiefly confined to the Fingoon and Warturnkurru Domains, although the Yandagooge Formation extends into the Butler Domain. Within the Fingoon Domain the Fingoon Quartzite becomes thinner to the northeast and the Yandagooge Formation becomes thicker to the southeast, although present thickness variations are probably partly tectonic. Way-up evidence is restricted to the upper part of the Larry Formation where fine-scale cross-bedding and graded bedding indicate younging towards the overlying Fingoon Quartzite.

In the Fingoon and Warturnkurru Domains, the Larry Formation is transitionally overlain by the Fingoon Quartzite. Thin quartzite bands are intercalated with an assemblage of pelitic schist and argillaceous arenites at the top of the Larry Formation. This transition could be interpreted either as a change from comparative deep to shallow environments, or as a transition between two types of shallow-water facies (e.g. estuarine or delta plain to shelf sands); however, insufficient diagnostic data are preserved.

One of the least tectonized contacts between the Fingoon Quartzite and Yandagooge Formation is preserved in the Warturnkurru Domain where quartzite and quartz–mica schist are intercalated at the base of the Yandagooge Formation. Quartzite forms thin layers throughout the Yandagooge Formation, but towards the northern part of the Fingoon Domain, feldspathic and argillaceous (poorly sorted) psammitic paragneiss makes up much of the formation. In the same direction, units of BIF and graphitic schist become less common and much thinner. These changes indicate a source of detritus to the northeast.

The Butler Creek Formation, a thick, monotonous succession of metamorphosed turbidite sediments and argillaceous units, abruptly overlies quartzite and pelitic schist in the Yandagooge Formation. The contact between the two formations is generally tectonized, but in one of the less deformed areas at the northwestern end of the Fingoon Range layer-parallel units across the boundary suggest stratigraphic continuity. The Butler Creek Formation is generally less than 1 km thick, but

becomes thicker to the east and northeast. The formation is disrupted by, and interleaved with, sheets of orthogneiss, and its upper stratigraphic contact is not exposed.

The Poynton Formation, an upward-fining succession of metamorphosed quartzite, greywacke, and minor pelite and banded iron-formation (BIF), is almost entirely confined to the Poynton Domain, where it is underlain by banded paragneiss of the Butler Creek Formation (Hickman and Bagas, 1998).

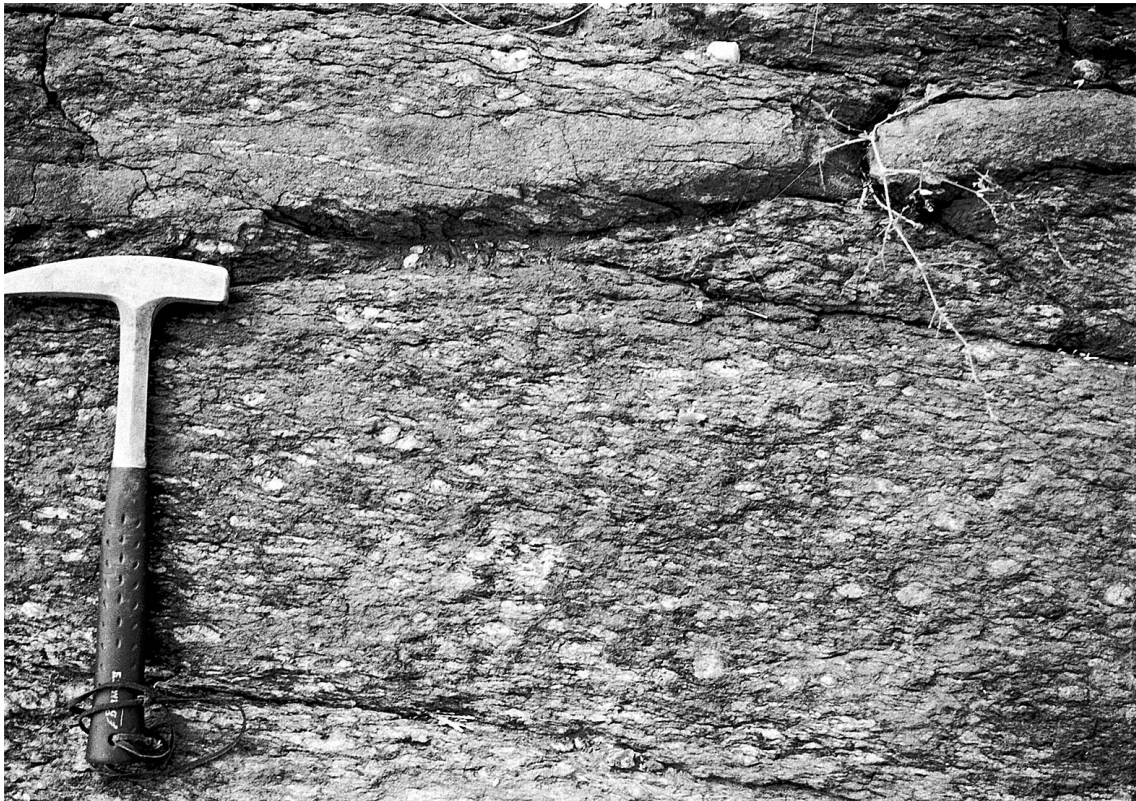
Considering that the southwestern boundary of the Poynton Domain is a major thrust (Connaughton Thrust, Figs 2 and 4), the interpretation that the Poynton Formation is the youngest sedimentary formation of the Rudall Complex depends on its relationship to the Butler Creek Formation. An alternative interpretation would equate the Poynton Formation with the Fingoon Quartzite, and would require correlating the Butler Creek Formation of the Poynton Domain with the Larry Formation of the Fingoon and Warturnkurru Domains. These correlations are less probable because they would require fortuitous juxtaposition of lithologically similar paragneiss units of different ages in the vicinity of the Connaughton Thrust. Moreover, the Poynton Formation appears to overlie the Butler Creek Formation in the Butler Domain.

Metasedimentary units of the Clayton Domain may belong to the Fingoon Quartzite and Yandagooge Formation, but sheets of orthogneiss and tectonic slicing of the area obscure stratigraphic relations.

## Orthogneiss

About 80% of the orthogneiss in the Talbot Terrane is a microcline–quartz–plagioclase–biotite augen gneiss (*LRga*) containing deformed megacrysts of K-feldspar, and is of age between 1765 and 1790 Ma (Hickman and Bagas, 1998). A further 10% of the orthogneiss is lithologically layered gneiss (*LRgx*) with xenoliths of amphibolite, serpentinite, BIF, and paragneiss. The remaining 10% is described in detail by Hickman and Bagas (1998), and will not be repeated here.





AHH81

17.02.99

Figure 6.  $S_2$ -foliated augen orthogneiss ( $PR_{ga}$ ), located 1 km north of Butler Creek at AMG 450927



AHH82

17.02.99

Figure 7.  $S_2$  in augen orthogneiss ( $PR_{ga}$ ) folded by  $F_4$  folds, located 2 km north-northwest of the Tom Tit Prospect at AMG 201030



Figure 8.  $S_2$  in augen orthogneiss ( $BRga$ ), folded and crenulated by  $F_4$  folds (AMG 201030)

Protoliths for the augen orthogneiss ( $BRga$ ) were porphyritic granite and monzogranite sheets and veins, which intruded most levels of the paragneiss succession, and the lithologically layered orthogneiss. A possible exception was the psammitic gneiss ( $BRss$ ) in the northwestern part of the terrane, which may represent a post-augen orthogneiss ( $BRga$ ) sedimentary unit. This relationship suggests that the granitoid protoliths of these two varieties of gneiss crystallized during separate intrusive events, consistent with current geochronological data (Hickman and Bagas, 1998). Furthermore, the layer-parallel foliation ( $S_1$ ) in the lithologically layered orthogneiss ( $BRgx$ ) is tightly folded ( $F_2$ ), whereas no  $S_1$  has been recognized in the augen orthogneiss ( $BRga$ ). The augen orthogneiss, however, contains augen of K-feldspar that are variably foliated by  $S_2$  mica alignment, and ranges from a poorly foliated porphyritic granite or monzogranite (Fig. 6) to a quartz-feldspar-muscovite schist (Fig. 7). The mica foliation is generally folded by  $F_4$  folds (Fig. 8) or crenulated ( $S_4$ ) by  $D_4$  (see **Structure**).

The lithologically layered orthogneiss ( $BRgx$ ) is almost entirely restricted to the Clayton Domain where contacts with unassigned metasedimentary units of the Rudall Complex are intrusive. However, it is possible that these metasedimentary rocks are older than the stratigraphic succession from the Larry Formation to the Poynton Formation. At no localities do units of the paragneiss succession unconformably overlie any types of orthogneiss, and no conglomerates

containing orthogneiss clasts have been identified. In summary, field evidence indicates that most of the augen orthogneiss protoliths were younger than the paragneiss succession, whereas the lithologically layered orthogneiss includes granitoid protoliths that are older.

## Yeneena Supergroup and Tarcunyah Group

Bagas et al. (1995) have redefined the stratigraphic name 'Yeneena Group' (Williams et al., 1976) into the Yeneena Supergroup (composed of the Throssell and Lamil Groups) and the Tarcunyah Group. The Tarcunyah Group now incorporates formations previously assigned to the 'Western Zone' succession of Williams (1990). Williams and Bagas (in prep.a) provide the fullest description of the Tarcunyah Group.

Recent work supports a Neoproterozoic age for the Tarcunyah Group (c. 800 Ma, Bagas et al., 1995), and isotopic evidence indicates that the age of the Throssell Group is probably younger than 1250 Ma, and probably older than 900 Ma (see **Geochronology**).

The contact between the Throssell and Lamil Groups is not exposed, although interpretation of aeromagnetic data suggests that it is a fault or unconformity (Hickman and Clarke, 1994; Hickman and Bagas, 1998).

Hickman and Bagas (1988) give detailed lithological descriptions of the Yeneena Supergroup and Tarcunyah Group on RUDALL.

## Dolerite dykes, quartz veins, and gossan

Dolerite (*d*) dykes have intruded the Rudall Complex in the northwestern part of the Talbot Terrane, and vary in trend from west-northwest to north-northwest. The dolerite exhibits low metamorphic grade and the dykes clearly post-date  $D_2$  and  $D_4$  structures. The later relationship establishes that they are younger than the Throssell Group, but no intrusion of the Throssell Group has been observed. Aeromagnetic data on THROSSELL and LAMIL show a suite of dolerite dykes striking north-northeast, and clearly later than  $F_4$  folds. Williams (1992) describes similar dykes in the 'Savory Basin', and implies a post-600 Ma age, although no direct geochronology has been undertaken. If the west-northwesterly striking dykes are related to the dominant north-northeast set of dykes west and northwest from RUDALL, they may occupy late tensional fractures produced by the  $D_6$  event (north-northeast to south-southwest compression). About 1.5 km south of the confluence of Gap Creek and the Rudall River, at AMG 178023\*, a dolerite dyke intrudes a minor north-northwesterly trending fault, apparently of  $D_6$  generation. The dolerite dyke is lenticular, poorly foliated along its margins, and has reacted with local orthogneiss to produce tachylitic veins of partly hybridized breccia. The dolerite is fine grained and consists of microphenocrysts of plagioclase in a granular matrix of augite, plagioclase, and opaque minerals.

Quartz veins (*q*) are widespread on RUDALL, and are generally located in faults and shear zones (Hickman and Bagas, 1998). Some of the veins (Appendix 1) are anomalous in cerium, lanthanum, barium, copper, arsenic, silver, and gold (see **Mineral resources**). Some veins also contain visible tourmaline or rutile.

Gossan or gossanous rock (*go*) units are limonite-goethite concentrations formed by surface oxidation of sulfide mineralization. Such sulfide mineralization is either epigenetic (generally accompanying quartz veining), or syngenetic and stratiform. All gossans identified during the mapping were sampled, and analytical results (Appendix 1) are discussed under **Mineral resources**.

## Structure

The Rudall Complex is the product of many depositional, intrusive, tectonic and metamorphic events, apparently operating over a period of more than 1000 m.y., which include the Yapungku, Miles, and Paterson Orogenies (Bagas et al., 1995). The RUDALL map conveys something

of the resulting geological complexity of the Talbot Terrane, but the true level of complexity is best appreciated at outcrop scale where isoclinally folded, compositionally layered paragneiss has commonly been 'sheeted' by granitoid phases, sheared and refolded. At outcrop scale, orthogneiss–paragneiss contacts are almost invariably parallel to compositional banding in the metasedimentary rocks, and it is generally impossible to determine the relative importance of tectonic interleaving and the intrusion of granitic sills.

Angular xenoliths of paragneiss and orthogneiss are visible in some outcrops of orthogneiss, but elsewhere lenticular paragneiss inclusions are clearly boundins or detached fold cores. At 1:25 000 and larger scales, intrusive contacts are indicated by discordant orthogneiss–paragneiss contacts without any evidence of oblique faulting. Most of the granitoid protoliths appear to have been emplaced as broadly concordant sheets, locally up to 3 km thick. These major intrusions have caused fragmentation of the stratigraphic succession, and in the process have limited the use of stratigraphic marker units for regional structural interpretation.

An important conclusion from the 1991–1992 mapping, and subsequent structural analysis, is that prior to deposition of the Yeneena Supergroup, the Rudall Complex was composed of nappes and thrust sheets, inclined and stacked towards the northeast.

Table 3 summarizes structures of the various deformation events that have affected the Talbot Terrane. Figures 2 and 3 illustrate the major structures, and Figures 9 and 10 show minor structures. Several important observations can be made from Figures 2, 3, 9, and 10. Firstly, major  $F_4$  anticlines and synclines, so well developed in the Yeneena Supergroup of BROADHURST (Hickman and Clarke, 1994, fig. 6), are seen to extend deep into the Rudall Complex. An example is the Dunn Antiform, which has been traced 30 km southeast from the Watrara Range (BROADHURST) to the May Antiform on RUDALL. Secondly, the major  $D_4$  faults continue into the Rudall Complex, and are interpreted to remain steeply inclined ( $>45^\circ$ ) at depths of 3–5 km below the unconformity. Thirdly, the existence of narrow, fault-bounded, synclinal outliers of Coolbro Sandstone within the Rudall Complex (e.g. along the Clayton Thrust, Fig. 2) demonstrates vertical movements of several kilometres along the larger faults. Fourthly, Figures 3 and 10 reveal a major, northeast-trending culmination or antiformal cross-fold through the centre of the Rudall Complex. Reversals of plunge of  $F_4$  folds also occur on BROADHURST (Fig. 5; Hickman and Clarke, 1994), but are generally en echelon, and consistent with heterogeneous strain rather than fold interference. Finally, the statistical analysis of minor structures in the Poynton and Rooney Domains reveals the pre-Throssell Group orientation of  $D_2$  structures (Fig. 11; discussed in detail under  **$D_2$  structures**).

Hickman and Clarke (1994) recognized six phases of deformation on BROADHURST,  $D_1$  and  $D_2$  occurring prior to deposition of the Throssell Group, and these have been included in the Yapungku Orogeny (Bagas and Smithies, 1997).

\* Localities are specified by the Australian Map Grid (AMG) standard six-figure reference system whereby the first group of three figures (eastings) and the second group (northings) together uniquely define position, on the RUDALL 1:100 000 sheet (unless otherwise noted), to within 100 m.

Table 3. Summary of deformation episodes affecting the Talbot Terrane, and the Throssell and Tarcunyah Groups

Event	Major structures	Minor structures	Metamorphism and magmatism
<b>Early Yapungku Orogeny</b> D <sub>1</sub> : Regional layer-parallel shear, direction unknown	Identified on BROADHURST	S <sub>1</sub> : Penetrative layer-parallel schistosity; alignment of mica, quartz, and feldspar	M <sub>1</sub> : Low-pressure, middle amphibolite facies conditions (not recognized on RUDALL); local melting; granitoid intrusion
<b>Yapungku Orogeny</b> D <sub>2</sub> : SW- and W- directed thrusting and overfolding	Tight to isoclinal F <sub>2</sub> folds (axes trend WNW to N and are overturned towards SSW); D <sub>2</sub> thrust zones	F <sub>2</sub> : Isoclinal folds S <sub>2</sub> : Schistosity due to alignment of mica and quartz L <sub>2</sub> : Stretching lineation within S <sub>2</sub>	M <sub>2</sub> : Medium-pressure amphibolite facies; some melting of pelitic rocks
<b>Early Miles Orogeny</b> D <sub>3</sub> : Local W- or NW-directed isoclinal-recumbent folding	Identified on BROADHURST	Local faulting and quartz veining of the Rudall Complex–Throssell Group unconformity	None identified
<b>Miles Orogeny</b> D <sub>4</sub> : Regional deformation in response to SW-directed compression	Upright, tight to isoclinal F <sub>4</sub> folding about NW-trending axes, strike-slip fault system	S <sub>4</sub> : Axial surface cleavage inclined steeply NE L <sub>4</sub> : Stretching lineations plunge down-dip on S <sub>4</sub>	M <sub>4</sub> : Low greenschist facies; locally intense cataclasis and dynamic recrystallization
D <sub>5</sub> : Local deformation; ?NE-directed stress release after D <sub>4</sub>	Identified on BROADHURST	Identified on BROADHURST	None identified
<b>Paterson Orogeny</b> D <sub>6</sub> : Brittle deformation in response to NNE-SSW compression	ENE- and N-striking near vertical strike-slip faults	S <sub>6</sub> : Strain-slip cleavage, axial to conjugate kink bands, deforming S <sub>4</sub>	None identified

## Pre-Yeneena Supergroup deformation

The Rudall Complex was multiply deformed and metamorphosed during the Yapungku Orogeny before deposition of the Yeneena Supergroup.

As described under **Tectonic evolution**, this deformation was related to plate collision, and involved progressive stacking of thrust slices. Thus, the present assignment of pre-Yeneena Supergroup structures to D<sub>1</sub> and D<sub>2</sub> episodes does not imply two distinct, short-term events. For D<sub>2</sub>, in particular, it is clear that F<sub>2</sub> and S<sub>2</sub> structures would have formed at different times in the different tectono-stratigraphic domains, and thrusting directions varied with time.

Metasedimentary rocks and the older varieties of orthogneiss (mainly *ERgx*) were deformed by the earliest recognized deformation, D<sub>1</sub>, sometime after crystallization of the 2015 Ma orthogneiss and before crystallization of the augen orthogneiss protoliths during the period 1787–1765 Ma. All major rock units of the complex were affected by deformation assigned to D<sub>2</sub>, which culminated at a currently unknown time after 1765 Ma (S<sub>2</sub> in *ERga*). This produced pervasive micaceous schistosity (grouped under S<sub>2</sub>) parallel to the axial planes of F<sub>2</sub> folds. The S<sub>2</sub> schistosity is extremely well developed in K-feldspar augen orthogneiss (*ERga*),

but an earlier schistosity (S<sub>1</sub>) has not been recognized in this unit. D<sub>1</sub> and D<sub>2</sub> structures are truncated by the unconformity at the base of the Throssell Group, and were deformed by post-Throssell Group folds (mainly F<sub>4</sub>). Consequently, the present orientations of D<sub>1</sub> and D<sub>2</sub> structures are commonly very different from their original orientations, and cannot be used as criteria for structural classification.

## Yapungku Orogeny

### D<sub>1</sub> structures

A regional deformation prior to D<sub>2</sub> is evident from the widespread existence of layer-parallel penetrative schistosity (S<sub>1</sub>), folded by F<sub>2</sub> isoclinal folds and in places visibly deformed by cross-cutting S<sub>2</sub>. The S<sub>1</sub> foliation is parallel to compositional layering in the paragneiss and quartzite units, suggesting that it is either an axial-plane foliation of major isoclinal (possibly recumbent) folds or it is associated with subhorizontal tectonic interleaving (thrusting). D<sub>2</sub> has obliterated any linear fabrics, which could have been used to establish the orientation of D<sub>1</sub> strain.

One kilometre north of the Rudall River (AMG 275030), a narrow shear zone folded by an isoclinal F<sub>2</sub> synform bounds a lenticular inlier of quartzite. If this quartzite belongs to the Fingoon Quartzite, the shear zone

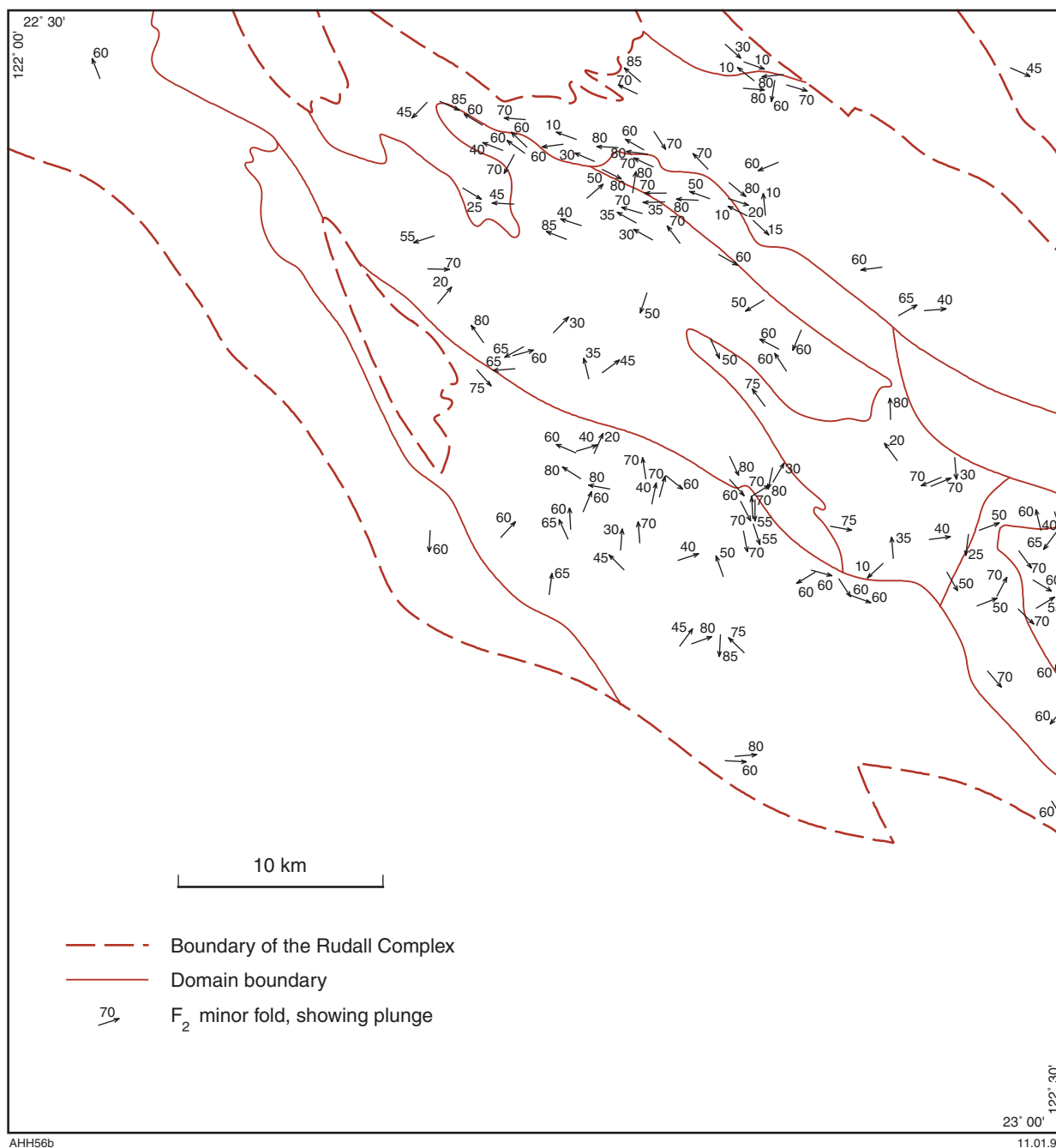


Figure 9. Minor structures on the RUDALL 1:100 000 map area, showing the plunge directions of minor F<sub>2</sub> folds

must be a pre-F<sub>2</sub> thrust because here the F<sub>2</sub> fold has deformed an inverted succession. To the southwest of this locality the main outcrop of Fingoon Quartzite contains large isoclinal F<sub>2</sub> folds deforming an early foliation (S<sub>1</sub>), and refolded by the F<sub>4</sub> Dunn Antiform.

### D<sub>2</sub> structures

Prior to mapping RUDALL, it was established that D<sub>2</sub> was characterized by tight to isoclinal folding in which a regional schistosity (S<sub>2</sub>) was developed in all major rock units of the Rudall Complex (Clarke, 1991; Hickman and

Clarke, 1994). The S<sub>2</sub> foliation is now (after rotation by F<sub>4</sub> folds) generally steeply inclined principally towards the northeast or southwest, but in F<sub>4</sub> axial regions it commonly dips northwest or southeast. Clarke (1991) used structural observations in the Yandagooze and Watrara Inliers of BROADHURST to propose that F<sub>2</sub> folds were originally recumbent, and formed in response to a regional northeast-trending shear regime. However, this interpretation made no allowance for reorientation of D<sub>2</sub> structures during D<sub>4</sub>, an event that Clarke (1991) considered to have had negligible effect on the Rudall Complex.

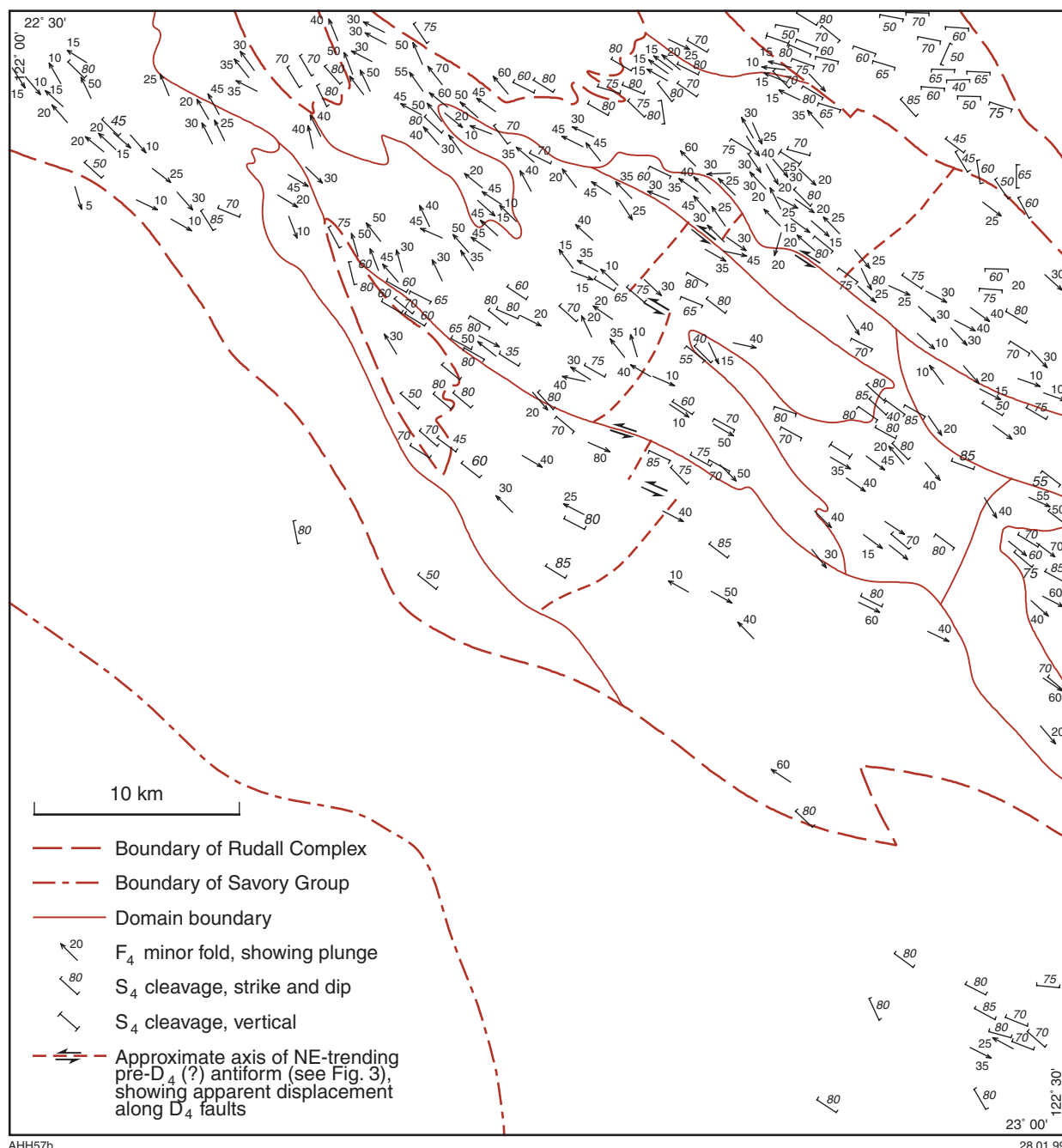
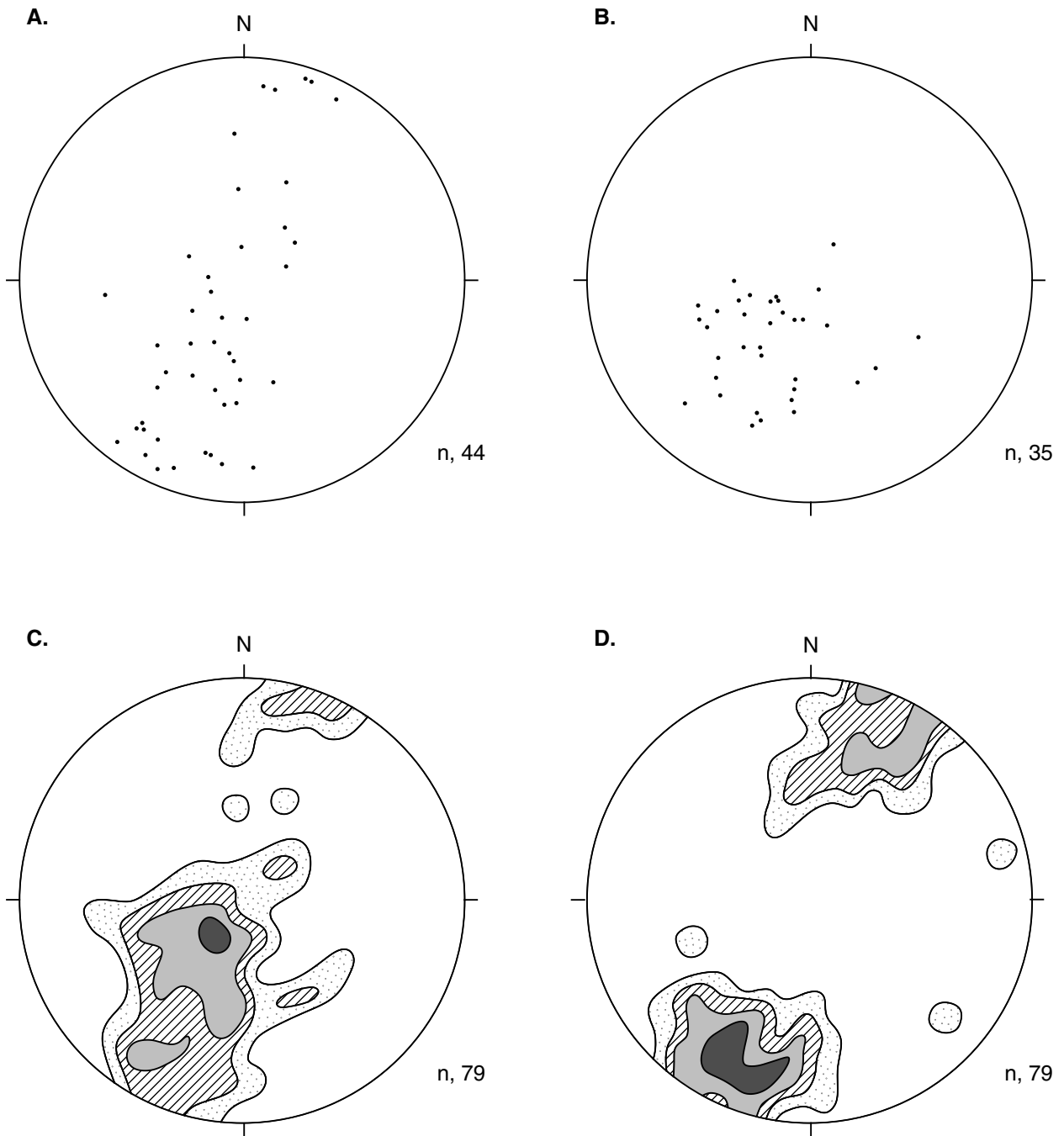


Figure 10. Minor structures on the RUDALL 1:100 000 map area, showing the plunge of F<sub>4</sub> folds, and S<sub>4</sub> cleavage

It must be emphasised that D<sub>2</sub> was not a single, short-term event affecting all parts of the Rudall Complex at precisely the same time. This is established by D<sub>2</sub> thrust stacking (see **Tectonic evolution**), with structures in the northeast and east apparently overriding earlier structures to the southwest.

In an attempt to remove D<sub>4</sub> tilting from S<sub>2</sub>, and thus determine the attitude of S<sub>2</sub> immediately prior to deposition of the Throssell Group, S<sub>2</sub> observations within 1 km of the Rudall Complex–Throssell Group unconformity have been paired with observations of bedding

in the immediately overlying Coolbro Sandstone (significantly deformed by only D<sub>4</sub>). Over a strike length of 50 km in the Poynton and Rooney Domains stereographic unfolding of 79 S<sub>2</sub> observations firmly establishes that before D<sub>4</sub> the local strike of S<sub>2</sub> was west-northwest, and its dip was dominantly between 20° and 40° towards the north-northeast (Fig. 11a–c). Given that minor F<sub>2</sub> folds are tight to isoclinal, and that S<sub>2</sub> is the axial-plane foliation of these structures, it is concluded that in the northeastern part of RUDALL the axes of any major F<sub>2</sub> folds must have trended west-northwest, and the folds were overturned towards the south-southwest. The plunge of



**A.** Rooney Creek area,  $S_2$  unfolded to remove  $F_4$  tilt  
**B.** Poynton Synform,  $S_2$  unfolded to remove  $F_4$  tilt  
**C.** Contoured poles, a + b,  $S_2$  unfolded to remove  $F_4$  tilt,  
1, 2.5, 5, 10% per 1% area  
**D.** Contoured poles, current (post- $D_4$ ) attitude of  $S_2$   
(all observations are plotted on the lower hemisphere)

**Figure 11. Stereographic projections plotting  $S_2$  foliations to estimate the pre-Throssell Group orientation of  $S_2$  in the Poynton and Rooney Domains**

mesoscopic  $F_2$  folds in northeastern RUDALL (Fig. 9) is now generally moderate to steep towards the west-northwest. In this region  $F_4$  folds plunge northwest at about  $15$  to  $45^\circ$  (Fig. 10), implying that prior to  $F_4$  the west-northwesterly plunge of  $F_2$  folds was low.

Major pre- $F_4$  folds occur in the Martu and Parngurr Domains. Observations from CONNAUGHTON indicate that the folds are isoclinal, and prior to refolding during  $D_4$  had subhorizontal axes trending in a northerly to northeasterly direction (Bagas and Smithies, 1998). The isoclines of the Martu and Parngurr Domains are probably late  $D_2$  structures, but they could belong to a separate phase.

To the north of the Rudall River, in the northern part of the Fingoon Domain, large, intraformational  $F_2$  isoclines occur within the Fingoon Quartzite on the northeastern limb of the Dunn Antiform. These folds are interpreted to be parasitic isoclines on the tectonically attenuated, north-northeastern limb of the major  $F_2$  anticline (Fig. 12). The northeastern boundary of the quartzite is a zone of extreme attenuation and faulting in which the Yandagoo and Butler Creek Formations are abnormally thin, or even absent. The Butler Creek Formation, however, shows a major increase in thickness in the May Creek area of the Butler Domain. The formation is probably thickened by complex isoclinal folding in the core of a  $F_2$  synform.

The original orientation of  $D_2$  structures in the central part of the Fingoon Domain, and in the Warturkurru Domain has been obscured by complex tight to isoclinal  $F_4$  folding, although  $F_2$  folds have also been observed in  $F_4$  axial regions near the Dione prospect (AMG 256906). These folds are isoclinal and plunge shallowly towards the north. Away from the  $F_4$  axial regions and in areas of shearing, such as around 1 km southeast of Dione (AMG 265903),  $F_2$  folds are parallel to  $F_4$  folds. This observation indicates that  $F_2$  folds have most likely been rotated towards parallelism with  $F_4$  folds during progressive shearing. Therefore, the local  $F_4$  effects on  $F_2$  are generally difficult or impossible to determine in the field, especially in the Fingoon Quartzite.

The  $D_4$  event reactivated  $D_2$  shear zones, which would have been zones of weakness. Consequently, the recognition of  $D_2$  shear zones within  $D_4$  thrusts and normal (lag) faults depends on criteria such as extreme attenuation inconsistent with adjacent  $F_4$  folds, associated minor  $F_2$  folds and faults, or sheared pre- $D_4$  intrusions of microgranite, aplite, or pegmatite. The  $D_2$  shear zone along the northern boundary of the Fingoon Domain was refolded by the Dunn–May Antiform, and may extend southeast into the southwestern limb of the Poonemerlarras Syncline (Fig. 2). To the northwest of the Fingoon Range, the shear zone coincides with a  $D_4$  fault near the Tom Tit prospect, but lenses of sheared quartzite are preserved 3 km east from Rudall Crossing, where this structure crosses the Rudall River (AMG 145065).

Another example of large-scale  $F_2$  folding occurs 2 km south of Poynton Creek at AMG 310045. Here, northwest-plunging  $F_4$  folds refold a westerly striking  $F_2$

synclinal core of Poynton Formation, which flanked by ultramafic bodies and Butler Creek Formation.

Lenticular bodies of ultramafic rocks outcrop around the Rudall River. These rocks are apparently partially controlled by  $D_2$  shear zones, and are orientated parallel to  $S_2$ . This implies that the  $D_2$  event included the emplacement of sheets of ultramafic rocks. Figure 3 shows that the distribution of ultramafic rocks is largely restricted to three west-northwesterly striking zones. The zones north of Rudall River and in the headwaters of Larry Creek, partly coincide with  $D_2$  attenuation zones adjacent to the Fingoon Quartzite. Carr (1989) concluded that the ultramafic bodies of the Rudall River area might be Proterozoic analogues of ‘Alpine-type’ peridotites, and favoured solid-state emplacement.

## Post-Yeneena Supergroup deformation

Four phases of deformation,  $D_3$  to  $D_6$ , have been recognized in the Throssell Group (Hickman and Clarke, 1994). Of these, local pre- $D_4$  movement along the Rudall Complex–Throssell Group unconformity probably represents  $D_3$ ,  $D_4$  was the dominant event responsible for the major northwest-trending folds in the area, and  $D_6$  faults crosscut and reactivate earlier structures.  $D_3$  and  $D_4$  are considered as progressive deformation events forming the Miles Orogeny (Bagas et al., 1995). Structures belonging to  $D_5$  in the tectonic history of BROADHURST have not been observed elsewhere, probably due to the scarcity of good exposures of the Broadhurst Formation, however, to facilitate structural comparisons between different areas of the Paterson Orogen the tectonic nomenclature used on BROADHURST is retained. The  $D_6$  event has been redefined as the Paterson Orogen by (Bagas et al., 1995; Bagas and Smithies, 1998).

Post- $D_4$  folds, faults and cleavage in the Savory Group, to the southwest of the study area, are assigned to the Paterson Orogeny ( $D_6$ ; Hickman and Bagas, 1998). Williams (1992) has presented sedimentological and structural evidence that these structures formed after  $D_4$ , and that they are younger than 670 Ma.

## Miles Orogeny

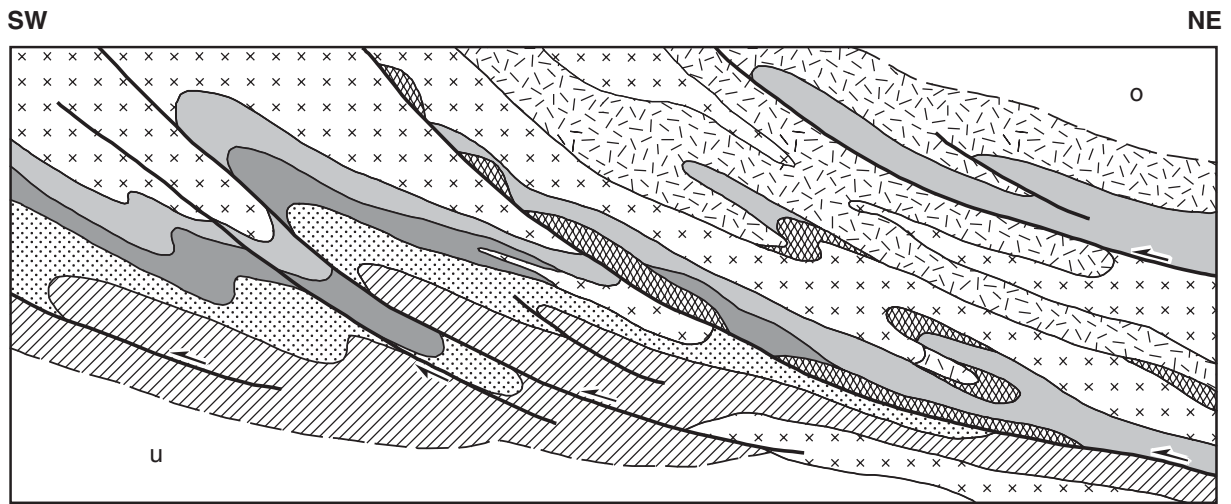
### $D_3$ structures

The Rudall Complex–Throssell Group unconformity along the southwestern limb of the Poynton Synform is faulted and quartz-veined parallel to bedding. This tectonic contact is transgressed and offset by northwest-striking  $D_4$  faults, implying significant horizontal or subhorizontal movement prior to  $D_4$ , and post- $D_2$ .

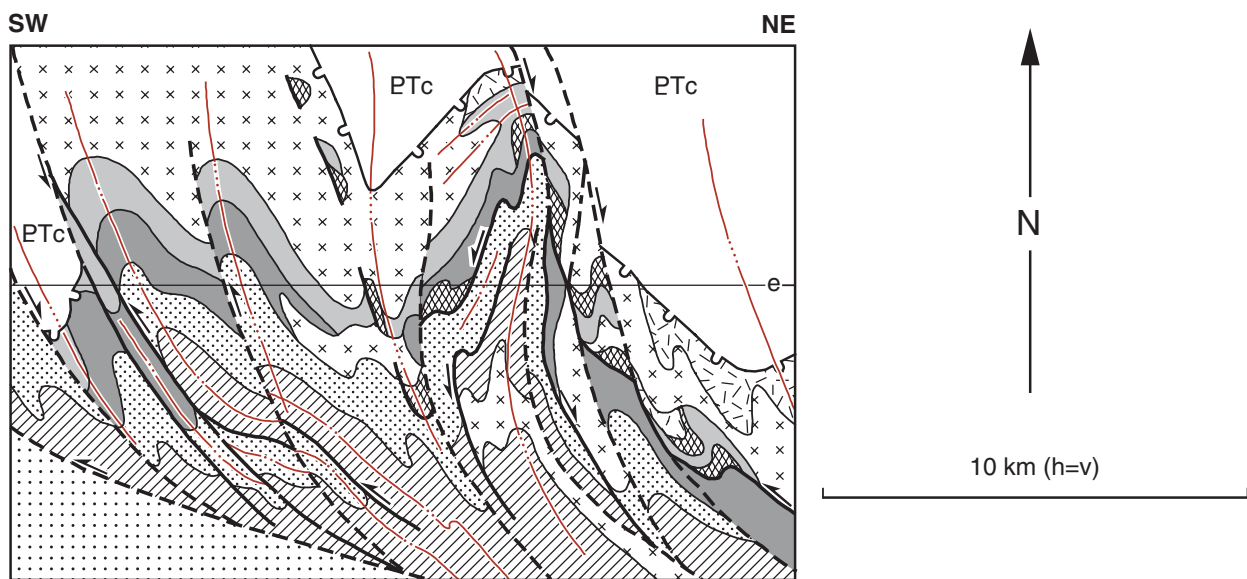
### $D_4$ structures

The  $D_4$  event represents the main phase of the Miles Orogeny and produced structures trending about  $300$ – $320^\circ$  in the Talbot Terrane of the Rudall Complex, and the Throssell Group.

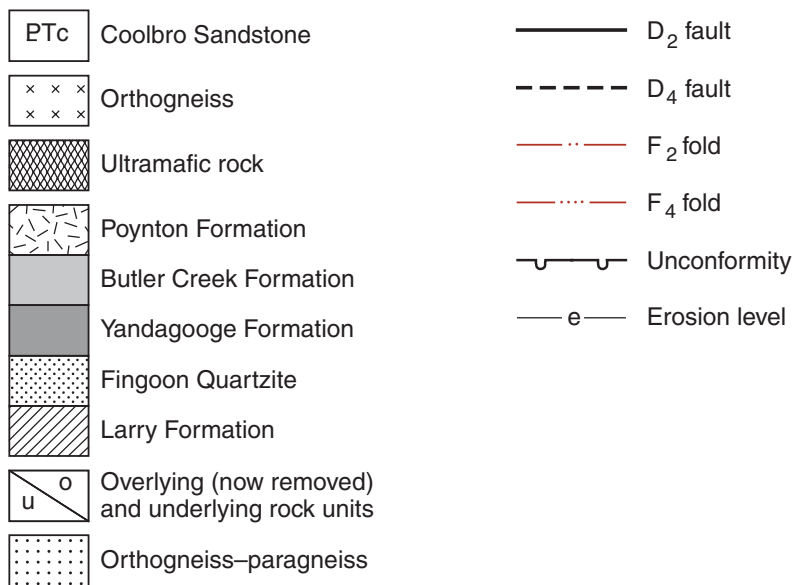




A. Post-D<sub>2</sub>



B. Post-D<sub>4</sub>



AHH45b

25.05.99

Figure 12. Diagrammatic cross section through Rudall River, showing major D<sub>2</sub> and D<sub>4</sub> structures

The major structures in the Throssell Group on RUDALL and BROADHURST are upright to overturned, tight to isoclinal, northwesterly to west-northwesterly trending folds that are overturned to the southwest, and contain a variably developed axial-plane cleavage ( $S_4$ ) dipping steeply northeast. The  $F_4$  folds display reversals of plunge, and both the  $D_4$  faults and folds exhibit en echelon patterns. This en echelon pattern suggests that most of the  $D_4$  faults and folds may be related to strike-slip movement under broadly northeast–southwest compressive stress (see **Tectonic evolution**).

The limbs of  $F_4$  folds are generally disrupted by northwesterly striking thrust or normal (lag) faults and shear zones that exhibit both down-dip and strike-slip movement. Vertical displacement along the  $D_4$  thrusts and normal faults range from a few hundred metres to at least 3 km (e.g. Clayton Thrust at AMG 070010). The southwestern limbs of the anticlines are associated with high-angle thrusts, and complementary normal (lag) faults occur on their northeastern limbs. On a regional scale the faults intersect at acute angles and, overall, present an anastomosing system. The major  $D_4$  folds and faults are shown on Figure 3, and minor  $D_4$  structures are plotted on Figure 10.

The geometry of  $F_4$  folds in the Talbot Terrane is complicated by their superimposition on pre-existing structures. Minor  $F_4$  folds in the Rudall Complex commonly plunge far more steeply than  $F_4$  folds in the Throssell Group, they are tight to isoclinal, have a more variable plunge in a northwest or southeast direction, and their axial surfaces are more steeply inclined. These characteristics make minor  $F_4$  folds hard to distinguish from  $F_2$  folds in the field, but the distinction between the fold generations can be made where  $F_4$  folds deform  $S_2$  (Figs 7 and 8).

## Paterson Orogeny

### $D_6$ structures

$D_6$  structures consist of northerly to northwesterly striking dextral faults, east-northeasterly striking sinistral faults, strain-slip cleavage ( $S_6$ ), and easterly trending open folds. These structures indicate a maximum compression in a north-northeast to south-southwest direction, which would have resulted in  $D_6$  dextral movement along the  $D_4$  faults. This movement would have formed oblique, transpressional  $F_6$  folds trending easterly. The  $D_6$  stress regime was similar to that during  $D_4$ , making the distinction between the two generations of structures difficult; however, the  $D_6$  structures are far less intense than those formed during earlier episodes of deformation.

## Metamorphism

The metamorphic history of the Paterson Orogen is related to its deformation (Table 3).

Deformation and metamorphism attributed to the Miles Orogeny ( $D_3$ – $D_4$ ) have overprinted earlier

structures, and earlier metamorphic mineral assemblages are incompletely preserved. Even so, there is evidence that the Talbot Terrane of the Rudall Complex underwent low-pressure metamorphism ( $M_1$ ) at amphibolite facies during  $D_1$  (Clarke, 1991), and abundant evidence that the terrane underwent moderate- to high-pressure metamorphism ( $M_2$ ) at amphibolite facies (Smithies and Bagas, 1997). Evidence for  $M_1$  is only rarely preserved in the Yandagooge Formation on BROADHURST (Hickman and Clarke, 1991), or in garnet cores that preserve sigmoidal trains of fine-grained epidote, hornblende, and titanite representing an early  $S_1$  foliation (Bagas and Smithies, 1998).

Greenschist metamorphism ( $M_4$ ), associated with  $D_4$  of the Miles Orogeny, affected both the Rudall Complex and Throssell Group, but it is also possible that some greenschist assemblages in the Rudall Complex represent late  $M_2$  retrogression. The Tarcunyah Group underwent little metamorphic alteration, with burial temperatures unlikely to have risen above 180°C (Bagas, et al., 1995). Any metamorphism of the group is restricted to dynamic effects close to faults.

## Previous work

Chin et al. (1980) recognized two metamorphic events prior to deposition of the Throssell Group. The first event was associated with  $D_1$ , and produced middle- to upper-amphibolite mineral assemblages, with development of sillimanite, staurolite, and kyanite. Chin et al. (1980) imply associated partial melting to produce granitoid magmas. The second event accompanied  $D_2$  and was considered to be lower grade, with prograde garnet, muscovite and biotite (and possibly andalusite), and retrograde sericite, chlorite, tremolite, and epidote. Dynamic effects were said to characterize  $D_2$ , with granulation of  $D_1$  gneissic fabrics, alignment of platy minerals, and development of feldspar augen. Post-Throssell Group metamorphism was low grade, and dominated by dynamic effects associated with  $D_4$  ( $D_3$  of Chin et al., 1980).

Clarke (1991) considered that, on the limited evidence preserved,  $M_1$  was a low-pressure, middle-amphibolite facies event in the Yandagooge Inlier, with development of andalusite and staurolite, and probably accompanied by partial melting. Clarke (1991) stated that  $M_2$  included prograde middle-amphibolite facies assemblages with kyanite, biotite and staurolite, and garnet, biotite and staurolite (both assemblages including muscovite and quartz and, locally, plagioclase). Retrogressive chlorite, sericite, and fibrous sillimanite were considered to be syn- or post- $D_2$ .

Hickman and Clarke (1994) observed that  $M_4$  metamorphism, associated with  $D_4$ , did not exceed greenschist facies on BROADHURST. The principal effects were recrystallization of quartz, particularly in deformation zones, regrowth of calcite and dolomite along  $S_4$ , and sericitic alteration.

## Metamorphism in the Talbot Terrane

Any study of the metamorphic history of the western exposures of the Rudall Complex will be complicated by factors such as structural complexity, polymetamorphism with retrogression of early medium- to high-grade mineral assemblages characteristic of amphibolite facies, and the predominantly quartzofeldspathic composition of the unit.

It is clear that the Talbot Terrane of the Rudall Complex was metamorphosed to the amphibolite facies preceding deposition of the unconformably overlying Throssell Group that was metamorphosed to the lower greenschist facies. However, it is difficult to identify  $M_2$  mineral assemblages because of  $M_2$  recrystallization and  $M_4$  retrogression. Even so,  $M_2$  prograde metamorphic minerals are locally preserved, particularly in schists (Clarke, 1991; Hickman and Bagas, 1998). Metamorphic grades attained by quartzite, psammitic gneiss and most orthogneiss units are generally difficult to establish in the absence of useful index minerals. Quartzite and orthogneiss typically contain only retrogressive mineral assemblages, but exceptions include prograde garnet in orthogneiss and some relict sillimanite in quartzite.

Of approximately 400 samples petrographically examined from the Talbot Terrane only 90 provided useful mineral indicators of pressure-temperature conditions (Fig. 13). Figure 13 shows that most of the Talbot Terrane has been subjected to prograde amphibolite-facies metamorphism, and a post-peak  $M_2$  and syn- $M_4$  retrogressive greenschist-facies metamorphism.

Clarke (1991) found relict andalusite and staurolite, apparently pre-dating  $S_2$ , on BROADHURST, and assigned these to  $M_1$ . Similar features have not been recognized on RUDALL. It is assumed that all, or virtually all, the medium- to high-grade minerals on Figure 13 form parts of  $M_2$  assemblages. Metamorphic mineral assemblages vary according to protolith composition, and are summarized by Hickman and Bagas (1998).

The prograde mineral assemblages in pelitic schist are consistent with amphibolite facies metamorphism (Hickman and Bagas, 1998). The apparent absence of cordierite and andalusite, combined with the common abundance of garnet, indicates medium- to high-pressure conditions (Yardley, 1991, p. 78–82).

Protolith compositional changes from quartz sandstone to feldspathic sandstone, argillaceous sandstone, siltstone, and greywacke have resulted in more diverse metamorphic mineral suites. Most paragneiss consists of quartz and oligoclase (variably altered to sericite), with minor muscovite (commonly sericite), and variable biotite (partly altered to chlorite), chlorite, and epidote (locally enveloping biotite). Chlorite has commonly replaced (post-peak  $M_2$ ) hornblende or actinolite, leaving relics of these medium-grade metamorphic minerals. Garnet (almandine) is common, but staurolite and kyanite are rare, which reflects the

relatively low aluminium contents of most paragneiss protoliths. The mineral assemblages are consistent with prograde amphibolite facies metamorphism and greenschist facies retrogression.

The mineral assemblages of amphibolite units in the Rudall Complex indicate upper greenschist to amphibolite facies metamorphism. The absence of garnet suggests low- to medium-pressure conditions, and the relatively calcic compositions of plagioclase are consistent with amphibolite-facies metamorphism (Yardley, 1991, p. 93). Hornblende is generally green rather than blue-green, which indicates metamorphic grades similar to those applying to the staurolite, kyanite, and sillimanite zones of pelitic rocks (Yardley, 1991, p. 99). At AMG 351959, plagioclase is altered to calcium-rich scapolite, and contains later sericite and epidote, and recrystallized oligoclase contains epidote, clinozoisite, chlorite, and sericite (GSWA sample 106925).

The presence of scapolite in several amphibolite units suggests local high-temperature alteration of plagioclase by acidic solutions (Winkler, 1965, p. 90). Furthermore, it is notable that scapolite appears to be associated with the contacts of intrusive granitoids (now orthogneiss). Examples can be found 1 km to the north of the Rudall River at AMG 278032 (sample 111833) and 3 km to the south of the junction of the Rudall River and Poonemerlarr Creek (AMG 351959; sample 106925).

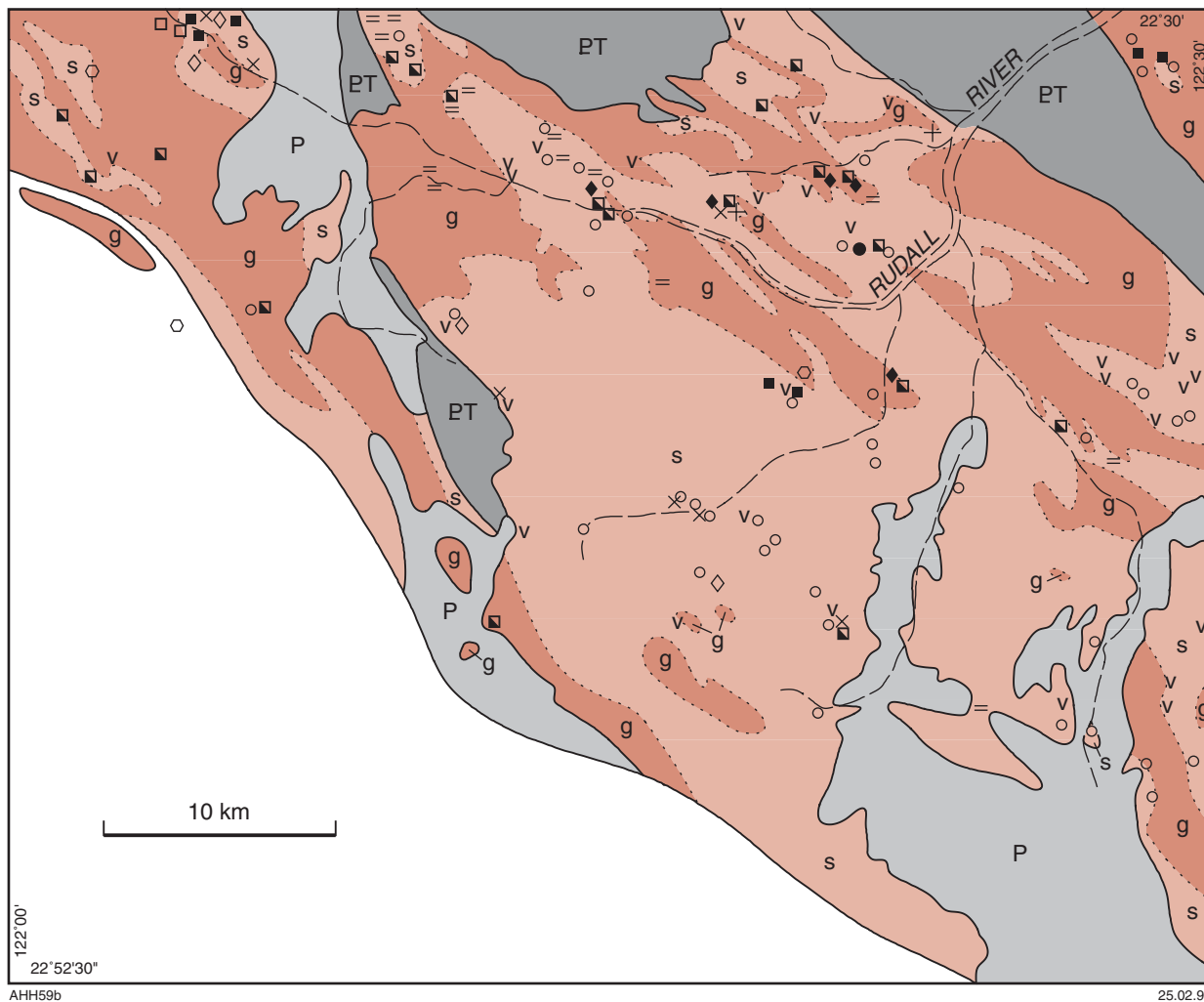
Grunerite is generally present in the iron-rich layers of metamorphosed banded iron-formation. This indicates metamorphism at a grade between the garnet and sillimanite zones of pelitic rocks (amphibolite metamorphic facies: Turner and Verhoogen, 1960, p. 494). Garnet and minor actinolite accompany grunerite in banded iron-formation at AMG 984170, about 5 km north of RUDALL on BROADHURST, and on RUDALL biotite is retrogressed to chlorite and sericite (Sample 106917 at AMG 322955).

Anthophyllite in metamorphosed ultramafic rocks (serpentine to serpentine-tremolite-chlorite(-tal) and actinolite-epidote rocks) is locally present, suggesting amphibolite facies, hornblende-hornfels facies or metasomatic conditions (Yardley, 1991), but the other minerals are characteristic of the greenschist facies.

## Metasomatism

Large proportions of the metamorphosed sedimentary rocks of the Talbot Terrane are in close contact with sheet-like bodies of orthogneiss. In these contact zones dykes and veins of microgranite, pegmatite, and quartz are commonly ubiquitous, demonstrating widespread penetration by magmatic and hydrothermal fluids.

The preserved metasomatic minerals include tourmaline, scapolite, and sulfides. Tourmaline is widespread (Fig. 13), and occurs in veins of quartz and pegmatite, quartzite, quartz-muscovite schist, BIF, and tourmaline-quartz pods near orthogneiss contacts. These tourmaline occurrences indicate introduction of boron during granitoid emplacement.



AHH59b

25.02.99

**AMPHIBOLITE FACIES  
METAMORPHIC MINERALS**

High pressure:

- Kyanite
- ◇ Staurolite

Intermediate pressure (generally):

- Garnet

High temperature:

- Sillimanite
- Cordierite
- ◆ Scapolite

Low-medium temperature and pressure:

- ▣ Green hornblende
- + Anthophyllite
- × Grunerite
- = Actinolite

Retrogressed:

- Sericitized aluminosilicate

Metasomatic:

- v Tourmaline

- P Permian
- PT Throssell Group
- Rudall Complex
  - g orthogneiss
  - s metasedimentary rocks
- ..... Generalized boundary

**Figure 13. Prograde metamorphic minerals of the Rudall Complex on the RUDALL 1:100 000 map**

Scapolite in amphibolite, as noted above, probably indicates penetration by chloride- and sulfate-bearing  $H_2O-CO_2$  fluids. Sulfidation (inferred from limonitic gossans) is a feature of the wallrocks of certain minor felsic intrusions and many quartz veins, but mineralization widths are generally restricted to less than one metre. Potash metasomatism may explain the common occurrence of muscovite-rich schist along orthogneiss–paragneiss contacts, but this possibility has not been tested by geochemistry.

Contacts between ultramafic–mafic bodies and metasedimentary rocks locally exhibit contact metasomatism. For example, at AMG 315043, around 7 km southwest of Talbot Soak, banded paragneiss within 3 m of serpentinite has been converted to calc-silicate gneiss containing 21%  $Al_2O_3$ , 9% CaO, 5%  $Na_2O$ , 1189 ppm Sr, and depleted  $SiO_2$  (sample 112486, Appendix 1). Lime metasomatism of non-calcareous sedimentary rocks in contact with ultramafic bodies may be due to Ca enrichment in residual solutions after crystallization of these bodies, or to Ca liberation during serpentinization (Turner and Verhoogen, 1960, p. 572). Calc-silicate gneiss associated with gabbro–paragneiss contacts outcrops 5 km to the south-southwest of Rudall Crossing (AMG 105020) and 3 km north-northeast of the Tom Tit prospect (AMG 215045). A similar association between calc-silicate gneiss and amphibolite was reported on BROADHURST (Hickman and Clarke, 1994, p. 12). At AMG 215045, north-northeast of the Tom Tit prospect, calc-silicate gneiss (*ERaa*) within psammitic gneiss and schist is interpreted, on petrographic evidence, as altered gabbro. Two samples (112303, 112304, Appendix 1) studied are composed of actinolite, plagioclase, clinozoisite and minor quartz, and include veins of epidote and epidote–carbonate–scapolite. Notable chemical features include high  $Al_2O_3$  (~28%), CaO (~13–15%), Ni (~230 ppm), and low FeO(tot) (~2.5%), MgO (~4%) and V (~25 ppm). Ultramafic rocks are not exposed.

## Metamorphism of the Throssell Group

The Throssell Group has been metamorphosed to the lower Greenschist facies. This metamorphism ( $M_4$ ) is associated with  $D_4$  of the Miles Orogeny, and its effects are most clearly seen in pelite and carbonate rocks of the Broadhurst Formation. The characteristic metamorphic assemblages are sericite, as growth and recrystallization of quartz in siltstone, chlorite growth in carbonate rocks, and calcite and dolomite regrowth along  $S_4$ .

## Summary of metamorphism

Pre-Yeneena Supergroup metamorphism of the Rudall Complex was mainly Barrovian. Pelitic schist, paragneiss and amphibolite units were metamorphosed at amphibolite facies, but present mineral assemblages are generally characteristic of lower grades due to retrograde alteration after the peak of  $M_2$ , and during  $M_4$ .

Local high-temperature, low- to medium-pressure metamorphism and metasomatism are contact metamorphic effects that are associated with the intrusion of granitoids and, to a much lesser degree, the mafic bodies.

A more detailed study would be required to distinguish  $M_1$  and  $M_2$  assemblages, but available evidence suggests that  $M_1$  assemblages are rarely preserved (Smithies and Bagas, 1997).

The Throssell Group was metamorphosed to the greenschist facies during the Miles Orogeny ( $D_3$ – $D_4$ ), but the Tarcunyah (late- to post- $D_4$ ) was regionally metamorphosed below the greenschist facies.

## Geochronology

Table 4 summarizes the geochronological results, sources of data, and cited interpretations obtained from the Paterson Orogen.

The Rudall Complex includes orthogneiss interpreted, by field observations, to represent two main pre- $D_2$  granitoid suites (*ERgx* and *ERga*). Both have recently been dated using zircon ion-microprobe U–Pb isotopic data (Nelson, 1995), and the younger orthogneiss (*ERga*) was also dated using the Rb–Sr method, by Chin and de Laeter (1981).

The mixed-zircon population ages of 2715–2577 Ma and  $2015 \pm 26$  Ma, and the single-zircon population age of  $1787 \pm 12$  Ma (Nelson, 1995) were obtained from the banded orthogneiss complex (*ERgx*). The sample giving the oldest date is a garnet–biotite–muscovite gneiss from drillcore. This gneiss may have been derived from, or may include material from, a sedimentary protolith. The  $2015 \pm 26$  Ma age may date a granitoid component, but uncertainty as to the precise nature of the sample requires follow-up investigations. The  $1787 \pm 12$  Ma result was obtained on drillcore of orthogneiss (probably *ERga* intruding the *ERgx* orthogneiss complex). Numerous K-feldspar augen orthogneiss (*ERga*) samples have been dated at between 1790 and 1765 Ma (Table 4). This suggests that the granitoid protoliths for this suite were intruded at slightly different times in different parts of the Rudall Complex. Biotite granodiorite orthogneiss (*ERgd*), which intrudes quartzite correlated with the Larry Formation south of the Rudall River, has been dated at  $1778 \pm 17$  Ma. The monzogranite protolith of an orthogneiss, that intruded the Larry Formation south of Graphite Valley, has been dated at  $1801 \pm 4$  Ma. The zircon data and field relations between orthogneiss and paragneiss (this Report) indicate that protoliths of much of the paragneiss were deposited before about 1780 Ma. The orthogneiss with  $2015 \pm 26$  Ma zircons contains abundant paragneiss enclaves and zircon xenocrysts dated between 2715 and 2577 Ma (Nelson, 1995). In the east Pilbara, 2750–2680 Ma rocks occur in the Gregory Range. From evidence presented in the section on **Tectonic evolution** it is probable that the eastern part of the Pilbara Craton was the main source region for sedimentary rocks

Table 4. Geochronological results for the Paterson Orogen

Age (Ma)	Rock suite	Dating method	Reference	Interpretation in reference <sup>(a)</sup>
2715–2577	orthogneiss ( <i>ERgx</i> ) <sup>(b)</sup>	Ion microprobe U–Pb	Nelson (1995)	crystallization age of xenocrystic zircons
2425 ± 7	orthogneiss ( <i>ERga</i> ) <sup>(b)</sup>	Ion microprobe U–Pb	Nelson (1995)	crystallization age of xenocrystic zircons
2015 ± 26	orthogneiss ( <i>ERgx</i> ) <sup>(b)</sup>	Ion microprobe U–Pb	Nelson (1995)	age of granitoid crystallization
1972 ± 4	orthogneiss ( <i>ERgg</i> ) <sup>(b)</sup> (sample 112310)	Ion microprobe U–Pb	Nelson (1995)	age of crystallization of early granitoid component of rock
1802 ± 14	orthogneiss ( <i>ERgg</i> ) <sup>(b)</sup> (sample 112310)	Ion microprobe U–Pb	Nelson (1995)	age of crystallization of late granitoid veins
1801 ± 4	orthogneiss ( <i>ERge</i> ) <sup>(b)</sup>	Ion microprobe U–Pb	Nelson (1995)	age of granitoid crystallization
1795 ± 17	orthogneiss ( <i>ERge</i> ) <sup>(b)</sup>	Ion microprobe U–Pb	Nelson (1995)	age of granitoid crystallization
1790 ± 17	orthogneiss ( <i>ERga</i> ) <sup>(b)</sup>	Ion microprobe U–Pb	Nelson (1995)	age of granitoid crystallization
1787 ± 5	orthogneiss ( <i>ERga</i> ) <sup>(b)</sup>	Ion microprobe U–Pb	Nelson (1995)	age of granitoid crystallization
1787 ± 12	orthogneiss (? <i>ERga</i> in <i>ERgx</i> ) <sup>(b)</sup>	Ion microprobe U–Pb	Nelson (1995)	age of granitoid crystallization
1778 ± 17	orthogneiss ( <i>ERgd</i> ) <sup>(b)</sup>	Ion microprobe U–Pb	Nelson (1995)	age of granitoid crystallization
1775 ± 10	orthogneiss ( <i>ERga</i> ) <sup>(b)</sup>	Ion microprobe U–Pb	Nelson (1995)	age of granitoid crystallization
1778 ± 16	aplite dyke <sup>(b)</sup>	Ion microprobe U–Pb	Nelson (1995)	age of aplite crystallization
1765±15	orthogneiss ( <i>ERga</i> ) <sup>(b)</sup>	Ion microprobe U–Pb	Nelson (1995)	age of granitoid crystallization
1533 ± 29	randomly selected samples from the Rudall River headwaters	Rb–Sr	Chin and de Laeter (1981)	uncertain
1333 ± 44	orthogneiss, CONNAUGHTON	Rb–Sr	Chin and de Laeter (1981)	age of D <sub>2</sub> ; maximum age of Yeneena Supergroup
1291 ± 10	pegmatite, CONNAUGHTON	Ion microprobe U–Pb	Nelson (1995)	crystallization age of pegmatite; pre- or syn-D <sub>2</sub> ; maximum age of Yeneena Supergroup
1132 ± 21	pegmatite veins intruding Rudall Complex <sup>(b)</sup>	Rb–Sr	Chin and de Laeter (1981)	possibly related to D <sub>4</sub> ; minimum age of Yeneena Supergroup post-dates D <sub>4</sub> ;
1080	Runtou Adamellite, TABLETOP	Two-point Rb–Sr	Chin and de Laeter (1981)	post-dates Yeneena Supergroup
1067 ± 260	Runtou Adamellite, TABLETOP	Pb–Pb	G. L. Clarke and N. McNaughton (unpubl. data)	post-dates D <sub>4</sub> ; post-dates Yeneena Supergroup
940	Warrabarty prospect, BRAESIDE	Pb–Pb	I Fletcher (pers. comm., 1993)	age of epigenetic galena in Broadhurst Formation age of epigenetic galena in
900	Nifty deposit, LAMIL	Pb–Pb	I. Fletcher (quoted in Blockley and Myers, 1990)	Broadhurst Formation
692 ± 6	mafic intrusion, BROADHURST	K–Ar	CRAE P/L data	age of crystallization
690 ± 48	Mount Crofton Granite, PATERSON RANGE	Pb–Pb	Goellnicht et al. (1991)	post-dates D <sub>4</sub>
633 ± 13	Minyari monzogranite, PATERSON RANGE	Ion microprobe U–Pb	Nelson (1995)	age of granitoid crystallization
c. 620	Mount Crofton Granite, PATERSON RANGE	Ion microprobe U–Pb	Nelson (1995)	age of granitoid crystallization
601 ± 42	Mount Crofton Granite, PATERSON RANGE	Rb–Sr	Williams (1992; data from Trendall, 1974)	post-dates D <sub>4</sub>
595 ± 27	orthogneiss ( <i>ERga</i> ) <sup>(b)</sup>	Rb–Sr	Chin and de Laeter (1981)	alteration event post-dating D <sub>4</sub>

NOTES: (a) Not necessarily accepted in this report  
(b) on RUDALL

of the Rudall Complex, but xenocrystic zircons of 2425–2000 Ma (Nelson, 1995) in the orthogneiss testify to additional unknown sources.

The age of  $D_2$ , and therefore  $M_2$ , is well constrained by isotopic data from an aplite dyke (GSWA sample 112341) east of Rudall airstrip. This dyke cuts a pyroxenite unit foliated by  $S_2$ , but does not itself contain  $S_2$ . The scatter of results (1870–1612 Ma) on individual zircon grains could be due to the contamination of the aplite, from the augen orthogneiss (*ERga*), and it is notable that seven grains have model ages of 1765–1703 Ma. A possible interpretation is that the aplite was intruded between 1765 and 1700 Ma. On this basis  $D_2$  is considered to be c. 1760 Ma.

Chin and de Laeter (1981) presented a Rb–Sr isochron at  $1333 \pm 44$  Ma for an orthogneiss (*ERgo*) from southwestern CONNAUGHTON (their 48929 series). They interpreted this date as the age of the pervasive metamorphism and deformation in the Rudall Complex ( $D_2$ ). It was also considered to represent the oldest possible age for the Yeneena Supergroup. The sampling site for the 1333 Ma orthogneiss is 60 km south-east of the Rudall River in an area where banded orthogneiss appears to have been intruded by a K-feldspar-rich and biotite-poor granitoid that contains amphibolite (metadolerite and metagabbro) xenoliths (Bagas and Smithies, 1998). The later granitoid is now a poorly foliated orthogneiss, and though affected by  $D_4$ , may be post- $D_2$ . The Throssell Group, about 700 m to the south, unconformably overlies these rocks. If the  $1333 \pm 44$  Ma result was obtained on the poorly foliated orthogneiss, this could provide an age for a felsic magmatic event after  $D_2$  (see **Tectonic evolution**).

A locally tectonized pegmatite on northwestern CONNAUGHTON, interpreted as post- $D_2$ , has a U–Pb zircon crystallization age of  $1291 \pm 10$  Ma confirming that  $D_2$  occurred prior to 1291 Ma. The relationship between this pegmatite and the Throssell Group has not been determined, but the total absence of any felsic igneous rocks in the Throssell Group suggests that the group may be younger than 1290 Ma.

Chin and de Laeter (1981) reported a Rb–Sr isochron age of  $1132 \pm 21$  Ma from pegmatite dykes cutting orthogneiss in the Rooney Creek area and interpreted this as the minimum age for the Throssell Group. No pegmatite veins have been found in the Throssell Group, despite being extremely common in the immediately underlying Rudall Complex. If the 1132 Ma result dates pegmatite intrusion, this age represents a maximum age for the Throssell Group. If it is a metamorphic age, this metamorphism could be either pre- or post-Throssell Group. Accordingly, the result has limited significance without determination of the crystallization age of this pegmatite suite.

On the southeastern margin of the Pilbara Craton metamorphic biotite that pre-dates the Tarcunyah Group has provided Rb–Sr ages of 1226 Ma and 1194 Ma (de Laeter et al., 1977). Subject to the isotopic composition of the biotite not having been reset by later

metamorphism, these results provide a maximum age for the Tarcunyah Group and establish a significant metamorphic event in the eastern part of the Pilbara Craton at about 1200 Ma.

The Runton Adamellite, from RUNTON, gave a poorly constrained two-point Rb–Sr isochron age of 1080 Ma (Chin and de Laeter, 1981) and a Pb–Pb age of  $1067 \pm 260$  Ma (Clarke, G. L., and McNaughton, N., 1993, pers. comm.). This monzogranite is non-foliated to weakly foliated. It may post-date  $D_4$  in the south-eastern part of the Paterson Orogen or it may be situated in a  $D_4$  low-strain zone. There are no contact relationships between the monzogranite and the Yeneena Supergroup, thus preventing any reliable interpretation of these isotopic data in relation to the age of the Yeneena Supergroup.

Galena sampled from the Broadhurst Formation has provided Pb model ages between 940 and 520 Ma (Blockley and Myers, 1990; Fletcher, I., 1993, pers. comm.; Hickman and Clarke, 1994). The regional distribution of the galena isotopic data appears to establish that the minimum age of the Broadhurst Formation is 900 Ma.

Preliminary geochronological and biostratigraphic data suggests that the Savory Sub-basin, which unconformably overlies the Tarcunyah Group in the south-western portion of RUDALL, evolved sometime between 900 and 600 Ma (Williams, 1992).

Several non-foliated to partly foliated granitoid intrusions, later than and sharply discordant to  $D_4$  structures, intrude the upper part of the Lamil Group near Telfer. One of the non-foliated granitoids, the Mount Crofton Granite, gave a Rb–Sr age of about  $601 \pm 42$  Ma (Williams, 1992 — recalculation of data in Trendall, 1974), Pb–Pb ages of  $690 \pm 48$  Ma (McNaughton and Goellnicht, 1990; Goellnicht et al., 1991), and a zircon U–Pb age of c. 620 Ma (Nelson, 1995). This demonstrates that  $D_4$  is older than 620 Ma in the northern part of the Paterson Orogen.

From the geochronological results reported here, and the geological knowledge of the Paterson Orogen, the chronological sequence of events is summarized in Table 5.

## Tectonic evolution

Understanding the tectonic evolution of a geological terrane such as the Paterson Orogen not only serves to explain the relationships between its components, but is essential to permit an informed evaluation of its mineral potential.

Completion of the mapping of RUDALL in 1992 provided sufficient evidence to warrant a new interpretation of the geological history of the orogen, and this has been presented by Hickman et al. (1994) and Hickman and Bagas (1995). Accordingly, only a brief outline of the tectonic evolution of the area need be given here.

**Table 5. Geochronological data relevant to the evolution of the Paterson Orogen**

<i>Isotopic age (Ma)</i>	<i>Geological event</i>
2015 ± 26	crystallization of some <i>ERgx</i> granitoid protoliths
pre-1800	deposition of Larry Formation
c. 1800	crystallization of some granitoid protoliths ( <i>ERge</i> and <i>ERgg</i> )
1790–1765	crystallization of granitoid protoliths of <i>ERga</i> and <i>ERgd</i>
pre-1780	deposition of Rudall Complex sedimentary protoliths
1765–1700	metamorphism, M <sub>2</sub> , accompanying D <sub>2</sub>
1333 ± 44	metamorphism of an orthogneiss ( <i>ERgo</i> ), CONNAUGHTON
1291 ± 10	crystallization of a pegmatite dyke, CONNAUGHTON
c. 1300	deposition of Manganese Subgroup of the Bangemall Group, unconformably underlying the Tarcunyah Group
c. 1200	metamorphic biotite in rocks of the Gregory Granitic Complex, unconformably underlying the Tarcunyah Group
1132 ± 21	crystallization or metamorphism of pegmatite dykes
1080	crystallization or metamorphism, Runton Adamellite
940–820	galena mineralization in Throssell Group
800–600	evolution of the Savory Sub-basin
c. 620	minimum age for emplacement of post-D <sub>4</sub> granitoids

## Rudall Complex

Mapping of the Talbot Terrane in the Rudall Complex has revealed geological features that show the Rudall Complex to be the product of continental collision (Hickman and Clarke, 1994; Bagas and Smithies, 1998; Hickman and Bagas, 1998). Given the geological constraints so far determined, the appropriate evolutionary model is provided by the Himalayas (Smithies and Bagas, 1997). Windley (1984) and Park (1988) provide good reviews of this type of orogenic belt.

In examining the stage-by-stage evolution of the Talbot Terrane, it is necessary to consider and attempt to explain the principal geological features, which are listed below:

- The Talbot Terrane occupies a broad imbricate zone of stacked northeast- and east-dipping thrust sheets. Individual thrusts are commonly convex towards the southwest, and cross-cutting relationships indicate progressively younger thrusts towards the northeast. Some of the thrusts are major faults separating distinct tectono-stratigraphic domains.
- The deformed rocks within the sheets are principally metamorphosed siliciclastic sedimentary rocks and granitoids; volcanic rocks are rare.
- At least three episodes of felsic magmatism are present, the oldest of which involved granitoid intrusion into part of the sedimentary succession.
- No basal unconformity to the sedimentary succession has been recognized, and no thrust slices of basement have been identified for the Talbot Terrane.
- The sedimentary succession is indicative of a siliciclastic shelf along a continental margin. Facies

and thickness changes suggest basin elongation north-south or northwest-southeast, with relatively deep-water mud and turbidite thickening eastwards.

- Sandstone with a high feldspar content indicates erosion of felsic volcanic or granitic rock, possibly from an adjacent penecontemporaneous volcanic arc.
- Long, narrow belts of sheared flysch-like sedimentary rocks; serpentized peridotite and lenses of amphibolite may represent allochthonous slices of an ophiolite succession.
- Most parts of the Talbot Terrane now exposed were metamorphosed to amphibolite facies, indicating that the present erosional surface reveals middle levels (15–20 km) of the Proterozoic crust. Deeper levels of at least 40 km have been recognized in the Connaughton Terrane to the east (Smithies and Bagas, 1997).

## Regional setting

To the west of the Paterson Orogen the Capricorn Orogen contains 2000–1600 Ma metasedimentary rocks lithologically similar to those of the Rudall Complex. The tectonic interpretations of the Capricorn Orogen by Thorne and Seymour (1991) and Tyler (1991) invoke a convergent plate-tectonic model involving B-subduction between the Pilbara and Yilgarn Cratons. Tyler (1991, p. 80–83) makes a case for oblique collision of these geologically different Archaean cratons at about 2000–1600 Ma. In the Gascoyne Complex this collision was accompanied by extensive intrusion of granitoids at 1800–1500 Ma (Muhling, 1988). Sedimentary rocks in the northern part of the Capricorn Orogen were deposited on the southern margin of the Pilbara Craton



in a foreland basin – active margin environment. Along the southern margin of the Capricorn Orogen, deposits of the former Glengarry Basin (now subdivided into the Yerrida, Bryah, and Padbury Basins by Pirajno et al., 1996) were derived from erosion of the Yilgarn Craton, probably in sag, rift, and foreland basin environments (Pirajno et al., 1996).

Although the limited geochronological data point to broadly contemporaneous evolution of the Rudall Complex and the Capricorn Orogen, there are clearly important geological differences between these tectonic units:

- Lack of imbricate interleaving of metasedimentary rocks and granitoids over the greater part of the Capricorn Orogen.
- Higher metamorphic grade of the Rudall Complex compared with that of most of the Capricorn Orogen (excluding the Gascoyne Complex).
- The east–west to northeast–southwest trend of the Capricorn Orogen compared to the northwest–southeast trend of the Rudall Complex (and corresponding difference in directions of thrusting).

Accordingly, the relevance to the Rudall Complex of information derived from the Capricorn Orogen mainly relates to the identification of the tectonic processes that were operating in northwestern Australia at about 2000–1600 Ma (Bagas and Smithies, 1997).

## Evidence from the Talbot Terrane

The first recognizable stage in the evolution of the Talbot Terrane involved the deposition of a c. 5000 m-thick siliciclastic succession, Larry Formation – Butler Creek Formation, probably prior to 1780 Ma. The succession indicates shoreline–shelf–slope environments in a subsiding foreland basin on the eastern margin of a continent. The felsic source region for parts of the Yandagoo Formation could have been either a volcanic arc or a fold-thrust belt lying to the northeast of the Talbot Terrane.

A pre-1765 Ma age for the Poynton Formation is inferred from the observations that it contains  $S_2$ , and that it was intruded by protoliths of the K-feldspar augen orthogneiss in the Poynton Domain (*PRga*, GSWA sample 112379; see **Geochronology**). The lowest part of the Poynton Formation consists of well-sorted quartz sands and minor pebble beds, a shallow-shelf facies quite distinct from the underlying turbidite units of the Butler Creek Formation. No angular unconformity has been observed, but a disconformity could be present.

The granitoids in the Rudall Complex are all assumed to bear an intrusive relationship to the sedimentary succession, and most are probably genetically related to the orogenic belt. The Rudall Complex exhibits features expected of a plate-tectonic regime and, in the absence of adequate geochemical data, its granitoids could currently be interpreted in terms of either magmatic arc or fold thrust belt environments (Smithies and Bagas,

1997). This is similar to other Proterozoic orogenic belts of Western Australia, but appears to differ from intracontinental environments of central Australia (Wyborn, 1988; Foden et al., 1988).

The layered orthogneiss (*BRgx*) in the Talbot Terrane contains both  $S_1$  and  $S_2$  foliation, but only  $S_2$  has been recognized in the K-feldspar orthogneiss (*PRga*). Providing this is not merely a consequence of the general homogeneity of the latter (making  $S_1$ – $S_2$  distinction difficult) the inference must be that the  $D_1$  event (sub-horizontal thrusting) occurred prior to crystallization of the K-feldspar orthogneiss protoliths (mainly biotite monzogranite and biotite granite). Thus,  $D_1$  could have led to partial melting, and the intrusion of sheets of the K-feldspar granitoids into the layered orthogneiss and the metasedimentary succession.

The stratigraphic succession of the Talbot Terrane contains no mafic volcanic rocks, but sheared serpentinitized ultramafic bodies (peridotite), associated with pelitic schist and turbiditic metasedimentary rocks, occurs in three west-northwesterly trending zones (Fig. 3). The best developed of these zones extends 50 km from southeast of Rudall Crossing to northeast of May Creek and coincides with a major tectonic break along the southwestern boundary of the Poynton Domain. Scattered mafic amphibolite lenses represent metamorphosed dolerite and gabbro. Lithologically, the assemblage is similar to compressed and attenuated ophiolitic units in many of the world's orogenic belts, for example the Himalayas (Windley, 1984). From a detailed study of the ultramafic units, Carr (1989) concluded that they represent slices of Proterozoic oceanic crust. On structural evidence the sedimentary rocks of the Rudall ultramafic zones originated northeast of the Talbot Terrane, and the assemblage is one which could have formed in a marginal basin environment.

The deformation and metamorphism assigned to  $D_2$ – $M_2$  indicate a major collision, based on isotopic data, culminating between 1760 and 1500 Ma (see **Geochronology**). An advancing plate (no remnants of this have yet been identified, but may be concealed beneath the Canning Basin) produced overfolding and thrusting from the northeast and east (Smithies and Bagas, 1997; see **Structure**). The extent of deformation suggests a continent–continent collision (Bagas and Smithies, 1997).

There are substantial isotopic data for an important event of metamorphism and felsic magmatism at 1250–1100 Ma, but there is currently no conclusive evidence that this preceded deposition of the Yeneena Supergroup. As mentioned above (see **Geochronology**), felsic intrusions have been dated at  $1247 \pm 5$  Ma (crystallization age),  $1132 \pm 21$  Ma (?metamorphic age), and c. 1080 Ma. On the southeastern margin of the Pilbara Craton sheared Archaean granitoids at Lookout Rocks provided Rb–Sr biotite ages of 1226 Ma and 1194 Ma (de Laeter et al., 1977). This biotite forms part of a metamorphic foliation in rocks that are unconformably overlain by strata now assigned to the Tarcunyah Group (de Laeter et al., 1977), which shows

that the Tarcunyah Group is younger than 1194 Ma. The age relationship of this foliation with the Yeneena Supergroup is, however, unknown. Clarke (1991) referred to the c. 1250 Ma episode as the 'Watrara Orogeny', but correlated it with  $D_2$ . This is no longer accepted because  $S_2$  (foliation produced by  $D_2$ ) is cut by aplite (GSWA sample 112341) that is dated at  $1778 \pm 16$  Ma (Nelson, 1995).

The total absence of felsic intrusions in the Throssell Group suggests that the c. 1250 Ma event occurred before deposition of the Yeneena Supergroup, but further geochronology is required to resolve this issue, particularly on post- $D_2$  pegmatite bodies underlying the Rudall Complex–Yeneena Supergroup unconformity.

## Throssell and Tarcunyah Groups

Despite important differences such as lower metamorphic grade and less structural complexity, the Yeneena Supergroup does have two features in common with the Rudall Complex:

- The overall lithological succession is that of a continental margin. For the Yeneena Supergroup the interpretation that a continental landmass lay to the southwest is supported by abundant palaeocurrent data, and by lateral facies changes.
- Deformation ( $D_4$ ) included northeast–southwest compression, upright folding, and thrusting from the northeast, and total crustal shortening of many kilometres.

These similarities suggest that the evolution of the Yeneena Basin (Fig. 1) might represent later stages in a long-lived and interrupted northeast–southwest convergence. The interpretation developed by Hickman et al. (1994) is that plate convergence was significantly retarded after the major collision of  $D_2$  (in much the same way as collision reduced convergence of the Indian and Eurasian plates during evolution of the Himalayan orogenic belt — Windley, 1984). Plate collision impeded further subduction with the result that strike-slip faulting mainly accommodated later crustal shortening. The Yeneena Basin developed as a strike-slip basin or, more probably, as a series of such basins.

## Regional setting

There is no evidence concerning the northern or eastern margins of the Yeneena Basin. The observation that the basal succession of the group on southern CONNAUGHTON (Bagas and Smithies, 1998) is very similar to that in the northeastern part of BALFOUR DOWNS (Williams, 1989) suggests that a northwesterly trending continental margin lay to the southwest of the Talbot Terrane, and to the west of the Telfer–Nifty region. Palaeocurrent data from the Throssell Group (Coolbro Sandstone), and Tarcunyah Group (Gunanya Sandstone, and Choorun Formation) support transport of clastic material from the southwest (Fig. 14).

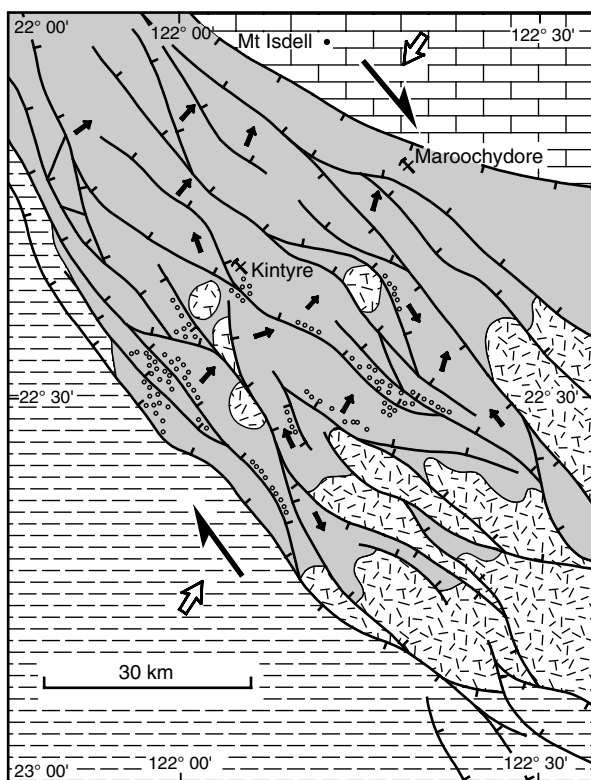
The extent and orientation of the Paterson Orogen demonstrate continental-scale convergence varying from northeast–southwest in the east Pilbara to north–south in central Australia. In view of the fact that orogenic belts are typically oriented parallel to the sedimentary basins that they deform, it is probable that the Yeneena Basin was elongate northwest–southeast.

## Evidence from the Throssell and Tarcunyah Groups

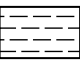
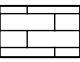

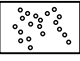

On sedimentological grounds, the sandstone–shale–carbonate succession of the Yeneena Supergroup could be either a continental-margin succession or part of an intra-continental basin. From the evidence already discussed it is clear that the source of clastic detritus lay to the southwest and west, and that the overall deepening of the basin was to the northeast. The succession commences with basal conglomerate in most areas, and this commonly fills channels cut into the underlying basement. Basal conglomerate is everywhere thin (generally <10 m), and conglomerate is absent from the overlying fluviodeltaic clastic rocks of the Coolbro Sandstone. Thus, deposition in the Yeneena Basin in the study area commenced in a continental environment of stream channels and alluvial fans, and progressed, probably due to subsidence, to a deltaic–shallow shelf environment. Stratigraphic and structural features described by Hickman et al. (1994) and Hickman and Bagas (1995) support a northwesterly striking strike-slip basin system produced by syn-depositional northeast–southwest compression (Fig. 14).

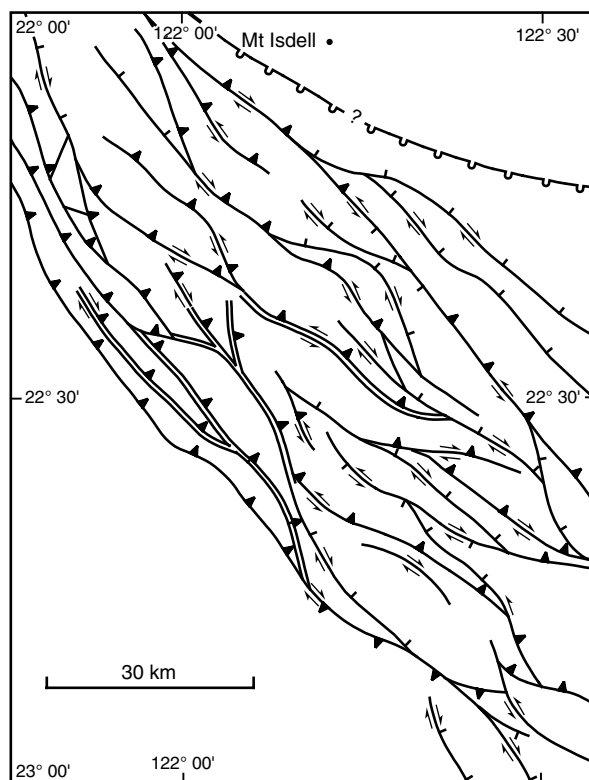
The northwest-trending  $D_4$  faults of the Miles Orogen exhibit both strike-slip and down-dip movement. The faults are curved and anastomosing, and break the area into lenticular, northwest-elongate blocks. This type of pattern is characteristic of strike-slip regimes elsewhere (Mitchell and Reading, 1986). In the Broadhurst Range–Rudall River area the curvatures and convergent relationships of the Southwest Thrust and the Mount Isdell magnetic lineament (Hickman and Clarke, 1994) would be consistent with strike-slip faults towards the northwestern end of a strike-slip basin (dextral movement). Such a basin would be deepest in the north and northeast (i.e. along the northern side of the Broadhurst Range). If the Mount Isdell fault was subaqueous (given the regional northeasterly slope off the Pilbara Craton), clastic sediment would be derived from the southwest. However, the supply of terrigenous material would be limited in southern RUDALL where the basin was shallower and the southwestern faulted margin curved eastwards (Fig. 14), preventing or limiting downthrow to the northeast.

Deformation of the Throssell Group occurred mainly during  $D_3$  and  $D_4$ .  $D_3$  was a phase of recumbent folding whereas  $D_4$  produced northwest- and southeast-plunging, tight to isoclinal, overturned folds with axial planes dipping steeply northeast. Most  $F_4$  fold limbs are sheared and partly replaced by high-angle faults (thrusts and lag faults). Where fault planes are exposed they generally show more than one linear fabric, testifying to reactivation, mostly during  $D_6$ .  $D_4$  movement appears to have



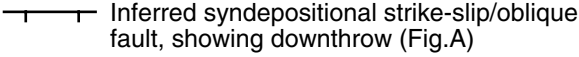

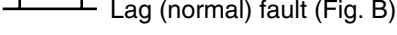
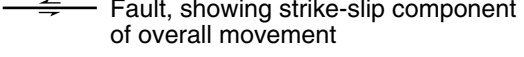
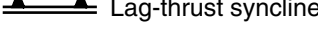



A. Coolbro Sandstone stage

-  Tarcunyah shelf (little or no deposition during this stage)
-  Isdell ?platform
-  Throssell Basin
-  Throssell Basin conglomerate (in Coolbro Sandstone, currently exposed)
-  Rudall Complex



B. D<sub>4</sub> fault system (reactivated strike-slip faults)

-  Generalized palaeocurrent direction
-  Inferred maximum compression
-  Inferred syndepositional strike-slip/oblique fault, showing downthrow (Fig.A)
-  Thrust fault
-  Lag (normal) fault (Fig. B)
-  Fault, showing strike-slip component of overall movement
-  Lag-thrust syncline
-  Inferred unconformity

AHH46b

22.04.99

Figure 14. Strike-slip faulting and deposition during the early stages of Yeneena Basin development, RUDALL–BROADHURST area

been down-dip, with lineations generally plunging between 50° north-northeast and 50° east. The folds themselves are arranged en echelon, and are now considered to be transpressional in origin. Such folds could be produced within a northwest-trending strike-slip fault system, under either dextral or sinistral movement. In either situation, the maximum compressive stress would have been close to northeast-southwest (~30°). Thus, the direction of crustal shortening during D<sub>4</sub> was similar to that during D<sub>2</sub>.

Only the Gunanya Sandstone and the Waters Formation represent the Tarcunyah Group on RUDALL. These are shallow-shelf sedimentary units, probably unconformably overlying the Throssell Group (Bagas et al., 1995).

### Late granitoids

The Mount Crofton Granite suite on PATERSON post-dates D<sub>4</sub> structures (Chin et al., 1982) and has been dated at c. 620 Ma (zircon U–Pb; Nelson D., 1993, pers. comm.). The suite is described by Goellnicht et al. (1991) who conclude that the granitoids are syn- to post-collisional. No representatives of this granitoid suite have been identified in the study area.

### Metallogenic implications

Interpretations of depositional and tectonic settings are used in assessing mineral potential, because particular types of mineral deposit are associated with specific

geological environments. Table 6 summarizes phases in the Proterozoic evolution of the Talbot Terrane, and suggests types of mineralization, which might be present. The following section describes known mineralization and past exploration, and comments on mineral potential.

## Mineral resources

The Paterson Orogen remained largely unexplored until the early 1970s because of remoteness, difficult terrain, and a lack of permanent water. The mineral potential of the Paterson Orogen became apparent with the discovery of the Telfer gold deposit on PATERSON in 1971 and the Kintyre uranium deposit on BROADHURST in 1985.

During the last twenty years of exploration, numerous subeconomic and rare economic stratabound mineral deposits and fault-controlled vein-type deposits, including gold, base metals, uranium and platinum-group elements (PGE), have been found throughout the Paterson Orogen. Many of the deposits in the Rudall Complex occur in carbonaceous or sulfidic schist, are hydrothermal in origin, formed late in the history of the complex, and are supergene-enriched to varying degrees.

As exploration is at an early stage, and mining companies are still investigating most mineral occurrences on RUDALL, no information on recent discoveries of mineralization has been published. Hickman and Bagas (1998) have described the exploration history of the area in detail.

## Geochemical investigation

During mapping of RUDALL, 395 samples were collected and analysed for trace elements, and 31 of the rock samples were analysed for major elements (Appendix 1). The analytical data were processed by selecting appropriate anomaly criteria, which are outlined on Figure 15. Application of these criteria defined 144 samples as 'geochemically anomalous'. Certain elements (Ag, As, Cd, Co, Ga, Ge, Nb, Sb, Sc, Sn, Ta, U) did not reach 'anomaly concentrations' in any of the 395 samples, although some elevated contents (e.g. Ag, Sn, and U between 10 and 50 ppm) are worth noting. The locations of anomalous samples are shown in Figures 15 and 16, and Figure 17 shows the main zones of known and interpreted mineral potential on RUDALL.

Two important features were revealed by the study:

1. Anomalous results for particular elements tend to cluster in specific areas or zones; and
2. Most anomalies are accompanied by recurring inter-element correlations that are consistent with particular types of mineralization.

The results and conclusions of the geochemical study are integrated with descriptions of mineralization identified by mineral exploration.

## Gold

The geochemical investigation, which accompanied the GSWA mapping, revealed four areas that contain gold anomalies (Figs 15 and 16). Two of these areas contain clusters of anomalous samples at Poynton Creek and Dunn Creek, both localities being situated close to the southwestern boundary of the Poynton Domain.

At Poynton Creek the gold occurs in gossanous quartz veins related to northwest-striking  $D_4$  faults, and ranges up to 4.07 ppm. However, results of a follow-up sampling program indicate that gold mineralization is erratic. Host rocks of the auriferous veins at Poynton Creek are mainly quartzite and banded paragneiss.

The Dunn Creek anomalies average about 0.1 ppm gold and occur mostly in pyritic quartz veins of  $D_2$  or  $D_4$  age. An exception is a unit of calc-silicate gneiss (samples 112303A, 112304A) in which 0.08–0.12 ppm gold and copper anomalies occur in metasomatized gabbro. The gneiss is situated in the core of the Dunn Antiform, and merits further investigation.

About 3 km northeast from Fandango (AMG 155954) an isolated gold anomaly (sample 112366) was detected in quartz veins in pelitic schist and BIF of the Yandagoo Formation. Tourmaline in the schist and BIF indicates locally extensive boron metasomatism. The locality is situated on a north-northwesterly striking  $D_4$  or  $D_6$  fault.

About 3 km east from Talbot Soak (AMG 408071) a semipelitic member of the Coolbro Sandstone includes quartzite (sample 111817) and metasiltstone (sample 111816). Both samples exhibit a strong yellow-brown discolouration due to alteration of disseminated pyrite, and contain gold (1.10 and 0.53 ppm respectively). A transported lateritic pseudogossan (samples 111818, 9) located 600 m to the northwest contains minor silver (8–17 ppm). The semipelitic unit is poorly exposed, but forms a valley between thick sandstone members of the formation. The unit has a distinctive aeromagnetic signature, which can be traced at least 30 km along strike. Samples of vein quartz and gossan (samples 111803–5, 9, 10) collected up to 7 km along strike contain anomalous gold associated with elevated Ba, but the most prospective units are pyritic sedimentary rocks.

## Uranium (and associated gold, copper, lead, and zinc)

Subeconomic traces of uraninite and coffinite have been located at the Bilbo (AMG 291898), Cassandra (around AMG 323853), Dione (around AMG 258905), and Minder (AMG 322806) prospects. The Cassandra and Minder deposits occur in  $D_4$  structures, and are related to late- or post- $D_4$  hydrothermal alteration.

The Bilbo and Dione mineralization is restricted to flat-lying regolith zones which are interpreted as secondary dispersions derived from primary shear-zone related mineralization. These zones contain uraninite in

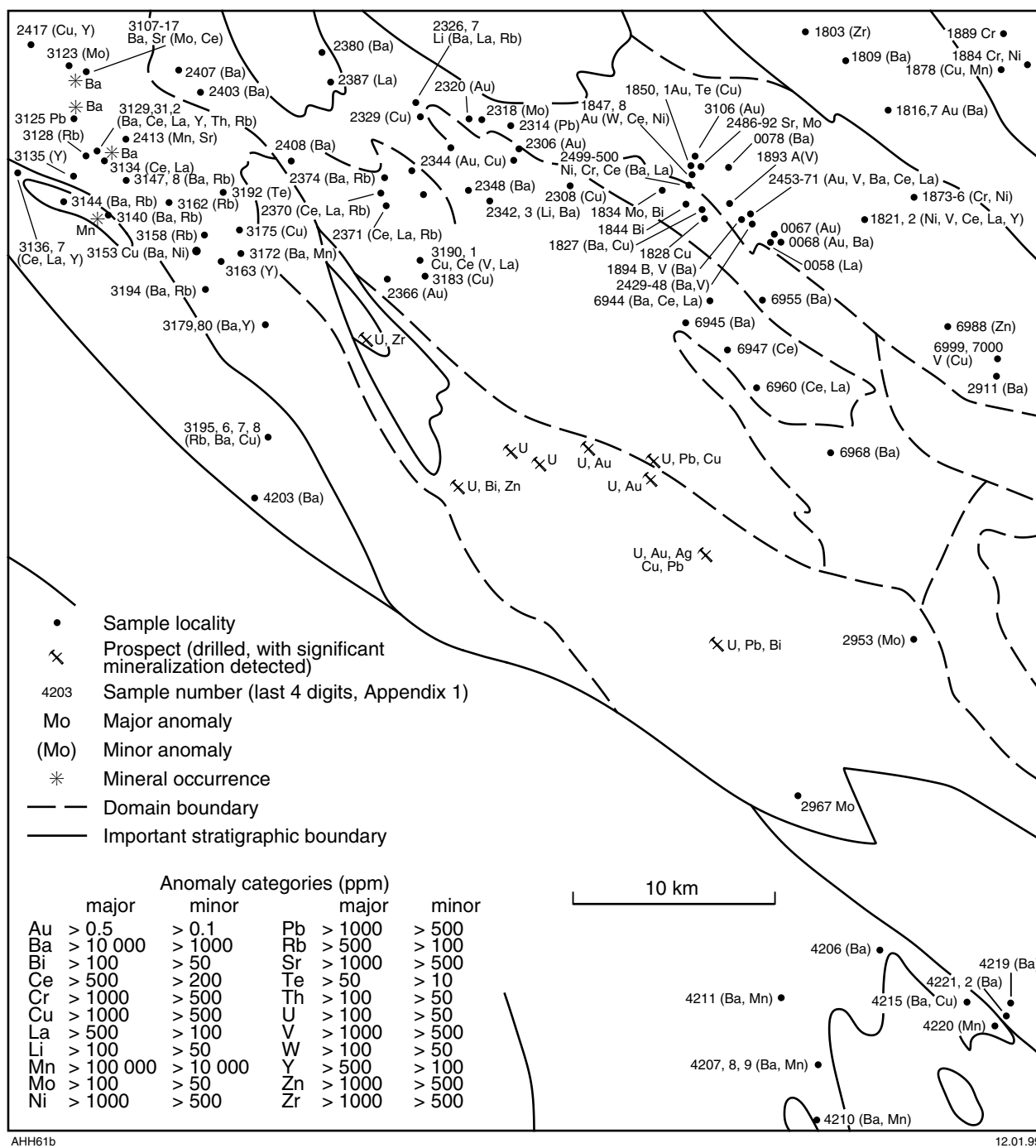


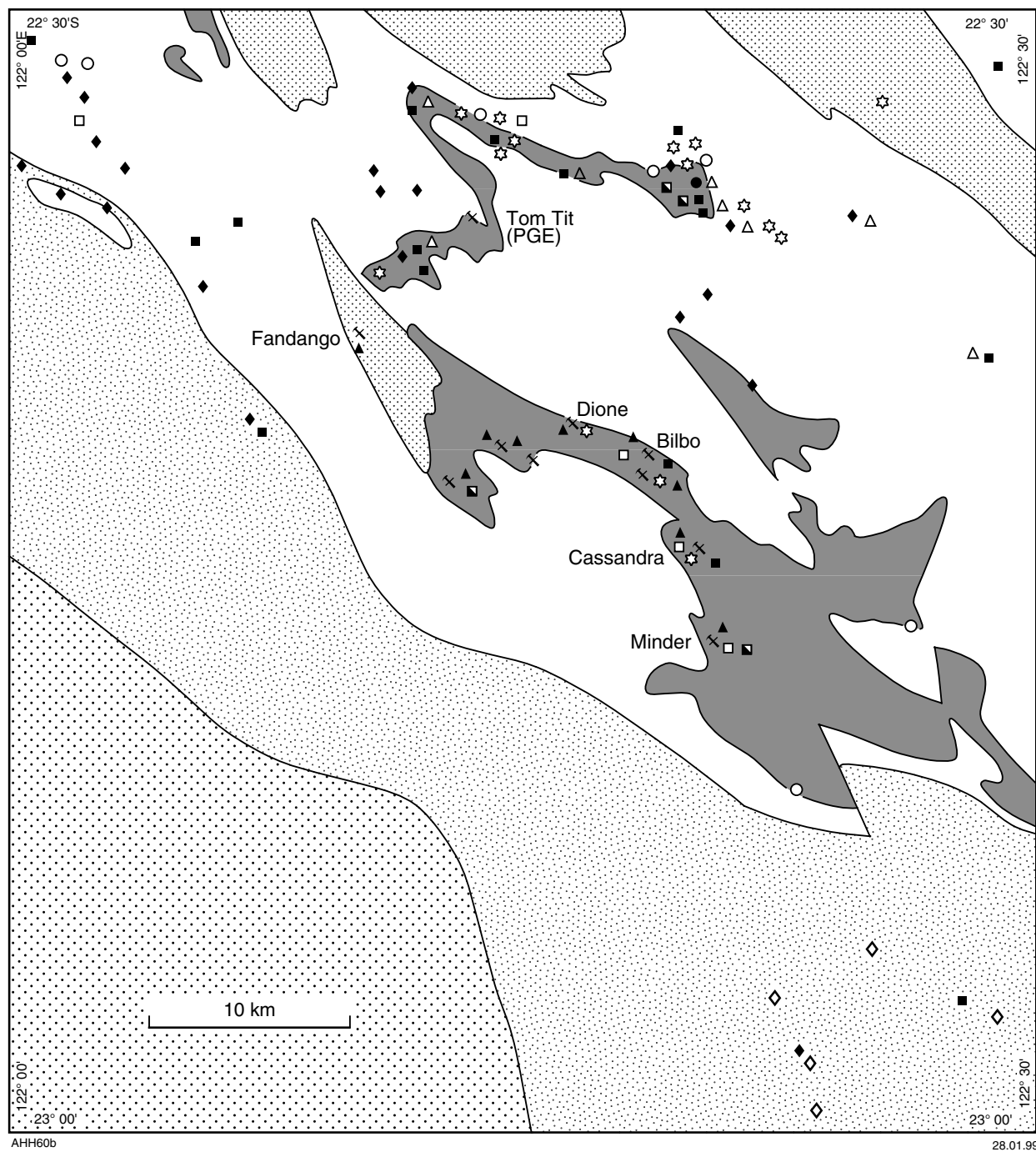
Figure 15. Locations of prospects, mineral occurrences, and mineral anomalies on the RUDALL 1:100 000 map area

association with traces of pyrite, galena, chalcopyrite, Ni–Co arsenate, and Bi–Sb minerals. Dione contains up to 0.1 ppm Au, and the nearby Io uranium prospect contains up to 0.19 ppm Au.

The Cassandra Prospect (AMG 322853) includes a number of uranium anomalies, in association with Au ( $\leq 3$  ppm), Ag, Cu, and Pb, in the Yandagooge Formation. The mineralization, including uraninite and coffinite, occurs as veins in  $D_4$  fractures and shears, and in association with silicified pegmatite and chlorite,

sericite, hematite, and albite hydrothermal alteration. This indicates that the mineralization is late- or post- $D_4$ .

The uranium mineralization at Minder is associated with Pb–Cu–Zn–Bi sulfides, and is in albite-altered shear zones in iron-rich pelite at or near pegmatite margins. Uraninite fills fractures in pyrite and the wallrocks show albite alteration indicative of hydrothermal activity. The mineralization includes traces of galena, chalcopyrite, sphalerite, and Pb–Bi sulfides.



AHH60b

28.01.99



Figure 16. Economic geology of the Talbot Terrane, and the Throssell and Tarcunyah Groups on the RUDALL 1:100 000 map area

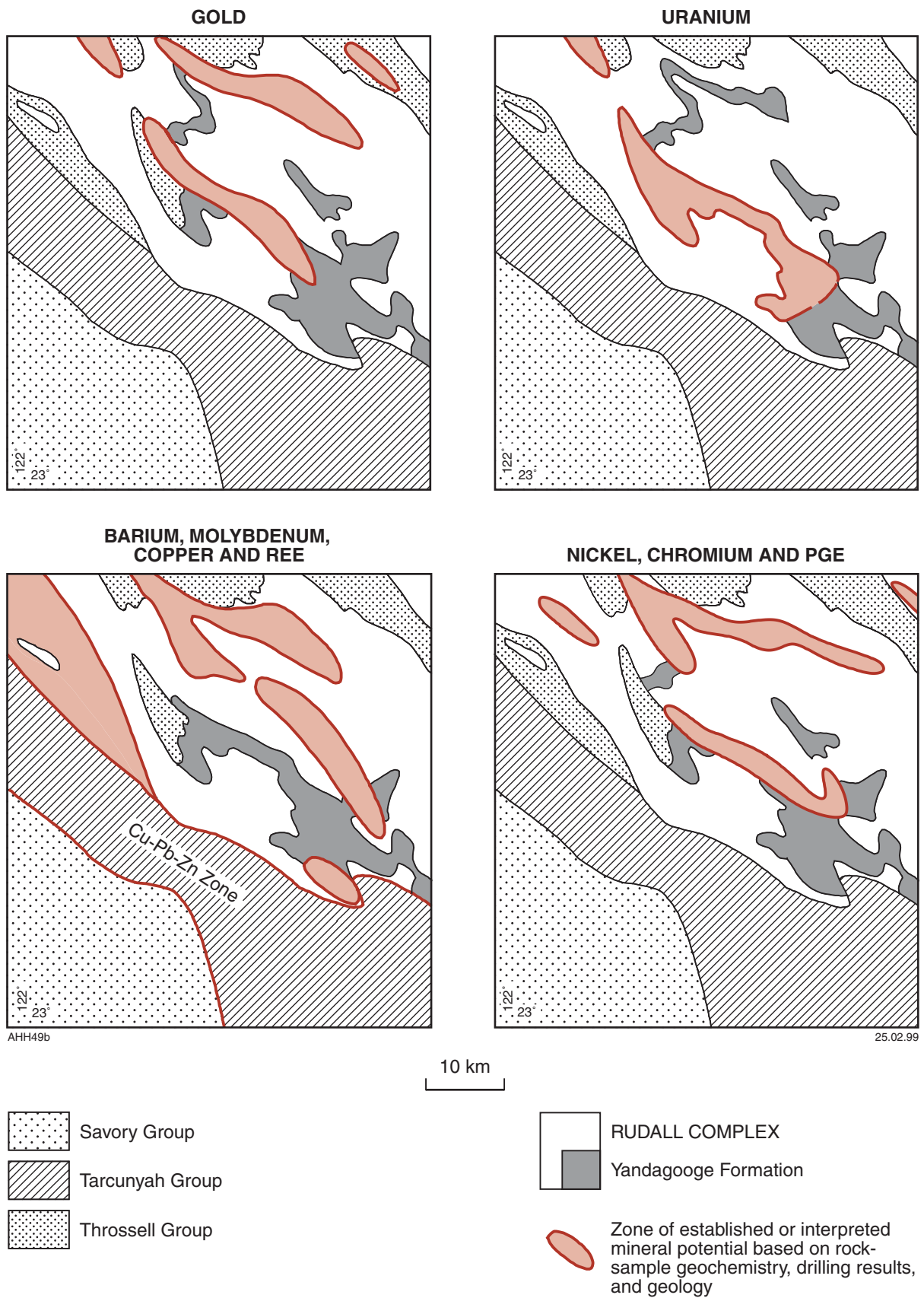


Figure 17. Summary of main zones of known and interpreted mineral potential on the RUDALL 1:100 000 map area

The Fandango uranium anomaly (AMG 150953) differs from the other uranium occurrences on RUDALL in that it is hosted by fractured Coolbro Sandstone, and is close to the contact of this formation with the Broadhurst Formation. The fractures occur close to the axis of the Camelot Syncline ( $F_4$ ) and are commonly filled with quartz–limonite veins. The sandstone host rock is strongly brecciated, with matrix material being extensively sericitized and kaolinized. This kaolinitic matrix is also rich in zircon (>1%) which must account for part of the uranium anomaly. The mineralization may be entirely structurally controlled, and late- or post- $D_4$ , or it could be due to hydrothermal alteration of a heavy mineral band.

GSWA geochemical investigations revealed no rocks containing more than 50 ppm U. Several samples were reported as containing about 30 ppm U, and these were mainly associated with copper anomalies in gossanous quartz veins.

## Copper, lead, and zinc

The Broadhurst Formation of the Throssell Group hosts stratabound and stratiform copper, lead, and zinc mineralization. These deposits occur at essentially the same stratigraphic level in shale–carbonate units and have been interpreted as Mount Isa-style base metal deposits. Examples include the Nifty deposit on LAMIL, and the Maroochydore deposits on BROADHURST, thus indicating that the Broadhurst Formation is prospective (Ferguson, 1999) over a large area. Copper in association with uranium also occurs at or near the Coolbro Sandstone – Broadhurst Formation contact, for example the Sunday Creek prospect on BROADHURST (Hickman and Clarke, 1994).

CRAE has shown that the Broadhurst Formation in the Camelot Syncline on RUDALL contains elevated As, Pb, U, Cu, Zn and Fe, and traces of Au in chloritic shale, graphitic schist, and carbonate. The western extension of the Camelot Syncline merits further exploration beneath Permian cover.

Geochemical analyses of the samples collected during mapping revealed significant copper anomalies (Cu >1000 ppm) at three localities (samples 111828, 113153, 113190) and minor anomalies at numerous localities (Figs 15 and 16, Appendix 1). The copper anomalies are commonly associated with elevated uranium contents, and positive inter-element correlations occur with Pb, Zn and Ni. As noted below, general low-level copper anomalies are also associated with major Mo, Au and Bi anomalies.

Field relationships of the quartz veins and gossans containing copper anomalies show four types of mineralization. About half of the anomalous samples are gossans or gossanous vein quartz occupying north-westerly striking faults (chiefly  $D_4$ ). Another group involves stratabound or stratiform sulfide mineralization in BIF, chiefly within the Yandagooge Formation, but also in the Poynton Formation. Calc-silicate gneiss, representing metasomatized mafic amphibolite (samples 112303A,

112304A, 112413), contains copper anomalies, and shale of the Broadhurst Formation west of the Southwest Thrust includes pyrite zones (gossan samples 113198, 99) containing weakly anomalous Cu and Zn.

Scattered lead and zinc anomalies are present in the Rudall Complex (Figs 15 and 16, Appendix 1). Concealed carbonate units in the Tarcunyah Group offer most scope for future exploration.

## Platinum-group elements (PGE)

Platinum and palladium occur as minor accessories in the Kintyre uranium deposit on BROADHURST, in trace concentrations in some U–Cu–Pb–Zn deposits in the Rudall Complex (Hickman and Clarke, 1994), and in anomalous concentrations in mafic and ultramafic rocks on RUNTON. This indicates that the potential for significant PGE mineralization is relatively high and is not restricted to areas of major ultramafic–mafic intrusions. Gold–platinum mineralization at Coronation Hill, in the South Alligator Valley of the Northern Territory, occurs in volcanic and sedimentary rocks of the Palaeoproterozoic El Sherana and South Alligator Groups included in the Pine Creek Inlier, although no ultramafic–mafic intrusions are known in the area. This PGE mineralization may have resulted from supergene enrichment of Proterozoic PGE placers, or by the introduction of hydrothermal fluids related to concealed felsic igneous activity (Stuart-Smith et al., 1988). The geology of the mineralization in the Pine Creek Inlier (Stuart-Smith et al., 1988) is somewhat similar to that of the Rudall Complex, therefore warranting further exploration for PGE in the Paterson Orogen.

## Other metals (molybdenum, tungsten, tin, bismuth, and vanadium)

The geochemical investigation by GSWA revealed isolated anomalies for certain metals, some of which may be significant for future exploration.

Molybdenum, mainly associated with copper, exceeded 100 ppm at three localities (Appendix 1). Two of those, located close to the Poynton Creek gold anomalies, occur in  $D_4$  quartz veins close to ultramafic lenses. Sample 111834 contains abundant granular tourmaline, and is hosted by sheared K-feldspar augen orthogneiss; in addition to molybdenum it contains 178 ppm Bi. Sample 112849 is hosted by calc-silicate gneiss (sample 112486) developed along a contact between banded paragneiss and serpentinized peridotite. The third significant molybdenum anomaly (sample 112967) occurs in a gossanous pelitic member of the Fingoon Quartzite about 10 km north of the McKay Range. Other molybdenum anomalies (Appendix 1) include an association with minor bismuth (sample 112318) in the area of the Dunn Creek gold anomalies. Here, lenticular, slightly sulfidic quartz lenses occupy a dextral west-northwesterly trending  $D_4$  fault.



Bismuth anomalies, apart from those associated with uranium and molybdenum, are relatively few. Of these, the most marked occurs in the southern part of the Poynton Creek area where a magnetite-bearing quartzite (sample 111844) at the top of the Fingoon Quartzite is folded by a northwest-plunging  $F_4$  anticline. The weak mineralization (Bi–Cu–Pb) is stratabound, and may be related to nearby pegmatite sheets.

Most of the 395 samples collected were not analysed for tungsten owing to probable contamination during ring-mill grinding. Where a chrome mill was used four samples (111822, 111847, 112308, 112329) were reported to contain between 30 and 55 ppm W. Three of the samples were collected from gossanous zones in turbiditic paragneiss close to the southern boundary of the Poynton Domain, and the fourth (sample 111822) from arenaceous paragneiss within the Poynton Domain. All have relatively high nickel contents (237–708 ppm Ni), and two are close to ultramafic bodies. Gold contents are anomalous, but not high.

No significant tin mineralization was detected during the mapping, and only one pegmatite and one orthogneiss were included in the geochemical investigation. Three samples (114208, 114211, 114213) from the Tarcunyah Group of the McKay Range were reported to contain weakly anomalous tin, and the molybdenum anomaly (sample 112967) in the Fingoon Quartzite 10 km north from the McKay Range returned 37 ppm Sn. This grouping of tin anomalies in a range of rock types from the McKay Range area suggests hydrothermal activity.

Vanadium anomalies are restricted to a zone close to the southern boundary of the Poynton Domain. Most are associated with limonitic argillaceous units, in which vanadium exhibits positive correlations with gallium, barium, and silver.

## Diamonds

CRAE has been conducting diamond exploration in the Paterson Orogen since 1978, and Stockdale explored the region in 1984. A number of kimberlitic indicators and microdiamonds have been detected, although no kimberlites have yet been found. These kimberlitic indicators and microdiamonds may have originated from Permian glacial sedimentary rocks.

## Barite

Chin et al. (1980), who discovered veins up to 0.3 m wide 4 km southwest from Watrara Pool, first reported barite mineralization on RUDALL. These veins were re-examined during the present investigation, and additional mineralization was recorded between this locality and an area around AMG 020048. Hickman and Bagas (1998) give a description of the veins.

Geochemical analyses (samples 111307–113117, Appendix 1) indicate that  $BaSO_4$  content of the veins ranges up to about 80% (47% Ba), the chief impurities being iron (hematite) and silica. Although the largest vein

is over 100 m long and up to 4 m thick, the general level of impurities and the remote location make the deposits subeconomic. Analytical data on the range of rock types collected from the veins reveal no significant base- or precious-metal mineralization, although one sample (113115) contains anomalous molybdenum and weakly anomalous copper. Strontium exhibits a strong positive correlation with barium.

In the Clayton Domain, and close to the southern boundary of the Poynton Domain, barium anomalies are associated with anomalous contents of rubidium, strontium, cerium, lanthanum, and yttrium (Figs 15 and 16; Appendix 1). Somewhat similar anomalies also occur around Larry Creek, 3–5 km south of the Rudall River confluence. In the Clayton Domain the association is accompanied by local copper, lead, and molybdenum anomalies, and may be partly related to post- $D_2$  felsic intrusions of microgranite, aplite, and felsite. Along the southern boundary of the Poynton Domain the Ba anomalies occur in the same zone as gold, copper, molybdenum, lead, bismuth, and tungsten anomalies. As discussed below (in **Mineral potential**), these anomaly belts appear to coincide with zones of major faulting.

Combined high concentrations of barium (>1000 ppm) and manganese (>10 000 ppm) are restricted to shallow-water sedimentary rocks of the Tarcunyah Group (Figs 15 and 16). This is interpreted to be a consequence of evaporitic and oxidizing environments during deposition of the Tarcunyah Group, and has no direct economic significance.

## Mineral potential

The Paterson Orogen has proven potential for gold, Cu–Pb–Zn and uranium mineralization. Additionally, mineral exploration and the present mapping and geochemical investigations have indicated significant prospectivity for Pb–Zn, molybdenum, bismuth, and possibly tungsten, nickel, chromium, and PGE mineralization.

No economic mineral deposits have yet been discovered within the area covered by this report, but exploration is still at an early stage and has so far been undertaken without the assistance of a detailed geological framework. Exploration has chiefly involved the examination and drilling of targets identified from airborne geophysics.

Figures 15 and 16 summarize the existing geochemical anomaly data on RUDALL, and Figure 17 interprets this information in terms of zones of mineral potential. Table 6 includes a more general and theoretical assessment of the mineral potential of the orogen based on regional geology and tectonic evolution. Figure 17 shows that three northwest-striking zones encompass all known significant gold anomalies in the area. The central zone includes the Poynton Creek and Dunn Creek gold anomalies, and is a belt of  $D_2$  and  $D_4$  faulting close to the southern boundary of the Poynton Domain. The overall movement along this zone is northeastern block down, with dextral displacement. The southern zone

Table 6. Summary of Proterozoic tectonic evolution on RUDALL, with theoretical metallogenic implications

	<i>Phase</i>	<i>Environment</i>	<i>Unit/feature</i>	<i>Structure</i>	<i>Potential mineralization</i>
STRIKE-SLIP REGIME	D <sub>6</sub> Late strike-slip	Brittle deformation	Quartz veins	Strike-slip faults and transpressional folds; reactivation of D <sub>4</sub> structures	Epigenetic Au in quartz veins
	Clastic deposition	Foreland basin	Savory Group		
	Development of the Tarcunyah Basin (in the greater Officer Basin)	Tarcunyah Basin: supratidal to shallow-water, locally fluvial-deltaic	Waters Formation and Gunanya Sandstone	Syn-depositional NNW- to WNW-trending faults, dominantly dextral strike-slip, but with accompanying vertical movement producing growth faults; slump folding from basin margin	Sabkha-type Cu-Pb-Zn, Copperbelt-type Cu-Co Epigenetic Au in quartz veins
	Erosion	Fold-thrust belt (inactive)	Unconformity		
	D <sub>4</sub> SW-directed movement and basin closure	Dominantly transpressional fold-thrust belt	Silicified shear zones	Upright to overturned, generally tight to isoclinal NW-trending folds and NE-inclined thrusts	Epigenetic Au in quartz veins. Hypothermal base metals
	Stable carbonate shelf	NE-deepening shelf, gradual subsidence	Isdell Formation		Mississippi Valley-type, carbonate-hosted Pb-Zn (most potential in shallow-water facies)
	Rapid subsidence	?Marine transgression Pelagic deposition	?Unconformity Broadhurst Formation		McArthur River-type Fe-Pb-Zn, Copperbelt-type Cu-Co
	Development of Broadhurst Range strike-slip basin	Dominantly transtensional basin, elongate NW-SE and deepening NE. Broadhurst basin	Coolbro Sandstone		Unconformity-related vein-style U (with associated Cu, Pb, Bi, PGE, and Au) on, or close to faults
Deep erosion	Inactive fold-thrust belt	Unconformity			
PLATE REGIME	Retarded convergence	Post-collisional deformation. Crustal thickening and melting	Microgranite, aplite, and pegmatite	Local NW-trending folds	U-enrichment in granitoids
	D <sub>2</sub> collision, SW-directed	Fold-thrust belt	?Syn-collisional granitoids. May include some <i>Erga</i>	Nappes, and NE- to E-inclined stacked thrust sheets	Greisen-related Sn-W, with Cu, Mo, and Li
	Widespread granitoid intrusion	Post-D <sub>1</sub> to early D <sub>2</sub> partial melting (thickening), or subduction-related magmatic arc	K-feldspar augen orthogneiss protoliths ( <i>Erga</i> )	Sill-form granitoid sheets, associated dykes, pegmatite and veins	Pegmatite minerals. Granitoid emplacement-related hydrothermal Au
	Clastic deposition, local volcanism	Rifted shelf, adjacent volcanic arc	Poynton Formation		Sandstone: stratabound U. Shale-BIF: sedex-type massive sulfides
	D <sub>1</sub> Subhorizontal tectonic interleaving	?Thin-skinned thrusting along fold-thrust belt margin	Lithologically layered orthogneiss ( <i>Ergx</i> )	Layer-parallel shear zones	Tectonically emplaced and mobilized pre-existing deposits
	Granitoid intrusion	?Partial melting beneath rifted basin	Granitoid protoliths for lithologically layered orthogneiss ( <i>Ergx</i> )	Sill-form granitoid sheets	Greisen-related Sn-W etc. (but probably too fragmented to be economic)

**Table 6.** (continued)

<i>Phase</i>	<i>Environment</i>	<i>Unit/feature</i>	<i>Structure</i>	<i>Potential mineralization</i>
← CONVERGENT- ↓	Clastic deposition	Subsiding foreland basin with shoreline, shelf and slope environments; probable rifting; adjacent marginal basin	Larry Formation, Fingoon Quartzite, Yandagooge Formation, and Butler Creek Formation	<ul style="list-style-type: none"> <li>(a) Shelf sand and mud: stratabound sandstone-type U.</li> <li>(b) Carbonaceous mud and BIF: sedex-type massive sulfides</li> <li>(c) Ultramafic–mafic: serpentinite-hosted Cr, Ni, or PGE. Metabasalt-hosted Cyprus-style Cu–Fe</li> </ul>

follows the southwestern boundary of the Fingoon Domain where overall movement is southwestern block down, with sinistral displacement (along the central and northwestern sections). Both zones include the Yandagooge Formation, with the central zone also involving mineralization of the Butler Creek and Poynton Formations.

Most of the gold mineralization is hosted by  $D_4$  faults and known deposits therefore appear to be syn- or post- $D_4$  in age. However, because  $D_4$  faults commonly coincide with  $D_2$  faults, and probably also with growth faults during deposition of the Throssell Group, the original age of gold mineralization is uncertain.

The northern zone of gold mineralization is confined to a shale-siltstone unit of the Coolbro Sandstone and, if epigenetic, clearly must be post-Throssell Group in age.

Uranium mineralization is confined to a relatively narrow northwest-striking belt along the southwestern boundary of the Fingoon Domain. This belt is essentially a  $D_4$  graben, and may have been a down-faulted block during deposition of the Coolbro Sandstone. Uranium deposits are hosted by fractures in the Yandagooge Formation, presumably not far below the level of the unconformity at the base of the Coolbro Sandstone. Figure 17 shows uranium potential declining southeast from the Minder area, based on the interpretation that the Coolbro Sandstone probably wedged out in this area (Fig. 14). Potential for uranium mineralization in the Poynton and Rooney Domains is considered to be low due to an absence of suitable pelitic or carbonate host-rocks close to the basal Coolbro Sandstone unconformity.

Nickel, chromium, and PGE mineralization may be present in the ultramafic rocks of the Rudall Complex, and PGE mineralization could be associated with uranium. However, because most of the ultramafic bodies are small and fragmented, mineral potential is considered to be relatively low.

Figure 17 shows four zones with Ba-REE-Cu-Mo potential. The western zone, in the Clayton Domain, coincides with a belt of major  $D_4$  thrusts and normal (lag) faults, but it is unclear to what extent these have acted as conduits for hydrothermal fluids. The northern zone partly corresponds to the central zone of gold mineralization (discussed above). Other shaded areas on Figure 17 chiefly involve the Yandagooge and upper Fingoon Formations where these units are dislocated by  $D_4$  and  $D_6$  faults. Although copper and molybdenum are commonly associated, the apparent absence of high-level intrusions and associated alteration, and the present deep erosion levels make it unlikely that mineralized porphyry-style systems are preserved.

The Tarcunyah Group on RUDALL is composed of shallow-water arenites, shale, and carbonate rocks. The succession occupies an area of about 1000 km<sup>2</sup> (Fig. 17), but is largely concealed and has not yet been explored. The geochemical investigation revealed local copper anomalies, and the belt is clearly prospective for sabkha-type Cu-Pb-Zn, and possibly Copperbelt-type Cu-Co or Mississippi Valley-type carbonate-hosted Pb-Zn deposits. The basal beds of this group are also known to be prospective for gold and copper mineralization on BLANCHE-CRONIN (Bagas and Smithies, in prep.).

## Acknowledgments

The authors thank Rio Tinto Exploration Pty Ltd (formerly CRAE) and PNC Exploration (Australia) Pty Ltd for their generous assistance during the fieldwork, access to colour aerial photographs, topographic maps, and helpful discussions.

## References

- BAGAS, L., 1998, Geology of the Gunanya 1:100 000 sheet, Western Australia: Western Australia Geological Survey, 1:100 000 Geological Series Explanatory Notes, 10p.
- BAGAS, L., GREY, K., and WILLIAMS, I. R., 1995, Reappraisal of the Paterson Orogen and Savory Basin: Western Australia Geological Survey, Annual Review 1994–95, p. 55–63.
- BAGAS, L., and SMITHIES, R. H., 1997, Palaeoproterozoic tectonic evolution of the Rudall Complex, and comparison with the Arunta Inlier and Capricorn Orogen: Western Australia Geological Survey, Annual Review 1996–97, p. 110–115.
- BAGAS, L., and SMITHIES, R. H., 1998, Geology of the Connaughton 1:100 000 sheet, Western Australia: Western Australia Geological Survey, 1:100 000 Geological Series Explanatory Notes, 38p.
- BAGAS, L., and SMITHIES, R. H., in prep., Geology of the Blanche–Cronin 1:100 000 sheet, Western Australia: Western Australia Geological Survey, 1:100 000 Geological Series Explanatory Notes.
- BLOCKLEY, J. G., and MYERS, J. S., 1990, Proterozoic rocks of the Western Australian Shield — geology and mineralization, *in* Geology of the Mineral Deposits of Australia and Papua New Guinea *edited by* F. E. HUGHES: Australasian Institute of Mining and Metallurgy, Monograph 14, p. 607–615.
- CARR, H. W., 1989, The geochemistry and platinum group element distribution of the Rudall River ultramafic bodies, Paterson Province, Western Australia: University of Western Australia, BSc Honours thesis (unpublished).
- CHIN, R. J., WILLIAMS, I. R., WILLIAMS, S. J., and CROWE, R. W. A., 1980, Rudall, Western Australia: Western Australia Geological Survey, 1:250 000 Geological Series Explanatory Notes, 22p.
- CHIN, R. J., and de LAETER, J. R., 1981, The relationship of new Rb–Sr isotopic dates from the Rudall Metamorphic Complex to the geology of the Paterson Province: Western Australia Geological Survey, Annual Report 1980, p. 132–139.
- CHIN, R. J., HICKMAN, A. H., and TOWNER, R. R., 1982, Paterson Range, Western Australia (2nd edition): Western Australia Geological Survey, 1:250 000 Geological Series Explanatory Notes, 29p.
- CLARKE, G. L., 1991, Proterozoic tectonic reworking in the Rudall Complex, Western Australia: Australian Journal of Earth Sciences, v. 38, p. 31–44.
- de LAETER, J. R., HICKMAN, A. H., TRENDALL, A. F., and LEWIS, J. D., 1977, Geochronological data concerning the eastern extent of the Pilbara Block: Western Australia Geological Survey, Annual Report 1976, p. 56–62.
- FERGUSON, K. M., 1999, Lead, zinc and silver deposits of Western Australia: Western Australia Geological Survey, Mineral Resources Bulletin 15, 314p.
- FODEN, J. D., BUICK, I. S., and MORTIMER, G. E., 1988, The petrology and geochemistry of granitic gneisses from the east Arunta Inlier, central Australia: implications for Proterozoic crustal development: Precambrian Research, v. 40/41, p. 233–259.
- GOELLNIGHT, N. M., GROVES, D. I., and McNAUGHTON, N. J., 1991, Late Proterozoic fractionated granitoids of the mineralized Telfer area, Paterson Province, Western Australia: Precambrian Research, v. 51, p. 375–391.
- HICKMAN, A. H., and BAGAS, L., 1995, Tectonic evolution and economic geology of the Paterson Orogen — a major reinterpretation based on detailed geological mapping: Western Australia Geological Survey, Annual Review 1993–94, p. 67–76.
- HICKMAN, A. H., and BAGAS, L., 1998, Geology of the Rudall 1:100 000 sheet, Western Australia: Western Australia Geological Survey, 1:100 000 Geological Series Explanatory Notes, 30p.
- HICKMAN, A. H., and CLARKE, G. L., 1994, Geology of the Broadhurst 1:100 000 sheet, Western Australia: Western Australia Geological Survey, 1:100 000 Geological Series Explanatory Notes, 40p.
- HICKMAN, A. H., WILLIAMS, I. R., and BAGAS, L., 1994, Proterozoic geology and mineralization of the Telfer–Rudall region, Paterson Orogen: Excursion Guidebook No. 5, 12th Australian Geological Convention, September 1994: Geological Society of Australia (WA Division), 56p.
- McNAUGHTON, N. J., and GOELLNIGHT, N. M., 1990, The age and radiothermal properties of the Mt Crofton Granite: Australian Journal of Earth Sciences, v. 37, p. 103–106.
- MITCHELL, A. H. G., and READING, H. G., 1986, Sedimentation and tectonics, *in* Sedimentary environments and facies *edited by* H. G. READING: Oxford, Blackwell Scientific Publications, p. 471–519.
- MUHLING, J. R., 1988, The nature of Proterozoic reworking of early Archaean gneisses, Mukalo area, Southern Gascoyne Province, Western Australia: Precambrian Research, v. 40/41, p. 341–362.
- NELSON, D. R., 1995, Compilation of SHRIMP U–Pb zircon geochronology data, 1994: Western Australia Geological Survey, Record 1995/3, 244p.
- PARK, R. G., 1988, Geological structures and moving plates: Glasgow, Blackie and Son Ltd., 337p.
- PIRAJNO, F., BAGAS, L., SWAGER, C. P., OCCHIPINTI, S. A., and ADAMIDES, N. G., 1996, A reappraisal of the Glengarry Basin: Western Australia Geological Survey, Annual Review 1995–96, p. 81–87.
- SMITHIES, R. H., and BAGAS, L., 1997, High pressure amphibolite–granulite facies metamorphism in the Paleoproterozoic Rudall Complex, central Western Australia: Precambrian Research, v. 83(4), p. 243–265.
- STUART-SMITH, P. G., NEEDHAM, R. S., and BAGAS, L., 1988, Stow Region, Northern Territory: Bureau of Mineral Resources, 1:100 000 Geological Series Explanatory Notes, 35p.
- THORNE, A. M., and SEYMOUR, D. B., 1991, Geology of the Ashburton Basin: Western Australia Geological Survey, Bulletin 139, 141p.
- TRENDALL, A. F., 1974, The age of a granite near Mount Crofton, Paterson Range Sheet: Western Australia Geological Survey, Annual Report 1974, p. 92–96.
- TURNER, F. J., and VERHOOGEN, J., 1960, Igneous and metamorphic petrology: New York, McGraw-Hill (International Series in the Earth Sciences), 403p.

- TYLER, I. M., 1991, The geology of the Sylvania Inlier and the southeast Hamersley Basin: Western Australia Geological Survey, Bulletin 138, 108p.
- WILLIAMS, I. R., 1989, Balfour Downs, W.A. (2nd edition): Western Australia Geological Survey, 1:250 000 Geological Series Explanatory Notes, 38p.
- WILLIAMS, I. R., 1990, Yeneena Basin, *in* Geology and mineral resources of Western Australia: Western Australia Geological Survey, Memoir 3, p. 277–282.
- WILLIAMS, I. R., 1992, Geology of the Savory Basin Western Australia: Western Australia Geological Survey, Bulletin 141, 115p.
- WILLIAMS, I. R., and BAGAS, L., in prep.a, Geology of the Throssell 1:100 000 sheet, Western Australia: Western Australia Geological Survey, 1:100 000 Geological Series Explanatory Notes.
- WILLIAMS, I. R., and BAGAS, L., in prep.b, Geology of the Poisonbush 1:100 000 sheet, Western Australia: Western Australia Geological Survey, 1:100 000 Geological Series Explanatory Notes.
- WILLIAMS, I. R., BRAKEL, A. T., CHIN, R. J., and WILLIAMS, S. J., 1976, The stratigraphy of the Eastern Bangemall Basin and Paterson Province: Western Australia Geological Survey, Annual Report, 1975, p. 79–83.
- WILLIAMS, I. R., and MYERS, J. S., 1990, Paterson Orogen, *in* Geology and mineral resources of Western Australia: Western Australia Geological Survey, Memoir 3, p. 274–75.
- WINDLEY, B. F., 1984, The evolving continents (2nd edition): Chichester, Wiley, 399p.
- WINKLER, H. G. F., 1965, Petrogenesis of metamorphic rocks: New York, Springer-Verlag, 220p.
- WYBORN, L. A. I., 1988, Petrology, geochemistry and origin of a major Australian 1880–1840 Ma felsic volcano-plutonic suite: a model for intracontinental felsic magma generation: Precambrian Research, v. 40/41, p. 37–60.
- YARDLEY, B. W. D., 1991, An introduction to metamorphic petrology: New York, Longman, 248p.

## Appendix 1

### Analytical data from the RUDALL 1:100 000 sheet

NOTES: All analyses performed by Chemistry Centre (W.A.).

Major- and trace-element analyses of mafic rocks by X-ray fluorescence (XRF) after fusion of samples within lithium tetraborate, except FeO, C, and volatiles, which were determined titrimetrically.

S was measured from the titration of SO<sub>2</sub> with KO<sub>3</sub>.

F was determined using a specific-ion electrode after decomposition of the sample by heating with concentrated H<sub>2</sub>SO<sub>4</sub>.

Trace-element concentrations were determined by XRF analysis of pressed-powder samples, with the following exceptions:

- Felsic rocks were determined by inductively coupled plasma atomic emission spectrometry (ICP-AES; for Co, Cr, Cu, Ni, V, and Zn) or inductively coupled plasma mass spectrometry (ICP-MS);
- Ce, La, Li, and Sc were determined by ICP-AES after a mixed (total) acid digest;
- Cs was determined by graphite furnace atomic absorption spectroscopy;
- Au was determined by classical fire assay with an atomic absorption finish.

Standard certified reference materials, analysed simultaneously with silicate analyses, included NBS-688, NIM-P, SY-2, NIM-G, and FER-1.

## Appendix 1

## Analytical data from the RUDALL 1:100 000 sheet

GSWA no.	Whole rock and trace element analysis							
	106944 paragneiss	106945 paragneiss	106955 paragneiss	106959 orthogneiss	106997 quartz vein	110051 meta-BIF	110052 limonitic schist	110065 quartzite
Latitude	22°37'43"	22°38'22"	22°37'43"	22°39'11"	22°38'38"	22°31'51"	22°31'41"	22°35'48"
Longitude	122°20'27"	122°19'52"	122°21'45"	122°21'51"	122°29'19"	122°22'18"	122°23'09"	122°22'15"
	<b>Percent</b>							
SiO <sub>2</sub>	73.00	76.60	73.00	71.30	95.70	48.50	25.90	87.20
TiO <sub>2</sub>	0.53	0.54	0.32	0.35	0.11	<0.05	0.34	0.18
Al <sub>2</sub> O <sub>3</sub>	13.60	11.50	14.50	14.70	3.12	0.76	5.32	2.81
Fe <sub>2</sub> O <sub>3</sub>	3.01	3.52	1.91	1.25	0.69	46.70	57.60	6.37
FeO	0.28	0.37	0.34	1.27	0.24	2.14	0.23	0.34
MnO	<0.05	<0.05	<0.05	0.06	<0.05	<0.05	0.06	<0.05
MgO	0.77	0.35	0.85	0.75	0.49	<0.05	0.48	0.13
CaO	0.13	1.16	0.73	2.54	<0.05	<0.05	<0.05	0.19
Na <sub>2</sub> O	<0.05	3.00	2.65	3.00	<0.05	<0.05	<0.05	<0.05
K <sub>2</sub> O	1.92	2.21	4.69	4.08	<0.05	0.14	1.96	0.13
P <sub>2</sub> O <sub>5</sub>	0.05	0.11	<0.05	0.08	<0.05	0.07	0.23	<0.05
LOI	6.50	1.29	1.86	1.33	0.61	1.19	7.95	2.15
S	0.09	0.03	<0.01	0.01	<0.01	<0.01	0.01	0.11
C	nd	nd	nd	nd	nd	nd	nd	nd
-O=	0.04	0.01	<0.01	<0.01	<0.01	<0.01	0.01	0.05
Others	0.58	0.31	0.25	0.23	0.02	0.08	0.11	0.06
<b>Total</b>	<b>100.4</b>	<b>101</b>	<b>101.2</b>	<b>101</b>	<b>100.9</b>	<b>99.5</b>	<b>100.2</b>	<b>99.6</b>
	<b>Parts per million</b>							
Au	<0.01	<0.01	<0.01	<0.01	<0.01	0.04	0.02	0.04
Ag	<5	<5	<5	<5	<5	<5	34	<5
As	<4	<4	<4	<4	<4	<4	5	<4
Ba	3 982	1 574	1 219	965	50	156	368	186
Bi	<4	<4	<4	<4	<4	<4	<4	<4
Cd	<5	<5	<5	<5	<5	<5	<5	<5
Ce	211	117	148	118	13	<6	35	17
Co	6	6	5	8	3	nd	nd	nd
Cr	41	<4	8	6	16	10	45	23
Cu	15	4	<4	<4	<4	21	<4	13
Ga	15	18	15	17	4	8	4	8
Ge	<3	<3	<3	<3	<3	3	3	<3
La	108	41	90	61	8	<5	20	15
Li	7	<6	8	18	<6	<6	8	<6
Mn	<380	<380	<380	465	<380	<380	465	<380
Mo	<6	<6	<6	<6	<6	<6	<6	6
Nb	15	25	11	10	<7	<7	<7	<7
Ni	14	<3	4	<3	5	4	27	4
Pb	10	5	15	40	<4	<4	8	20
Rb	105	50	144	146	<2	3	49	2
Sb	nd	nd	nd	nd	nd	<4	<4	4
Sc	11	9	5	5	<2	4	8	5
Sn	<4	<4	<4	<4	<4	41	6	<4
Sr	72	99	143	257	9	<2	15	23
Ta	<5	<5	<5	<5	<5	6	7	<5
Te	nd	nd	nd	nd	nd	<6	<6	<6
Th	33	24	30	26	4	<2	7	2
U	<2	3	3	3	<2	<2	<2	2
V	79	16	31	29	15	248	56	81
W	5	6	<4	<4	<4	nd	nd	nd
Y	39	80	23	20	3	2	21	6
Zn	32	38	7	39	7	9	50	10
Zr	251	485	202	207	32	<5	118	27



## Appendix 1 (continued)

GSWA no.	Whole rock and trace element analysis							
	110066 quartzite	110068 quartzite	110071 quartzite	110073 limonitic quartzite	111816 siltstone	111817 quartzite	111827 limonitic quartzite	111838 meta-BIF
Latitude	22°35'48"	22°36'00"	22°35'12"	22°35'23"	22°32'30"	22°32'30"	22°35'18"	22°33'50"
Longitude	122°22'15"	122°22'23"	122°22'24"	122°21'21"	122°25'27"	122°25'27"	122°20'03"	122°17'33"
	<b>Percent</b>							
SiO <sub>2</sub>	85.50	75.40	84.40	56.70	82.10	91.20	23.20	52.30
TiO <sub>2</sub>	0.15	0.09	0.22	0.08	0.31	0.10	0.20	0.09
Al <sub>2</sub> O <sub>3</sub>	2.75	13.50	4.33	1.28	6.68	1.62	4.02	0.91
Fe <sub>2</sub> O <sub>3</sub>	8.76	0.60	6.97	35.30	5.04	4.78	61.30	43.20
FeO	0.28	0.17	0.29	0.28	0.26	0.31	<0.10	0.62
MnO	<0.05	<0.05	<0.05	<0.05	<0.05	<0.05	0.09	<0.05
MgO	<0.05	0.18	0.07	<0.05	0.12	<0.05	<0.05	0.20
CaO	0.06	0.84	0.09	<0.05	<0.05	<0.05	<0.05	0.31
Na <sub>2</sub> O	<0.05	3.41	<0.05	<0.05	<0.05	<0.05	<0.05	<0.05
K <sub>2</sub> O	<0.05	4.58	1.09	0.06	0.92	<0.05	0.44	0.20
P <sub>2</sub> O <sub>5</sub>	<0.05	<0.05	<0.05	0.77	<0.05	<0.05	1.19	0.23
LOI	1.95	1.08	1.86	5.87	4.32	1.04	9.32	1.01
S	0.04	<0.01	0.07	0.02	0.02	0.07	0.03	0.03
C	nd	nd	nd	nd	nd	nd	nd	nd
-O=	0.02	<0.01	0.04	0.01	0.01	0.03	0.02	0.02
Others	0.05	0.23	0.17	0.05	0.19	0.22	0.30	0.08
<b>Total</b>	<b>99.5</b>	<b>100.1</b>	<b>99.5</b>	<b>100.4</b>	<b>100</b>	<b>99.3</b>	<b>100.1</b>	<b>99.1</b>
	<b>Parts per million</b>							
Au	0.05	0.96	0.07	2.15	0.53	1.10	0.05	0.03
Ag	<5	<5	<5	10	<5	<5	36	<5
As	<4	<4	<4	<4	<4	<4	<4	<4
Ba	105	1349	909	78	1 158	1 751	1 133	532
Bi	<4	<4	<4	<4	<4	<4	<4	<4
Cd	<5	<5	<5	<5	<5	<5	<5	<5
Ce	31	49	30	26	<6	29	61	8
Co	nd	nd	nd	nd	nd	nd	nd	nd
Cr	24	4	46	14	49	11	41	22
Cu	22	<4	8	7	<4	16	655	10
Ga	6	13	7	<3	7	<3	4	4
Ge	<3	<3	<3	<3	<3	<3	<3	4
La	9	28	15	11	5	16	33	<5
Li	<6	<6	<6	<6	<6	<6	<6	<6
Mn	<380	<380	<380	<380	<380	<380	697	<380
Mo	12	<6	<6	<6	<6	<6	<6	<6
Nb	<7	<7	<7	<7	<7	<7	<7	<7
Ni	<3	<3	6	83	6	5	112	4
Pb	40	28	31	<4	<4	4	<4	4
Rb	<2	103	41	<2	56	<2	10	3
Sb	<4	<4	<4	<4	<4	<4	<4	<4
Sc	7	3	7	8	10	<2	9	3
Sn	<4	<4	<4	<4	<4	<4	<4	<4
Sr	9	235	44	9	16	32	35	38
Ta	<5	<5	<5	<5	<5	<5	<5	5
Te	<6	<6	<6	<6	<6	<6	<6	<6
Th	3	22	16	3	13	7	5	<2
U	<2	2	4	2	<2	<2	30	2
V	73	9	46	42	49	18	94	19
W	nd	nd	nd	nd	nd	nd	nd	nd
Y	9	16	13	10	17	9	52	12
Zn	7	8	12	62	5	4	113	23
Zr	26	109	159	48	191	61	72	<5

## Appendix 1 (continued)

GSWA no. Rock type	Whole rock and trace element analysis							
	111844 quartzite	112303A gneiss	112304A gneiss	112312 meta-BIF	112324A meta-BIF	112326 pegmatite	112327 pelitic ferruginous schist	112367 meta-BIF
Latitude	22°35'05"	22°33'50"	22°33'50"	22°33'26"	22°32'35"	22°32'35"	22°32'35"	22°36'02"
Longitude	122°19'40"	122°14'35"	122°14'35"	122°15'25"	122°11'54"	122°11'54"	122°11'54"	122°11'42"
	<b>Percent</b>							
SiO <sub>2</sub>	89.30	46.70	46.30	46.60	46.00	37.50	24.50	39.60
TiO <sub>2</sub>	0.10	0.06	0.09	0.09	0.06	1.18	1.55	<0.05
Al <sub>2</sub> O <sub>3</sub>	0.83	28.6	27.00	1.53	0.75	31.30	17.70	0.81
Fe <sub>2</sub> O <sub>3</sub>	7.54	0.67	1.20	44.60	50.20	13.30	32.20	56.50
FeO	0.36	1.56	1.61	3.28	1.23	0.62	4.94	0.43
MnO	<0.05	0.05	0.06	0.25	0.15	0.05	1.21	0.17
MgO	<0.05	3.68	4.67	<0.05	<0.05	0.71	5.34	<0.05
CaO	<0.05	15.10	12.70	0.89	<0.05	0.91	1.48	<0.05
Na <sub>2</sub> O	<0.05	1.83	2.14	<0.05	<0.05	1.12	0.22	<0.05
K <sub>2</sub> O	0.09	0.24	0.92	<0.05	0.07	7.06	3.44	<0.05
P <sub>2</sub> O <sub>5</sub>	<0.05	<0.05	<0.05	<0.05	0.05	0.42	1.09	0.27
LOI	0.76	1.31	3.08	2.02	1.01	4.85	5.60	1.79
S	0.03	0.18	0.17	<0.01	0.01	0.05	<0.01	0.01
C	nd	nd	nd	0.03	0.03	nd	0.03	0.03
-O=	0.02	0.09	0.08	<0.01	0.01	0.02	<0.01	0.01
Others	0.13	0.13	0.19	0.05	0.12	0.55	0.25	0.03
<b>Total</b>	<b>99.1</b>	<b>100</b>	<b>100.1</b>	<b>99.3</b>	<b>99.7</b>	<b>99.6</b>	<b>99.6</b>	<b>99.6</b>
	<b>Parts per million</b>							
Au	0.05	0.08	0.12	0.07	0.06	0.07	0.06	0.07
Ag	<5	<5	<5	<5	<5	<5	<5	<5
As	<4	<4	<4	<4	<4	<4	<4	<4
Ba	596	15	162	204	883	2 829	349	38
Bi	118	<4	<4	7	<4	5	<4	<4
Cd	<5	<5	<5	<5	<5	<5	<5	<5
Ce	<6	<6	<6	11	<6	121	174	9
Co	nd	nd	nd	nd	nd	nd	nd	nd
Cr	14	88	110	17	10	186	163	15
Cu	117	317	602	<4	19	36	129	46
Ga	3	17	14	<3	<3	28	25	<3
Ge	<3	<3	<3	6	5	3	4	5
La	6	<5	<5	7	<5	73	113	5
Li	<6	<6	11	<6	<6	170	74	<6
Mn	<380	387	465	1 947	1 162	387	9 373	1 317
Mo	<6	<6	<6	<6	<6	<6	<6	<6
Nb	<7	<7	<7	<7	<7	19	9	<7
Ni	<3	225	233	23	21	18	116	23
Pb	71	10	14	15	<4	36	6	8
Rb	5	3	15	<2	2	254	142	<2
Sb	<4	<4	<4	<4	<4	<4	<4	<4
Sc	3	6	7	2	<2	17	27	<2
Sn	<4	<4	<4	<4	<4	6	7	<4
Sr	10	220	212	38	<2	222	28	13
Ta	<5	<5	<5	<5	<5	6	<5	<5
Te	<6	<6	<6	<6	<6	<6	<6	<6
Th	10	<2	<2	3	<2	33	25	<2
U	<2	<2	<2	<2	<2	4	2	<2
V	84	23	31	29	24	146	242	23
W	nd	nd	nd	nd	nd	nd	nd	nd
Y	2	<2	2	10	5	35	46	9
Zn	4	15	25	44	24	24	159	28
Zr	31	36	38	22	14	230	87	5

## Appendix 1 (continued)

GSWA no.	Whole rock and trace element analysis						
	112370	112371	112374	112375	112380	112387	112398
Rock type	breccia	breccia	breccia	breccia	conglomerate	conglomerate	meta-breccia
Latitude	22°34'34"	22°35'00"	22°34'16"	22°34'04"	22°30'56"	22°31'50"	22°31'05"
Longitude	122°10'48"	122°10'57"	122°10'43"	122°11'45"	122°09'15"	122°09'24"	122°05'54"
	<b>Percent</b>						
SiO <sub>2</sub>	81.10	71.80	61.40	73.20	93.30	55.00	46.50
TiO <sub>2</sub>	0.22	0.49	0.05	0.91	0.06	0.18	0.09
Al <sub>2</sub> O <sub>3</sub>	8.23	9.83	17.00	8.38	2.82	5.68	1.75
Fe <sub>2</sub> O <sub>3</sub>	2.31	7.55	4.31	7.08	0.28	21.00	48.2
FeO	0.19	0.31	<0.10	0.60	0.14	0.33	0.51
MnO	<0.05	<0.05	0.07	0.06	<0.05	<0.05	0.05
MgO	0.12	0.3	0.11	1.41	<0.05	2.68	<0.05
CaO	0.12	0.21	0.63	0.15	<0.05	3.44	0.05
Na <sub>2</sub> O	<0.05	<0.05	0.28	<0.05	<0.05	0.57	<0.05
K <sub>2</sub> O	6.37	7.78	14.40	5.34	2.26	2.72	0.05
P <sub>2</sub> O <sub>5</sub>	0.07	0.11	<0.05	0.17	<0.05	<0.05	0.18
LOI	0.71	1.23	1.17	1.84	0.22	7.37	1.72
S	<0.01	0.02	<0.01	<0.01	0.01	0.06	0.02
C	nd	nd	nd	nd	0.05	ND	0.05
-O=	<0.01	0.01	<0.01	<0.01	0.01	0.03	0.01
Others	0.23	0.23	0.43	0.41	0.22	0.23	0.04
<b>Total</b>	<b>99.7</b>	<b>99.9</b>	<b>99.9</b>	<b>99.6</b>	<b>99.4</b>	<b>99.2</b>	<b>99.2</b>
	<b>Parts per million</b>						
Au	0.07	0.07	0.06	0.05	0.06	0.06	0.07
Ag	<5	<5	<5	<5	<5	<5	<5
As	<4	<4	<4	<4	<4	<4	<4
Ba	989	875	3 285	627	1 713	665	56
Bi	<4	<4	<4	<4	<4	<4	<4
Cd	<5	<5	<5	7	<5	<5	<5
Ce	200	252	7	105	30	273	140
Co	nd	nd	nd	nd	ND	nd	nd
Cr	18	48	<4	20	17	28	21
Cu	<4	<4	<4	13	<4	<4	21
Ga	5	7	6	11	<3	7	4
Ge	<3	<3	<3	<3	<3	<3	3
La	153	173	9	779	16	102	7
Li	29	14	<6	54	<6	<6	nd
Mn	<380	<380	542	465	<380	<380	387
Mo	<6	<6	<6	<6	<6	<6	<6
Nb	<7	<7	<7	8	<7	8	<7
Ni	4	8	<3	17	<3	7	17
Pb	14	17	11	16	5	11	75
Rb	217	237	304	193	54	61	<2
Sb	<4	<4	<4	<4	<4	<4	<4
Sc	4	8	<2	10	<2	2	nd
Sn	<4	<4	<4	<4	<4	<4	<4
Sr	91	45	60	37	61	156	9
Ta	<5	<5	<5	<5	<5	<5	<5
Te	<6	<6	<6	<6	<6	<6	<6
Th	11	38	7	38	8	8	2
U	3	5	3	7	3	3	<2
V	27	59	62	131	8	354	28
W	nd	nd	nd	nd	nd	nd	nd
Y	53	22	15	174	40	64	22
Zn	7	14	5	42	7	<3	46
Zr	107	123	41	142	24	66	21

## Appendix 1 (continued)

GSWA no.	<i>Trace element analysis only</i>							
	106941	106947	106948	106960	106962	106968	106971	106977
Rock type	<i>gossan</i>	<i>gossan</i>	<i>meta-BIF</i>	<i>meta-BIF</i>	<i>gossan</i>	<i>meta-BIF</i>	<i>quartz vein</i>	<i>gossan</i>
Latitude	22°37'26"	22°38'59"	22°38'59"	22°40'01"	22°40'31"	22°41'36"	22°40'51"	22°40'18"
Longitude	122°19'07"	122°20'47"	122°20'47"	122°21'28"	122°21'44"	122°23'45"	122°25'50"	122°26'39"
	<b>Percent</b>							
Fe <sub>2</sub> O <sub>3</sub>	nd	nd	nd	nd	nd	nd	nd	nd
	<b>Parts per million</b>							
Au	0.06	0.06	0.06	0.06	0.06	0.08	0.07	0.06
Ag	nd	nd	nd	nd	nd	nd	nd	nd
As	8	<4	<4	<4	<4	<4	<4	5
Ba	243	96	154	382	802	1 923	383	172
Bi	<4	<4	<4	7	<4	<4	<4	<4
Cd	<5	<5	<5	<5	<5	<5	<5	<5
Ce	48	209	<6	377	120	11	<6	<6
Co	nd	nd	nd	nd	nd	nd	nd	nd
Cr	15	95	10	39	21	<4	8	11
Cu	124	58	<4	5	<4	<4	5	54
Ga	3	<3	3	3	<3	<3	<3	3
Ge	<3	<3	<3	9	10	4	<3	3
La	31	51	<5	131	51	<5	<5	<5
Li	<6	<6	<6	6	7	<6	<6	<6
Mn	nd	nd	nd	nd	nd	nd	nd	nd
Mo	<6	<6	6	7	<6	<6	11	<6
Nb	<7	<7	<7	<7	<7	<7	<7	<7
Ni	197	141	4	16	11	5	3	59
Pb	75	37	<4	8	10	<4	4	8
Rb	4	5	<2	5	<2	<2	5	<2
Sb	<4	<4	<4	<4	<4	<4	<4	<4
Sc	26	17	<2	7	3	<2	<2	35
Sn	5	<4	<4	<4	<4	<4	<4	<4
Sr	26	8	20	156	48	15	30	20
Ta	<5	<5	<5	<5	<5	<5	<5	<5
Te	<6	<6	<6	<6	<6	<6	6	<6
Th	2	3	2	26	2	3	2	<2
U	9	4	<2	7	2	<2	<2	3
V	72	41	24	95	76	23	17	300
W	nd	nd	nd	nd	nd	nd	nd	nd
Y	42	27	2	59	26	8	<2	45
Zn	210	145	10	76	12	10	3	164
Zr	21	26	14	80	21	<5	16	37

## Appendix 1 (continued)

GSWA no.	<i>Trace element analysis only</i>							
	106981	106988	106990	106991	106998	106999	107000	110057
Rock type	<i>gossan</i>	<i>gossan</i>	<i>gossan</i>	<i>meta-BIF</i>	<i>gossan</i>	<i>meta-BIF</i>	<i>gossan</i>	<i>gossan</i>
Latitude	22°40'57"	22°38'08"	22°38'24"	22°38'26"	22°39'00"	22°39'00"	22°38'00"	22°36'02"
Longitude	122°26'23"	122°27'20"	122°27'34"	122°27'44"	122°28'43"	122°28'37"	122°28'38"	122°22'05"
Fe <sub>2</sub> O <sub>3</sub>	nd	nd	nd	nd	nd	nd	nd	17.00
	<b>Percent</b>							
	<b>Parts per million</b>							
Au	0.04	0.03	0.05	0.04	0.04	0.04	0.04	0.01
Ag	nd	nd	nd	nd	nd	nd	nd	8
As	<4	51	31	<4	6	<4	<4	<4
Ba	121	42	117	45	914	111	264	162
Bi	<4	<4	<4	<4	<4	<4	<4	<4
Cd	<5	<5	<5	<5	<5	<5	<5	<5
Ce	19	9	57	6	48	96	62	132
Co	nd	nd	nd	nd	nd	nd	nd	11
Cr	13	17	13	11	10	58	143	nd
Cu	63	55	155	<4	62	709	552	38
Ga	<3	3	<3	<3	<3	6	4	6
Ge	<3	<3	3	9	<3	3	3	<3
La	13	8	24	<5	61	59	40	72
Li	<6	<6	<6	<6	<6	<6	<6	<6
Mn	nd	nd	nd	nd	nd	nd	nd	52
Mo	<6	9	<6	<6	<6	<6	<6	14
Nb	<7	<7	<7	<7	<7	8	<7	<7
Ni	4	30	55	25	373	99	111	38
Pb	<4	194	118	12	19	126	25	52
Rb	4	<2	<2	<2	2	<2	5	9
Sb	<4	<4	4	<4	<4	<4	<4	<4
Sc	10	<2	5	4	17	29	45	17
Sn	<4	<4	<4	<4	<4	<4	<4	<4
Sr	4	6	102	29	19	18	9	16
Ta	<5	<5	<5	<5	<5	<5	<5	<5
Te	<6	<6	<6	<6	<6	<6	<6	6
Th	3	<2	2	<2	<2	12	5	8
U	<2	5	<2	<2	<2	8	3	11
V	21	86	49	17	318	70	1 486	67
W	nd	nd	nd	nd	nd	nd	nd	<4
Y	3	12	35	8	252	48	40	30
Zn	6	823	448	107	390	202	242	40
Zr	13	11	31	10	12	122	38	44

## Appendix 1 (continued)

GSWA no.	<i>Trace element analysis only</i>							
	110058 gossan	110059 quartz vein	110060 gossan	110061 quartz vein	110062 quartz vein	110063 ferruginous quartz vein	110064 quartz vein	110067 quartz vein
Latitude	22°36'02"	22°35'42"	22°35'40"	22°35'40"	22°35'43"	22°35'43"	22°35'48"	22°35'52"
Longitude	122°22'05"	122°22'00"	122°21'59"	122°21'59"	122°22'05"	122°22'05"	122°22'15"	122°22'15"
	<b>Percent</b>							
Fe <sub>2</sub> O <sub>3</sub>	55.10	1.03	60.20	1.36	1.67	15.00	2.29	0.96
	<b>Parts per million</b>							
Au	0.02	0.01	0.01	0.01	0.01	0.04	0.01	0.21
Ag	<5	<6	<5	<6	<6	8	<6	<6
As	10	<4	4	<4	<4	<4	<4	<4
Ba	169	<11	2 656	26	12	49	111	<11
Bi	<4	<4	<4	<4	<4	<4	<4	<4
Cd	<5	<2	<5	2	<2	<2	<2	<2
Ce	90	<6	24	6	20	8	14	<6
Co	25	<3	39	<3	<3	6	<3	<3
Cr	nd	nd	nd	nd	nd	nd	nd	nd
Cu	109	<4	41	18	4	34	11	<4
Ga	4	<3	6	<3	<3	<3	<3	<3
Ge	3	<3	<3	<3	<3	<3	<3	<3
La	105	<5	18	<5	11	<5	12	<5
Li	<6	<6	<6	<6	<6	<6	<6	<6
Mn	132	12	231	32	18	183	38	23
Mo	<6	<2	<6	<2	<2	11	<2	<2
Nb	<7	<7	<7	<7	<7	<7	<7	<7
Ni	144	<3	79	4	4	34	8	3
Pb	48	<4	<4	4	19	27	9	<4
Rb	4	<2	<2	<2	<2	<2	<2	<2
Sb	<4	<4	<4	<4	<4	<4	<4	<4
Sc	12	<2	15	<2	<2	16	2	<2
Sn	<4	<4	<4	<4	<4	<4	<4	<4
Sr	22	<2	32	2	4	11	7	2
Ta	<5	<5	<5	<5	<5	<5	<5	<5
Te	<6	<1	<6	9	<1	2	2	1
Th	6	<2	3	<2	<2	<2	<2	<2
U	4	<2	9	<2	<2	10	<2	<2
V	93	4	224	15	8	114	15	3
W	17	<4	10	<4	<4	<4	<4	<4
Y	80	<2	40	<2	<2	7	4	2
Zn	240	<3	106	3	4	52	3	4
Zr	22	<5	10	<5	<5	7	<5	<5

## Appendix 1 (continued)

GSWA no.	<i>Trace element analysis only</i>							
	110070	110072	110077	110078	110080	110083	110085	110087
Rock type	quartz vein	gossan	gossan	ferruginous quartz vein	gossan	gossan	gossan	quartz vein
Latitude	22°35'20"	22°35'21"	22°34'07"	22°34'00"	22°34'03"	22°32'18"	22°32'18"	22°32'11"
Longitude	122°22'13"	122°21'21"	122°22'20"	122°20'54"	122°20'50"	122°21'26"	122°21'26"	122°18'33"
	<b>Percent</b>							
Fe <sub>2</sub> O <sub>3</sub>	3.46	77.6	74.9	8.09	77.10	77.40	61.30	2.23
	<b>Parts per million</b>							
Au	0.03	0.01	0.01	0.02	0.01	0.01	<0.01	0.01
Ag	<6	<5	<5	7	<5	<5	<5	<6
As	<4	<4	16	<4	14	<4	<4	<4
Ba	32	80	392	1 019	227	708	390	60
Bi	<4	<4	<4	<4	<4	<4	<4	<4
Cd	2	<5	<5	<5	<5	<5	<5	<2
Ce	<6	<6	42	94	43	109	20	10
Co	<3	39	41	8	18	55	24	<3
Cr	nd	nd	nd	nd	nd	nd	nd	nd
Cu	9	46	28	17	<4	47	41	<4
Ga	<3	3	<3	<3	3	<3	7	<3
Ge	<3	<3	<3	<3	5	3	3	<3
La	<5	<5	50	37	15	32	8	7
Li	<6	<6	<6	<6	<6	<6	<6	<6
Mn	15	104	319	979	67	248	403	282
Mo	<2	<6	<6	<6	<6	<6	<6	<2
Nb	<7	<7	<7	<7	<7	<7	<7	<7
Ni	12	60	176	149	214	218	164	6
Pb	<4	5	139	<4	28	16	4	<4
Rb	2	<2	<2	<2	<2	7	15	2
Sb	<4	<4	<4	<4	<4	<4	<4	<4
Sc	<2	34	30	<2	3	4	4	<2
Sn	<4	<4	<4	<4	<4	<4	<4	<4
Sr	2	8	21	39	20	41	26	4
Ta	<5	<5	<5	<5	<5	<5	<5	<5
Te	1	11	<6	<6	<6	<6	<6	<1
Th	<2	2	2	<2	5	<2	19	<2
U	<2	3	6	4	7	6	14	2
V	10	337	218	22	55	38	70	6
W	<4	6	17	<4	24	19	12	<4
Y	2	12	35	33	25	38	20	3
Zn	15	64	244	19	5	258	122	5
Zr	7	14	15	<5	8	26	47	<5

## Appendix 1 (continued)

GSWA no.	<i>Trace element analysis only</i>							
	111803 ferruginous quartz vein	111804 quartz vein	111805 quartz vein	111809 gossan	111810 gossan	111818 gossan	111819 gossan	111821 gossan
Latitude	22°30'30"	22°30'30"	22°30'30"	22°31'14"	22°31'14"	22°32'12"	22°32'12"	22°35'32"
Longitude	122°23'20"	122°23'20"	122°23'20"	122°24'25"	122°24'25"	122°25'17"	122°25'17"	122°24'50"
	<b>Percent</b>							
Fe <sub>2</sub> O <sub>3</sub>	27.60	5.29	5.73	44.60	73.80	49.60	34.30	10.90
	<b>Parts per million</b>							
Au	0.05	0.03	0.05	0.03	0.01	0.05	0.01	0.02
Ag	<6	<6	<6	<5	33	8	17	5
As	11	<4	5	16	12	5	7	<4
Ba	334	556	334	1 015	205	580	392	718
Bi	<4	<4	<4	<4	<4	<4	<4	<4
Cd	2	<2	<2	<5	<5	<5	<5	<5
Ce	27	9	<6	38	22	8	12	281
Co	6	4	8	64	35	6	<3	58
Cr	nd	nd	nd	nd	nd	nd	nd	nd
Cu	40	12	26	32	32	<4	<4	23
Ga	<3	<3	<3	<3	4	<3	3	<3
Ge	3	<3	<3	3	<3	<3	5	<3
La	5	<5	<5	18	8	12	6	242
Li	<6	9	<6	<6	<6	<6	<6	11
Mn	1 835	135	360	5 517	1 228	96	8	414
Mo	<2	<2	2	<6	<6	<6	<6	<6
Nb	<7	<7	<7	<7	<7	<7	<7	<7
Ni	57	13	18	209	66	29	15	198
Pb	8	4	<4	13	7	<4	5	8
Rb	5	<2	14	12	13	13	16	<2
Sb	<4	<4	<4	<4	<4	<4	<4	<4
Sc	3	<2	<2	<2	<2	<2	2	2
Sn	<4	<4	<4	<4	5	<4	<4	<4
Sr	<2	8	6	44	22	7	5	25
Ta	<5	<5	<5	<5	<5	<5	<5	<5
Te	2	1	<1	<6	<6	<6	<6	<6
Th	4	2	2	8	3	5	7	<2
U	13	<2	2	5	<2	<2	3	11
V	5	13	5	36	24	21	50	33
W	6	<4	<4	15	6	5	<4	5
Y	50	7	5	24	14	12	14	124
Zn	37	15	21	82	70	15	11	6
Zr	976	31	5	50	43	20	31	5



## Appendix 1 (continued)

GSWA no.	<i>Trace element analysis only</i>							
	111822	111825	111828	111829	111830	111834	111835	111839
Rock type	<i>gossan</i>	<i>silcrete</i>	<i>quartz vein</i>	<i>gossan</i>	<i>gossan</i>	<i>quartz vein</i>	<i>quartz vein</i>	<i>quartz vein</i>
Latitude	22°35'32"	22°36'28"	22°35'22"	22°35'22"	22°35'22"	22°34'35"	22°34'06"	22°34'02"
Longitude	122°24'50"	122°25'00"	122°20'03"	122°20'03"	122°20'03"	122°18'47"	122°18'27"	122°17'34"
	<b>Percent</b>							
Fe <sub>2</sub> O <sub>3</sub>	63.50	4.42	4.36	57.10	43.30	3.46	3.29	3.73
	<b>Parts per million</b>							
Au	0.02	0.01	0.05	0.01	<0.01	0.04	0.04	0.01
Ag	35	<5	6	34	<5	<6	<6	<6
As	6	5	<4	<4	<4	<4	<4	<4
Ba	985	943	68	198	250	137	17	<11
Bi	<4	<4	<4	<4	<4	178	8	<4
Cd	<5	<5	<2	<5	<5	2	<2	2
Ce	<6	32	26	16	87	12	<6	<6
Co	60	8	12	21	10	10	25	5
Cr	nd	nd	nd	nd	nd	nd	nd	nd
Cu	68	13	2 473	227	228	104	236	6
Ga	<3	12	<3	5	3	18	<3	<3
Ge	3	<3	<3	3	4	<3	<3	<3
La	8	15	12	<5	35	8	<5	<5
Li	<6	55	<6	<6	<6	<6	<6	<6
Mn	799	321	18	152	150	274	73	29
Mo	<6	<6	<2	<6	<6	125	2	<2
Nb	<7	9	<7	<7	<7	<7	<7	<7
Ni	524	20	29	161	53	21	10	13
Pb	61	12	37	4	18	21	5	<4
Rb	32	24	<2	18	<2	15	2	<2
Sb	<4	<4	<4	<4	<4	<4	<4	<4
Sc	<2	7	<2	8	<2	7	<2	<2
Sn	<4	<4	<4	<4	<4	<4	<4	<4
Sr	28	62	4	10	8	50	<2	<2
Ta	<5	<5	<5	<5	<5	<5	<5	<5
Te	<6	<6	<1	<6	<6	8	4	2
Th	2	12	<2	10	3	25	<2	<2
U	6	2	14	10	32	<2	2	<2
V	822	103	9	91	41	79	7	3
W	39	<4	<4	16	7	<4	<4	<4
Y	25	12	8	23	30	6	2	<2
Zn	85	15	13	152	47	77	5	13
Zr	11	267	5	105	12	99	<5	<5

## Appendix 1 (continued)

GSWA no.	<i>Trace element analysis only</i>							
	111840. gossan	111841 ferruginous quartz vein	111842 quartz vein	111845 gossan	111846 ferruginous quartz vein	111847 gossan	111848 ferruginous quartz vein	111850 gossan
Latitude	22°35'12"	22°35'03"	22°35'03"	22°34'10"	22°34'10"	22°34'13"	22°34'13"	22°33'55"
Longitude	122°19'17"	122°19'10"	122°19'10"	122°19'55"	122°19'55"	122°19'53"	122°19'53"	122°19'45"
	<b>Percent</b>							
Fe <sub>2</sub> O <sub>3</sub>	50.90	41.20	5.13	72.50	42.20	75.40	5.19	13.20
	<b>Parts per million</b>							
Au	0.01	0.02	0.02	0.01	0.07	0.02	0.75	4.07
Ag	<5	<6	<6	29	<6	36	<5	9
As	5	<4	<4	<4	<4	<4	<4	4
Ba	409	266	24	332	76	35	<11	78
Bi	<4	<4	<4	<4	<4	<4	<4	<4
Cd	<5	<2	<2	<5	<2	<5	<5	<5
Ce	<6	70	<6	24	14	432	<6	<6
Co	16	22	4	18	6	52	6	13
Cr	nd	nd	nd	nd	nd	nd	nd	nd
Cu	171	101	21	285	305	219	26	658
Ga	<3	4	<3	3	<3	3	<3	<3
Ge	<3	3	<3	<3	3	3	<3	<3
La	<5	33	<5	23	6	78	<5	<5
Li	<6	<6	<6	<6	<6	<6	<6	<6
Mn	93	597	63	413	465	184	27	69
Mo	<6	4	2	<6	<2	<6	<6	8
Nb	<7	<7	<7	<7	<7	<7	<7	<7
Ni	72	208	16	159	283	708	63	8
Pb	11	6	19	64	93	115	9	10
Rb	<2	10	<2	5	<2	<2	<2	<2
Sb	<4	<4	<4	<4	<4	<4	<4	<4
Sc	16	5	<2	8	3	5	<2	<2
Sn	<4	<4	<4	<4	<4	4	<4	4
Sr	8	19	6	13	5	<2	<2	8
Ta	<5	<5	<5	<5	<5	<5	<5	<5
Te	<6	2	3	<6	<1	<6	<6	51
Th	<2	7	13	4	<2	2	<2	<2
U	3	18	4	7	7	9	3	<2
V	213	102	31	99	102	41	14	10
W	9	17	<4	17	25	53	<4	<4
Y	42	41	10	9	10	42	2	<2
Zn	58	171	21	48	80	125	18	17
Zr	<5	36	10	25	<5	26	5	<5

## Appendix 1 (continued)

GSWA no.	<i>Trace element analysis only</i>							
	111851 <i>gossan</i>	111873 <i>metagabbro</i>	111874 <i>metadiorite</i>	111875 <i>metagabbro</i>	111876 <i>ultramafic</i>	111877 <i>meta-BIF</i>	111878 <i>gossan</i>	111879 <i>gossan</i>
<i>Latitude</i>	22°33'55"	22°35'13"	22°35'13"	22°35'13"	22°35'13"	22°31'35"	22°31'35"	22°31'35"
<i>Longitude</i>	122°19'45"	122°26'05"	122°26'05"	122°26'05"	122°26'05"	122°28'43"	122°28'48"	122°28'48"
	<b>Percent</b>							
Fe <sub>2</sub> O <sub>3</sub>	17.60	6.99	4.00	8.99	12.00	76.90	49.10	51.90
	<b>Parts per million</b>							
Au	0.74	0.02	0.01	0.01	0.01	0.01	0.01	0.01
Ag	11	<2	<2	<2	<2	<2	<2	<2
As	5	<4	<4	<4	<4	6	6	<4
Ba	168	492	82	200	552	19	448	<11
Bi	4	<4	<4	<4	<4	<4	<4	<4
Cd	<5	<5	<5	<5	<5	<5	<5	<5
Ce	<6	<6	<6	<6	<6	19	82	26
Co	10	nd	nd	nd	nd	nd	nd	nd
Cr	nd	613	97	117	159	4	24	<4
Cu	935	30	43	7	11	28	647	78
Ga	<3	10	14	10	8	<3	<3	4
Ge	<3	<3	<3	<3	<3	3	3	3
La	<5	<5	<5	<5	<5	16	64	11
Li	<6	nd	nd	nd	nd	nd	nd	nd
Mn	53	1 105	639	1 029	1 073	868	50 710	1 540
Mo	11	<2	<2	<2	<2	<2	5	2
Nb	<7	<7	<7	<7	<7	21	16	21
Ni	6	247	138	608	712	14	56	59
Pb	<4	<4	13	6	4	<4	8	6
Rb	<2	11	7	2	2	<2	<2	<2
Sb	<4	<4	<4	<4	<4	<4	<4	<4
Sc	<2	nd	nd	nd	nd	nd	nd	nd
Sn	<4	<4	<4	<4	<4	8	8	<4
Sr	12	98	160	61	36	25	152	63
Ta	<5	<5	<5	<5	<5	<5	<5	<5
Te	17	<6	<6	<6	<6	<6	<6	7
Th	<2	2	<2	<2	<2	<2	3	<2
U	4	<2	<2	<2	<2	<2	<2	<2
V	37	76	62	28	40	11	50	12
W	<4	nd	nd	nd	nd	nd	nd	nd
Y	<2	5	5	2	3	13	20	27
Zn	10	49	32	62	64	35	165	75
Zr	<5	33	53	18	12	11	50	11

## Appendix 1 (continued)

GSWA no. Rock type	<i>Trace element analysis only</i>							
	111880 quartz vein	111881 quartz vein	111882 quartz vein	111883 quartz vein	111884 felsic rock	111885 quartz vein	111886 quartz vein	111887 quartz vein
Latitude	22°31'35"	22°31'35"	22°31'35"	22°31'35"	22°31'21"	22°34'44"	22°34'46"	22°34'46"
Longitude	122°28'48"	122°28'48"	122°28'48"	122°28'48"	122°29'42"	122°20'50"	122°20'51"	122°20'51"
	<b>Percent</b>							
Fe <sub>2</sub> O <sub>3</sub>	3.00	1.0	<0.07	<0.07	5.00	0.44	0.76	0.69
	<b>Parts per million</b>							
Au	0.01	0.01	0.01	0.01	0.01	0.02	0.02	<0.01
Ag	<2	<2	<2	<2	<2	<5	<5	<5
As	<4	<4	<4	<4	<4	<4	<4	<4
Ba	<11	26	12	16	52	28	26	52
Bi	<4	<4	<4	<4	<4	<4	<4	<4
Cd	<5	<5	<5	<5	<5	<5	<5	<5
Ce	<6	7	<6	<6	<6	<6	<6	92
Co	nd	nd	nd	nd	nd	nd	nd	nd
Cr	<4	<4	<4	<4	2 666	13	23	17
Cu	<4	<4	<4	<4	<4	<4	<4	<4
Ga	<3	<3	<3	<3	<3	<3	<3	<3
Ge	<3	<3	<3	<3	<3	<3	<3	<3
La	<5	<5	<5	<5	<5	<5	<5	32
Li	nd	nd	nd	nd	nd	nd	nd	nd
Mn	249	13 560	44	1 084	579	nd	nd	nd
Mo	<2	<2	<2	<2	<2	<6	<6	<6
Nb	<7	<7	<7	<7	<7	<7	<7	<7
Ni	5	8	5	5	2 203	5	6	5
Pb	<4	<4	4	<4	<4	<4	<4	23
Rb	<2	<2	3	<2	<2	<2	<2	<2
Sb	<4	<4	<4	<4	<4	<4	<4	<4
Sc	nd	nd	nd	nd	nd	nd	nd	nd
Sn	<4	<4	<4	<4	<4	<4	<4	<4
Sr	7	32	<2	2	2	<2	<2	22
Ta	<5	<5	<5	<5	<5	<5	<5	<5
Te	<6	<6	<6	<6	<6	<6	<6	<6
Th	<2	<2	2	<2	2	<2	<2	5
U	<2	<2	<2	<2	<2	<2	<2	<2
V	<3	<3	<3	<3	55	<3	21	33
W	nd	nd	nd	nd	nd	nd	nd	nd
Y	2	3	<2	<2	<2	<2	<2	5
Zn	6	13	<3	3	43	<3	<3	<3
Zr	<5	10	<5	<5	<5	<5	<5	11

## Appendix 1 (continued)

GSWA no. Rock type	<i>Trace element analysis only</i>							
	111888 quartz vein	111889 ultramafic	111890 quartzite	111891 quartz vein	111892 quartz vein	111893A gossan	111893B quartz vein	111893C quartz vein
Latitude	22°34'46"	22°30'28"	22°34'50"	22°34'50"	22°34'50"	22°34'57"	22°34'57"	22°34'57"
Longitude	122°20'51"	122°28'50"	122°20'55"	122°20'55"	122°20'55"	122°20'54"	122°20'54"	122°20'54"
	<b>Percent</b>							
Fe <sub>2</sub> O <sub>3</sub>	1.09	17.30	4.18	1.22	3.98	25.20	0.56	0.90
	<b>Parts per million</b>							
Au	<0.01	0.01	0.01	<0.01	0.01	0.01	0.02	0.01
Ag	<5	14	<5	<5	<5	18	<5	<5
As	<4	<4	<4	<4	<4	<4	<4	<4
Ba	31	83	594	498	35	321	<11	<11
Bi	<4	<4	<4	<4	<4	<4	<4	<4
Cd	<5	<5	<5	<5	<5	<5	<5	<5
Ce	<6	11	<6	10	<6	130	<6	<6
Co	nd	nd	nd	nd	nd	nd	nd	nd
Cr	18	1 095	44	13	9	89	8	9
Cu	<4	105	21	<4	<4	10	<4	<4
Ga	<3	14	3	7	19	26	<3	<3
Ge	<3	<3	<3	<3	<3	<3	<3	<3
La	<5	5	<5	<5	<5	44	<5	<5
Li	nd	nd	nd	nd	nd	nd	nd	nd
Mn	nd	nd	nd	nd	nd	nd	nd	nd
Mo	<6	8	<6	<6	<6	7	<6	<6
Nb	<7	<7	<7	<7	<7	<7	<7	<7
Ni	7	411	15	6	11	73	6	4
Pb	<4	<4	<4	<4	<4	6	<4	<4
Rb	<2	3	<2	12	<2	<2	<2	<2
Sb	<4	<4	<4	<4	<4	<4	<4	<4
Sc	nd	nd	nd	nd	nd	nd	nd	nd
Sn	<4	<4	<4	<4	<4	7	<4	<4
Sr	2	187	9	3	12	33	<2	<2
Ta	<5	<5	<5	<5	<5	<5	<5	<5
Te	<6	<6	<6	<6	<6	<6	<6	<6
Th	<2	<2	4	5	<2	9	<2	<2
U	<2	<2	<2	3	<2	5	<2	<2
V	15	299	194	14	37	574	<3	3
W	nd	nd	nd	nd	nd	nd	nd	nd
Y	<2	12	2	16	<2	21	<2	<2
Zn	5	127	13	3	22	57	<3	<3
Zr	<5	68	18	71	7	34	<5	<5

## Appendix 1 (continued)

GSWA no.	<i>Trace element analysis only</i>							
	111893D	111893E	111894A	111894B	111894C	111895A	111895B	111895C
Rock type	quartz vein	quartz vein	quartz vein	ironstone	quartz vein	gossan	quartz vein	quartz vein
Latitude	22°34'57"	22°34'57"	22°35'26"	22°35'26"	22°35'26"	22°35'16"	22°35'16"	22°35'16"
Longitude	122°20'54"	122°20'54"	122°21'17"	122°21'17"	122°21'17"	122°21'07"	122°21'07"	122°21'07"
	<b>Percent</b>							
Fe <sub>2</sub> O <sub>3</sub>	0.92	1.34	11.70	62.20	0.99	25.00	1.32	0.80
	<b>Parts per million</b>							
Au	0.01	0.01	0.01	0.02	<0.01	<0.01	<0.01	<0.01
Ag	<5	<5	8	11	<5	17	<5	<5
As	<4	<4	<4	<4	<4	<4	<4	<4
Ba	21	28	243	1 887	27	135	13	50
Bi	<4	<4	<4	<4	<4	<4	<4	<4
Cd	<5	<5	<5	<5	<5	<5	<5	<5
Ce	24	9	46	38	<6	9	6	<6
Co	nd	nd	nd	nd	nd	nd	nd	nd
Cr	14	15	34	112	8	31	7	9
Cu	<4	<4	12	64	<4	57	<4	<4
Ga	<3	<3	<3	6	<3	4	<3	<3
Ge	<3	<3	<3	<3	<3	<3	<3	<3
La	6	5	30	40	<5	7	<5	<5
Li	nd	nd	nd	nd	nd	nd	nd	nd
Mn	nd	nd	nd	nd	nd	nd	nd	nd
Mo	<6	<6	<6	<6	<6	9	<6	<6
Nb	<7	<7	<7	<7	<7	<7	<7	<7
Ni	3	5	16	53	5	37	5	3
Pb	5	9	<4	6	<4	<4	<4	<4
Rb	<2	<2	<2	<2	<2	<2	<2	<2
Sb	<4	<4	<4	<4	<4	<4	<4	<4
Sc	nd	nd	nd	nd	nd	nd	nd	nd
Sn	<4	<4	<4	<4	<4	<4	<4	<4
Sr	7	7	21	35	2	35	<2	<2
Ta	<5	<5	<5	<5	<5	<5	<5	<5
Te	<6	<6	<6	<6	<6	<6	<6	<6
Th	<2	<2	<2	3	<2	<2	<2	<2
U	<2	<2	4	8	<2	4	<2	<2
V	<3	8	136	1 025	5	271	7	4
W	nd	nd	nd	nd	nd	nd	nd	nd
Y	<2	<2	4	13	<2	8	<2	<2
Zn	<3	5	19	68	<3	46	<3	<3
Zr	<5	<5	12	43	<5	16	<5	<5

## Appendix 1 (continued)

GSWA no.	<i>Trace element analysis only</i>							
	111895D	111895E	111895F	112306	112307	112308	112309	112314
Rock type	ironstone	quartz vein	quartz vein	quartz vein	quartz vein	ferruginous quartz vein	quartz vein	ferruginous quartz vein
Latitude	22°35'16"	22°35'16"	22°35'16"	22°33'27"	22°33'27"	22°34'33"	22°34'10"	22°32'55"
Longitude	122°21'07"	122°21'07"	122°21'07"	122°13'47"	122°13'47"	122°16'18"	122°17'08"	122°14'33"
	<b>Percent</b>							
Fe <sub>2</sub> O <sub>3</sub>	68.10	1.34	1.09	0.95	0.64	29.40	8.56	13.90
	<b>Parts per million</b>							
Au	<0.01	<0.01	<0.01	0.10	0.08	0.08	0.07	0.10
Ag	6	<5	<5	<5	<5	<5	<5	9
As	<4	<4	<4	<4	<4	6	<4	9
Ba	166	12	<11	33	<11	310	110	116
Bi	<4	<4	<4	<4	<4	<4	<4	4
Cd	<5	<5	<5	<5	<5	<5	<5	<5
Ce	28	56	<6	7	<6	<6	29	<6
Co	nd	nd	nd	<3	<3	479	4	10
Cr	110	11	8	nd	nd	nd	nd	nd
Cu	102	<4	<4	<4	6	817	95	207
Ga	4	<3	<3	<3	<3	<3	<3	3
Ge	<3	<3	<3	<3	<3	4	<3	<3
La	12	17	<5	5	<5	<5	11	<5
Li	nd	nd	nd	<6	<6	<6	<6	<6
Mn	nd	nd	nd	28	17	569	41	30
Mo	<6	<6	<6	<6	<6	<6	7	28
Nb	<7	<7	<7	<7	<7	<7	<7	<7
Ni	37	4	4	4	4	414	21	13
Pb	4	<4	<4	<4	<4	350	6	574
Rb	<2	<2	<2	3	<2	<2	3	2
Sb	<4	<4	<4	<4	<4	<4	<4	<4
Sc	nd	nd	nd	<2	<2	<2	5	<2
Sn	<4	<4	<4	<4	<4	<4	<4	<4
Sr	44	6	<2	4	<2	25	34	4
Ta	<5	<5	<5	<5	<5	<5	<5	<5
Te	<6	<6	<6	<6	<6	<6	<6	<6
Th	2	<2	<2	<2	<2	<2	2	2
U	3	<2	<2	<2	<2	<2	2	<2
V	346	3	<3	4	<3	184	9	16
W	nd	nd	nd	<4	<4	30	7	<4
Y	18	<2	<2	2	<2	5	20	<2
Zn	75	<3	<3	3	<3	148	21	47
Zr	76	<5	<5	<5	<5	<5	11	6

## Appendix 1 (continued)

GSWA no.	Trace element analysis only								
	112318	112320	112322	112328	112329	112337	112342	112343	112344
Rock type	quartz vein	quartz vein	gossan	gossan	gossan	quartz vein	quartz vein	quartz vein	quartz vein
Latitude	22°32'43"	22°32'44"	22°32'24"	22°32'12"	22°32'12"	22°32'47"	22°34'48"	22°34'48"	22°34'48"
Longitude	122°13'43"	122°13'23"	122°12'03"	122°11'52"	122°11'52"	122°10'15"	122°13'58"	122°13'58"	122°13'58"
	<b>Percent</b>								
Fe <sub>2</sub> O <sub>3</sub>	1.80	5.66	58.30	58.30	66.80	2.43	1.04	5.85	3.05
	<b>Parts per million</b>								
Au	0.08	0.10	0.07	0.07	0.07	0.08	0.08	0.07	0.07
Ag	<5	<5	<5	<5	<5	<5	<5	<5	<5
As	<4	<4	<4	<4	<4	<4	<4	4	<4
Ba	38	44	137	380	94	19	210	1 478	179
Bi	35	4	<4	<4	<4	<4	<4	<4	<4
Cd	<5	<5	<5	<5	<5	<5	<5	<5	<5
Ce	<6	<6	64	25	43	21	194	8	9
Co	21	13	10	8	32	<3	<3	64	<3
Cr	nd	nd	nd	nd	nd	nd	nd	nd	nd
Cu	132	125	39	360	810	<4	6	14	6
Ga	<3	<3	10	7	5	<3	<3	<3	3
Ge	3	<3	3	<3	3	<3	<3	<3	<3
La	<5	<5	37	11	25	11	89	<5	7
Li	<6	<6	<6	<6	<6	<6	51	<6	18
Mn	41	23	122	268	303	32	118	38	41
Mo	72	6	<6	<6	<6	<6	<6	6	<6
Nb	<7	<7	<7	<7	<7	<7	<7	<7	<7
Ni	10	13	21	71	237	8	4	11	5
Pb	45	5	5	5	13	6	14	10	5
Rb	<2	<2	<2	51	7	<2	4	<2	13
Sb	<4	<4	<4	<4	<4	<4	<4	<4	<4
Sc	<2	<2	50	6	6	<2	3	<2	4
Sn	<4	<4	<4	5	<4	<4	<4	<4	<4
Sr	3	<2	10	27	8	2	92	18	9
Ta	<5	<5	<5	<5	<5	<5	<5	<5	<5
Te	<6	<6	<6	<6	<6	<6	<6	<6	<6
Th	5	<2	<2	4	7	2	11	<2	5
U	<2	<2	6	4	14	<2	<2	9	3
V	7	<3	605	53	90	16	19	63	33
W	<4	<4	6	10	34	<4	<4	<4	<4
Y	<2	<2	24	32	56	6	18	<2	8
Zn	15	8	78	147	188	<3	3	3	3
Zr	<5	<5	67	40	49	<5	39	<5	62



## Appendix 1 (continued)

GSWA no.	Trace element analysis only						
	112345 quartz vein	112346 gossan	112347 quartz vein	112348 gossan	112349 quartz vein	112350 quartz vein	112351 gossan
Latitude	22°34'48"	22°34'47"	22°34'47"	22°34'40"	22°34'47"	22°34'47"	22°35'23"
Longitude	122°13'58"	122°13'44"	122°13'44"	122°13'28"	122°13'18"	122°13'18"	122°13'24"
	<b>Percent</b>						
Fe <sub>2</sub> O <sub>3</sub>	4.06	62.50	1.35	65.40	1.08	0.56	63.4
	<b>Parts per million</b>						
Au	0.09	0.07	0.08	0.07	0.07	0.07	0.07
Ag	<5	<5	<5	<5	<5	<5	<5
As	5	4	<4	<4	<4	<4	<4
Ba	233	520	858	1 341	98	16	36
Bi	<4	<4	<4	<4	16	<4	<4
Cd	<5	<5	<5	<5	<5	<5	<5
Ce	10	52	13	16	<6	<6	<6
Co	99	30	<3	31	7	<3	51
Cr	nd	nd	nd	nd	nd	nd	nd
Cu	12	30	5	448	39	<4	111
Ga	<3	5	6	3	<3	<3	14
Ge	<3	3	<3	<3	<3	<3	4
La	<5	31	7	16	<5	<5	<5
Li	<6	<6	19	<6	<6	<6	<6
Mn	20	390	76	243	44	16	1 390
Mo	<6	<6	<6	<6	<6	<6	<6
Nb	<7	<7	<7	<7	<7	<7	<7
Ni	14	91	5	132	6	5	279
Pb	16	44	7	41	7	<4	<4
Rb	<2	18	<2	2	<2	2	<2
Sb	<4	<4	<4	<4	<4	<4	<4
Sc	<2	6	<2	29	<2	<2	42
Sn	<4	<4	<4	<4	<4	<4	<4
Sr	13	325	39	39	5	2	47
Ta	<5	<5	<5	<5	<5	<5	6
Te	<6	<6	<6	<6	<6	<6	<6
Th	<2	4	<2	4	3	<2	<2
U	2	8	<2	15	<2	<2	<2
V	25	34	7	321	5	3	222
W	<4	9	<4	12	<4	<4	<4
Y	<2	21	2	31	<2	<2	19
Zn	3	237	5	159	6	<3	80
Zr	5	70	10	26	<5	<5	26

## Appendix 1 (continued)

GSWA no.	<i>Trace element analysis only</i>							
	112352	112353	112359	112360	112361	112366	112368	112376
Rock type	<i>gossan</i>	<i>quartz vein</i>	<i>quartz vein</i>	<i>quartz vein</i>	<i>ferruginous quartz vein</i>	<i>quartz vein</i>	<i>gossan</i>	<i>ferruginous quartz vein</i>
Latitude	22°35'47"	22°36'19"	22°34'46"	22°34'46"	22°34'46"	22°36'55"	22°36'10"	22°34'04"
Longitude	122°13'25"	122°14'17"	122°12'03"	122°12'03"	122°12'03"	122°11'05"	122°12'45"	122°11'45"
	<b>Percent</b>							
Fe <sub>2</sub> O <sub>3</sub>	48.30	1.14	0.84	1.66	9.88	7.36	75.70	10.30
	<b>Parts per million</b>							
Au	0.06	0.07	0.08	0.09	0.08	0.11	0.07	0.07
Ag	5	<5	<5	<5	5	<5	<5	<5
As	5	<4	<4	<4	5	<4	73	28
Ba	991	27	95	1011	191	46	160	199
Bi	<4	<4	<4	<4	<4	<4	<4	<4
Cd	<5	<5	<5	<5	<5	<5	<5	<5
Ce	50	<6	6	669	19	42	<6	<6
Co	30	<3	<3	<3	4	8	16	61
Cr	nd	nd	nd	nd	nd	nd	nd	nd
Cu	16	41	<4	4	12	17	90	11
Ga	19	<3	<3	<3	<3	8	10	6
Ge	3	<3	<3	<3	<3	<3	4	3
La	22	<5	<5	413	15	23	<5	<5
Li	<6	<6	<6	9	<6	13	<6	49
Mn	189	33	35	263	378	172	456	288
Mo	<6	<6	<6	<6	6	<6	<6	<6
Nb	8	<7	<7	<7	<7	<7	<7	<7
Ni	<3	6	5	7	8	15	<3	738
Pb	6	<4	<4	7	26	<4	<4	<4
Rb	63	<2	10	36	<2	64	6	7
Sb	5	<4	<4	<4	<4	<4	<4	<4
Sc	7	3	<2	<2	<2	<2	21	<2
Sn	<4	<4	<4	<4	<4	<4	<4	<4
Sr	92	2	10	41	7	5	85	33
Ta	<5	<5	<5	<5	<5	<5	<5	<5
Te	<6	<6	<6	<6	<6	<6	<6	<6
Th	2	2	3	14	4	10	<2	<2
U	<2	<2	<2	3	6	2	<2	<2
V	189	168	9	19	46	51	262	109
W	12	<4	<4	4	<4	<4	22	21
Y	15	6	<2	59	11	14	21	14
Zn	6	5	4	4	9	71	178	23
Zr	147	8	8	24	8	71	45	35

## Appendix 1 (continued)

GSWA no.	Trace element analysis only							
	112377	112378	112386	112394	112395	112401	112402	112403
Rock type	quartz vein	gossan	quartz vein	quartz vein	gossan	quartz vein	ferruginous quartz vein	gossan
Latitude	22°34'04"	22°34'04"	22°32'03"	22°26'33"	22°26'33"	22°32'03"	22°32'03"	22°32'03"
Longitude	122°11'45"	122°11'45"	122°09'29"	122°02'20"	122°02'20"	122°05'32"	122°05'32"	122°05'32"
	<b>Percent</b>							
Fe <sub>2</sub> O <sub>3</sub>	4.40	27.00	1.90	1.67	26.50	2.00	28.00	64.90
	<b>Parts per million</b>							
Au	0.07	0.07	0.07	0.07	0.12	0.01	0.01	<0.01
Ag	<5	<5	<5	<5	<5	<2	<2	<2
As	<4	<4	<4	<4	10	<4	<4	76
Ba	172	623	50	47	1 203	373	36	3 983
Bi	<4	<4	<4	<4	<4	<4	<4	<4
Cd	<5	<5	<5	<5	<5	<5	<5	<5
Ce	190	50	84	<6	<6	59	7	24
Co	<3	47	<3	5	25	nd	nd	nd
Cr	nd	nd	nd	nd	nd	36	170	5
Cu	4	6	5	61	909	<4	20	173
Ga	10	17	<3	<3	<3	<3	<3	3
Ge	<3	<3	<3	<3	5	<3	3	4
La	92	30	40	<5	6	45	<5	10
Li	42	33	<6	<6	<6	nd	nd	nd
Mn	38	315	120	26	42	21	<5	3 073
Mo	<6	<6	<6	<6	<6	<2	3	9
Nb	<7	7	<7	<7	<7	<7	14	<7
Ni	4	<3	6	13	262	10	66	172
Pb	7	24	4	36	13	23	11	7
Rb	<2	136	<2	<2	<2	24	<2	6
Sb	<4	<4	<4	<4	<4	<4	<4	<4
Sc	<2	15	<2	<2	<2	nd	nd	nd
Sn	<4	<4	<4	<4	<4	<4	<4	<4
Sr	18	175	4	5	347	18	3	51
Ta	<5	<5	<5	<5	<5	<5	<5	<5
Te	<6	<6	<6	<6	18	<6	<6	<6
Th	5	14	3	<2	<2	4	<2	7
U	2	3	2	<2	2	<2	9	10
V	26	12	31	13	76	19	62	92
W	5	27	<4	<4	19	nd	nd	nd
Y	34	5	4	<2	2	3	4	28
Zn	<3	44	4	9	21	7	36	239
Zr	7	151	<5	<5	23	25	<5	23

## Appendix 1 (continued)

GSWA no.	<i>Trace element analysis only</i>							
	112404 quartz vein	112405 gossan	112406 quartz vein	112407 ferruginous quartz vein	112408 quartz vein	112412 amphibolite	112413 ferruginous carbonate	112415 quartz vein
Latitude	22°32'03"	22°31'55"	22°31'31"	22°31'31"	22°33'55"	22°33'16"	22°33'16"	22°31'04"
Longitude	122°05'32"	122°05'32"	122°04'57"	122°04'57"	122°08'20"	122°03'35"	122°03'35"	122°01'25"
	<b>Percent</b>							
Fe <sub>2</sub> O <sub>3</sub>	5.00	59.90	1.00	12.00	3.00	16.00	41.00	2.00
	<b>Parts per million</b>							
Au	0.01	0.01	0.01	0.01	0.01	0.01	0.01	0.01
Ag	<2	<2	<2	<2	<2	<2	<2	<2
As	<4	7	<4	<4	<4	<4	7	<4
Ba	17	132	34	1 074	5 226	159	2 142	156
Bi	<4	<4	<4	<4	<4	<4	<4	7
Cd	<5	<5	<5	<5	<5	<5	<5	<5
Ce	<6	7	<6	25	12	24	<6	88
Co	nd	nd	nd	nd	nd	nd	nd	nd
Cr	21	51	4	<4	18	111	7	5
Cu	7	72	17	29	22	<4	446	133
Ga	<3	<3	<3	<3	<3	17	<3	<3
Ge	<3	3	<3	<3	<3	<3	4	<3
La	18	9	<5	15	<5	9	20	61
Li	nd	nd	nd	nd	nd	nd	nd	nd
Mn	27	193	39	52	69	2 372	26 220	64
Mo	<2	4	<2	<2	<2	2	4	6
Nb	<7	19	<7	<7	<7	8	19	<7
Ni	7	201	5	16	20	94	129	8
Pb	12	4	66	13	13	9	14	19
Rb	<2	<2	<2	38	4	45	<2	3
Sb	<4	<4	<4	<4	4	<4	<4	<4
Sc	nd	nd	nd	nd	nd	nd	nd	nd
Sn	<4	<4	<4	<4	<4	<4	44	<4
Sr	11	13	5	19	171	106	617	52
Ta	<5	<5	<5	<5	<5	<5	<5	<5
Te	<6	<6	<6	<6	<6	<6	<6	<6
Th	<2	<2	2	7	2	4	<2	<2
U	3	2	<2	2	2	<2	28	5
V	21	60	5	23	9	380	467	20
W	nd	nd	nd	nd	nd	nd	nd	nd
Y	2	27	<2	15	17	34	12	31
Zn	12	255	8	20	12	153	215	<3
Zr	<5	31	<5	101	43	88	85	28

## Appendix 1 (continued)

GSWA no.	<i>Trace element analysis only</i>							
	112416	112417	112418	112419	112420	112421	112422	112423
Rock type	quartz vein	gossan	gossan	quartz vein	quartz vein	quartz vein	quartz vein	quartz vein
Latitude	22°31'04"	22°30'41"	22°31'51"	22°35'34"	22°35'34"	22°35'34"	22°35'34"	22°35'34"
Longitude	122°01'25"	122°0'45"	122°0'10"	122°21'25"	122°21'25"	122°21'25"	122°21'25"	122°21'25"
	<b>Percent</b>							
Fe <sub>2</sub> O <sub>3</sub>	1.00	42.00	12.00	1.47	2.32	1.43	1.59	1.29
	<b>Parts per million</b>							
Au	0.01	0.02	0.01	<0.01	0.01	<0.01	<0.01	<0.01
Ag	<2	<2	<2	<5	<5	<5	<5	<5
As	<4	28	<4	<4	<4	<4	<4	<4
Ba	23	189	91	43	78	74	14	15
Bi	<4	6	<4	<4	<4	<4	<4	<4
Cd	<5	<5	<5	<5	<5	<5	<5	<5
Ce	<6	129	<6	10	16	43	<6	<6
Co	nd	nd	nd	nd	nd	nd	nd	nd
Cr	<4	13	<4	21	30	27	18	12
Cu	4	518	9	<4	<4	<4	<4	<4
Ga	<3	<3	<3	<3	<3	<3	<3	<3
Ge	<3	3	<3	<3	<3	<3	<3	<3
La	<5	55	<5	<5	8	16	<5	<5
Li	nd	nd	nd	nd	nd	nd	nd	nd
Mn	24	206	5	nd	nd	nd	nd	nd
Mo	<2	2	2	<6	<6	<6	<6	<6
Nb	<7	19	<7	<7	<7	<7	<7	<7
Ni	5	169	6	4	9	6	6	4
Pb	<4	14	8	<4	<4	<4	<4	<4
Rb	<2	11	7	<2	2	3	<2	<2
Sb	<4	<4	5	<4	<4	<4	<4	<4
Sc	nd	nd	nd	nd	nd	nd	nd	nd
Sn	<4	<4	<4	<4	<4	<4	<4	<4
Sr	<2	26	4	2	<2	6	<2	<2
Ta	<5	<5	<5	<5	<5	<5	<5	<5
Te	<6	<6	<6	<6	<6	<6	<6	<6
Th	<2	4	<2	3	5	5	2	<2
U	<2	3	2	<2	<2	<2	<2	<2
V	4	22	8	46	14	28	4	6
W	nd	nd	nd	nd	nd	nd	nd	nd
Y	<2	121	2	5	6	5	<2	<2
Zn	<3	236	3	<3	4	<3	<3	<3
Zr	<5	29	<5	36	77	74	<5	<5

## Appendix 1 (continued)

GSWA no.	<i>Trace element analysis only</i>							
	112424 quartzite	112425 quartz vein	112426 quartz vein	112427 quartz vein	112428 gossan	112429B felsic rock	112430 quartz vein	112431 gossan
Latitude	22°35'29"	22°35'29"	22°35'29"	22°35'29"	22°35'29"	22°35'37"	22°35'37"	22°35'37"
Longitude	122°21'27"	122°21'27"	122°21'27"	122°21'27"	122°21'27"	122°21'28"	122°21'28"	122°21'28"
	<b>Percent</b>							
Fe <sub>2</sub> O <sub>3</sub>	2.86	3.19	1.50	1.04	10.10	8.54	1.13	49.90
	<b>Parts per million</b>							
Au	<0.01	<0.01	0.01	0.01	<0.01	<0.01	0.02	0.02
Ag	<5	<5	<5	<5	7	7	<5	<5
As	<4	<4	<4	<4	<4	<4	<4	<4
Ba	481	78	77	44	184	1 168	63	360
Bi	<4	<4	<4	<4	<4	<4	<4	<4
Cd	<5	<5	<5	<5	<5	<5	<5	<5
Ce	69	36	14	<6	149	171	<6	<6
Co	nd	nd	nd	nd	nd	nd	nd	nd
Cr	41	27	19	19	54	16	20	323
Cu	<4	<4	<4	<4	<4	<4	<4	50
Ga	4	<3	<3	<3	5	25	<3	12
Ge	<3	<3	<3	<3	<3	<3	<3	<3
La	62	28	11	<5	80	69	<5	<5
Li	nd	nd	nd	nd	nd	nd	nd	nd
Mn	nd	nd	nd	nd	nd	nd	nd	nd
Mo	<6	<6	<6	<6	<6	<6	<6	<6
Nb	<7	<7	<7	<7	<7	11	<7	<7
Ni	9	6	5	4	14	20	4	<3
Pb	7	16	<4	<4	28	23	<4	18
Rb	21	<2	<2	<2	<2	4	<2	<2
Sb	<4	<4	<4	4	4	<4	<4	<4
Sc	nd	nd	nd	nd	nd	nd	nd	nd
Sn	<4	<4	<4	<4	<4	<4	<4	<4
Sr	18	9	3	<2	13	57	<2	7
Ta	<5	<5	<5	<5	<5	<5	<5	<5
Te	<6	<6	<6	<6	<6	<6	<6	<6
Th	11	4	4	<2	15	6	<2	4
U	<2	<2	<2	<2	2	<2	<2	<2
V	31	26	8	3	163	314	4	785
W	nd	nd	nd	nd	nd	nd	nd	nd
Y	7	<2	2	<2	3	2	<2	3
Zn	3	3	<3	<3	7	58	<3	29
Zr	88	12	28	<5	23	251	<5	75

## Appendix 1 (continued)

GSWA no.				Trace element analysis only				
	112432	112433	112434	112435	112436	112437	112438	112439
Rock type	<i>gossan</i>	<i>gossan</i>	<i>gossan</i>	<i>ferruginous quartz vein</i>	<i>ferruginous quartz vein</i>	<i>gossan</i>	<i>quartz vein</i>	<i>ferruginous quartz vein</i>
Latitude	22°35'37"	22°35'37"	22°35'37"	22°35'24"	22°35'24"	22°35'24"	22°35'21"	22°35'21"
Longitude	122°21'28"	122°21'28"	122°21'28"	122°21'22"	122°21'22"	122°21'22"	122°21'25"	122°21'25"
	<b>Percent</b>							
Fe <sub>2</sub> O <sub>3</sub>	25.00	25.30	25.20	3.95	4.68	25.30	4.60	9.12
	<b>Parts per million</b>							
Au	0.01	0.01	0.01	0.01	0.01	0.01	<0.01	0.01
Ag	15	14	14	<5	5	14	<5	5
As	<4	4	<4	4	<4	<4	<4	<4
Ba	625	1 399	822	720	1 099	835	16	47
Bi	<4	<4	<4	<4	<4	<4	<4	<4
Cd	<5	<5	<5	<5	<5	<5	<5	<5
Ce	20	35	<6	12	24	10	<6	10
Co	nd	nd	nd	nd	nd	nd	nd	nd
Cr	103	30	187	40	40	149	10	13
Cu	17	<4	9	<4	<4	<4	<4	<4
Ga	8	14	9	3	<3	5	<3	<3
Ge	<3	<3	<3	<3	<3	<3	<3	<3
La	11	16	<5	5	19	5	<5	8
Li	nd	nd	nd	nd	nd	nd	nd	nd
Mn	nd	nd	nd	nd	nd	nd	nd	nd
Mo	7	<6	8	<6	<6	10	<6	<6
Nb	<7	<7	<7	<7	<7	<7	<7	<7
Ni	20	44	18	7	9	13	12	31
Pb	<4	10	6	<4	4	22	<4	6
Rb	<2	<2	<2	2	2	2	<2	<2
Sb	<4	<4	<4	<4	<4	<4	<4	<4
Sc	nd	nd	nd	nd	nd	nd	nd	nd
Sn	<4	5	4	<4	<4	<4	<4	<4
Sr	18	27	14	9	16	38	2	4
Ta	<5	<5	<5	<5	<5	<5	<5	<5
Te	<6	<6	<6	<6	<6	6	<6	<6
Th	6	5	5	6	7	21	<2	2
U	3	3	3	<2	<2	2	<2	<2
V	317	561	383	32	44	266	7	26
W	nd	nd	nd	nd	nd	nd	nd	nd
Y	9	5	6	7	5	6	<2	4
Zn	38	52	42	<3	3	19	9	17
Zr	79	155	89	112	88	61	<5	12

## Appendix 1 (continued)

GSWA no.	<i>Trace element analysis only</i>							
	112440	112441	112442B	112443	112444	112445	112446	112447
Rock type	quartz vein	ferruginous quartz vein	felsic rock	quartz vein	quartz vein	gossan	gossan	gossan
Latitude	22°35'21"	22°35'21"	22°35'24"	22°35'24"	22°35'24"	22°35'24"	22°35'24"	22°35'24"
Longitude	122°21'25"	122°21'25"	122°21'22"	122°21'22"	122°21'22"	122°21'22"	122°21'22"	122°21'22"
	<b>Percent</b>							
Fe <sub>2</sub> O <sub>3</sub>	2.92	2.10	6.21	1.12	1.53	54.50	15.60	25.00
	<b>Parts per million</b>							
Au	0.01	0.01	0.01	0.01	0.11	0.01	0.02	<0.01
Ag	<5	<5	<5	<5	<5	<5	10	11
As	<4	<4	<4	<4	<4	6	<4	<4
Ba	298	88	304	<11	<11	163	15	114
Bi	<4	<4	<4	<4	<4	<4	<4	<4
Cd	<5	<5	<5	<5	<5	<5	<5	<5
Ce	13	21	27	<6	<6	<6	<6	<6
Co	nd	nd	nd	nd	nd	nd	nd	nd
Cr	30	25	86	9	18	130	64	314
Cu	<4	<4	8	<4	<4	35	13	12
Ga	<3	<3	28	<3	<3	5	3	5
Ge	<3	<3	<3	<3	<3	<3	<3	<3
La	8	11	26	<5	<5	<5	<5	<5
Li	nd	nd	nd	nd	nd	nd	nd	nd
Mn	nd	nd	nd	nd	nd	nd	nd	nd
Mo	<6	<6	<6	<6	<6	<6	6	<6
Nb	<7	<7	8	<7	<7	<7	<7	<7
Ni	10	10	15	5	6	87	24	42
Pb	<4	<4	10	<4	<4	7	5	9
Rb	5	2	<2	<2	<2	<2	<2	<2
Sb	<4	<4	<4	<4	<4	<4	<4	<4
Sc	nd	nd	nd	nd	nd	nd	nd	nd
Sn	<4	<4	<4	<4	<4	<4	<4	<4
Sr	5	3	24	<2	<2	24	2	2
Ta	<5	<5	<5	<5	<5	<5	<5	<5
Te	<6	<6	<6	<6	<6	<6	<6	<6
Th	5	6	4	<2	2	5	3	5
U	<2	<2	<2	<2	<2	2	<2	2
V	16	15	362	5	14	560	127	326
W	nd	nd	nd	nd	nd	nd	nd	nd
Y	8	7	4	<2	<2	13	6	2
Zn	4	5	14	<3	<3	87	21	35
Zr	74	75	145	5	<5	54	14	29



## Appendix 1 (continued)

GSWA no.	Trace element analysis only						
	112448	112449	112450	112451	112452	112453	112454
Rock type	<i>gossan</i>	<i>gossan</i>	<i>ferruginous quartz vein</i>	<i>quartz vein</i>	<i>gossan</i>	<i>gossan</i>	<i>quartzite</i>
Latitude	22°35'27"	22°35'27"	22°35'18"	22°35'18"	22°35'18"	22°35'18"	22°35'18"
Longitude	122°21'20"	122°21'20"	122°21'21"	122°21'21"	122°21'21"	122°21'21"	122°21'21"
	<b>Percent</b>						
Fe <sub>2</sub> O <sub>3</sub>	25.00	25.00	9.40	1.04	25.00	25.00	5.46
	<b>Parts per million</b>						
Au	0.01	0.01	<0.01	<0.01	0.02	<0.01	0.01
Ag	13	13	6	<5	12	14	<5
As	<4	<4	<4	<4	<4	<4	<4
Ba	219	198	52	<11	113	298	122
Bi	<4	<4	<4	<4	<4	<4	<4
Cd	<5	<5	<5	<5	<5	<5	<5
Ce	<6	<6	<6	<6	<6	<6	54
Co	nd	nd	nd	nd	nd	nd	nd
Cr	300	41	40	10	136	47	36
Cu	18	20	4	<4	15	15	<4
Ga	8	4	<3	<3	9	13	6
Ge	<3	<3	<3	<3	<3	<3	<3
La	<5	<5	<5	<5	<5	<5	20
Li	nd	nd	nd	nd	nd	nd	nd
Mn	nd	nd	nd	nd	nd	nd	nd
Mo	<6	6	<6	<6	<6	6	<6
Nb	<7	<7	<7	<7	8	<7	<7
Ni	41	19	13	5	48	15	13
Pb	6	<4	<4	<4	4	5	<4
Rb	<2	13	<2	<2	<2	2	<2
Sb	<4	<4	<4	<4	<4	<4	<4
Sc	nd	nd	nd	nd	nd	nd	nd
Sn	<4	<4	<4	<4	<4	<4	<4
Sr	4	5	<2	<2	4	13	7
Ta	<5	<5	<5	<5	<5	<5	<5
Te	<6	<6	<6	<6	<6	<6	<6
Th	3	2	2	<2	5	4	9
U	5	3	<2	<2	5	4	<2
V	513	174	81	5	282	668	39
W	nd	nd	nd	nd	nd	nd	nd
Y	10	8	2	<2	8	7	7
Zn	33	15	8	<3	40	28	7
Zr	58	52	8	<5	57	73	79

## Appendix 1 (continued)

GSWA no.	<i>Trace element analysis only</i>							
	112455 felsic rock	112456 gossan	112457 gossan	112458 gossan	112459 gossan	112460 gossan	112461 quartz vein	112462 gossan
Latitude	22°35'18"	22°35'18"	22°35'18"	22°35'18"	22°35'18"	22°35'18"	22°35'16"	22°35'16"
Longitude	122°21'21"	122°21'21"	122°21'21"	122°21'21"	122°21'21"	122°21'21"	122°21'19"	122°21'19"
	<b>Percent</b>							
Fe <sub>2</sub> O <sub>3</sub>	9.11	21.20	64.10	52.10	55.10	25.00	10.50	25.50
	<b>Parts per million</b>							
Au	0.01	0.16	<0.01	0.01	<0.01	0.01	0.02	0.02
Ag	<5	11	6	7	5	12	7	16
As	<4	<4	<4	<4	<4	<4	<4	<4
Ba	279	380	466	378	247	280	115	2090
Bi	<4	<4	<4	<4	<4	<4	<4	<4
Cd	<5	<5	<5	<5	<5	<5	<5	<5
Ce	36	77	126	<6	373	10	12	<6
Co	nd	nd	nd	nd	nd	nd	nd	nd
Cr	66	43	105	171	91	51	8	50
Cu	<4	13	73	34	43	16	84	39
Ga	22	7	9	9	8	4	4	19
Ge	<3	<3	<3	<3	<3	<3	<3	<3
La	18	54	86	<5	239	6	9	<5
Li	nd	nd	nd	nd	nd	nd	nd	nd
Mn	nd	nd	nd	nd	nd	nd	nd	nd
Mo	<6	8	<6	<6	<6	7	<6	10
Nb	7	<7	<7	<7	<7	<7	<7	11
Ni	21	21	31	19	47	34	14	26
Pb	4	5	<4	<4	5	5	<4	6
Rb	4	<2	<2	<2	<2	<2	<2	<2
Sb	<4	<4	<4	<4	<4	<4	<4	<4
Sc	nd	nd	nd	nd	nd	nd	nd	nd
Sn	<4	<4	<4	<4	<4	<4	<4	6
Sr	24	102	148	6	365	11	7	20
Ta	<5	<5	<5	<5	<5	<5	<5	<5
Te	<6	<6	<6	<6	<6	<6	<6	<6
Th	4	3	<2	7	<2	5	3	10
U	<2	3	4	5	4	7	<2	3
V	393	140	615	736	421	227	14	70
W	nd	nd	nd	nd	nd	nd	nd	nd
Y	2	5	7	8	10	11	8	6
Zn	53	29	42	64	81	49	12	35
Zr	165	61	72	53	99	45	46	241

## Appendix 1 (continued)

GSWA no.	Trace element analysis only							
	112463	112464	112465	112466	112467	112468	112469	112470
Rock type	<i>gossan</i>	<i>gossan</i>	<i>ferruginous quartz vein</i>	<i>felsic rock</i>	<i>gossan</i>	<i>gossan</i>	<i>gossan</i>	<i>gossan</i>
Latitude	22°35'16"	22°35'16"	22°35'17"	22°35'17"	22°35'17"	22°35'17"	22°35'17"	22°35'17"
Longitude	122°21'19"	122°21'19"	122°21'18"	122°21'18"	122°21'18"	122°21'18"	122°21'18"	122°21'18"
	<b>Percent</b>							
Fe <sub>2</sub> O <sub>3</sub>	66.50	25.20	9.50	9.21	67.10	25.20	60.90	25.20
	<b>Parts per million</b>							
Au	0.01	0.01	0.01	0.01	<0.01	0.01	0.01	0.04
Ag	7	12	6	6	11	14	10	12
As	<4	<4	<4	<4	4	<4	<4	<4
Ba	1 316	734	241	264	382	658	494	447
Bi	<4	<4	<4	<4	<4	<4	<4	<4
Cd	<5	<5	<5	<5	<5	<5	<5	<5
Ce	<6	<6	<6	14	<6	48	62	<6
Co	nd	nd	nd	nd	nd	nd	nd	nd
Cr	51	30	15	10	53	99	23	239
Cu	58	14	10	18	61	14	37	24
Ga	3	9	<3	26	7	7	4	6
Ge	<3	<3	<3	<3	<3	<3	<3	<3
La	<5	<5	<5	7	<5	21	36	<5
Li	nd	nd	nd	nd	nd	nd	nd	nd
Mn	nd	nd	nd	nd	nd	nd	nd	nd
Mo	<6	<6	<6	<6	<6	8	<6	<6
Nb	<7	<7	<7	9	<7	<7	<7	<7
Ni	47	15	6	25	7	14	24	37
Pb	10	6	10	7	10	13	13	12
Rb	<2	<2	<2	<2	<2	<2	<2	<2
Sb	<4	<4	<4	<4	<4	<4	<4	4
Sc	nd	nd	nd	nd	nd	nd	nd	nd
Sn	<4	<4	<4	<4	<4	<4	<4	<4
Sr	8	9	22	8	15	13	38	8
Ta	<5	<5	<5	<5	<5	<5	<5	<5
Te	<6	<6	<6	<6	<6	<6	<6	<6
Th	2	6	2	5	2	4	7	6
U	6	<2	<2	<2	3	5	3	<2
V	172	24	23	300	817	143	199	979
W	nd	nd	nd	nd	nd	nd	nd	nd
Y	17	10	<2	2	4	5	13	4
Zn	63	46	9	31	57	41	37	61
Zr	27	121	10	189	40	108	97	37

## Appendix 1 (continued)

GSWA no.				<i>Trace element analysis only</i>				
	112471	112472	112473	112474	112475	112476	112477	112478
Rock type	<i>gossan</i>	<i>gossan</i>	<i>gossan</i>	<i>quartz vein</i>	<i>quartz vein</i>	<i>quartz vein</i>	<i>quartz vein</i>	<i>quartz vein</i>
Latitude	22°35'17"	22°35'33"	22°35'33"	22°35'30"	22°35'36"	22°35'36"	22°34'07"	22°34'07"
Longitude	122°21'18"	122°21'34"	122°21'34"	122°21'34"	122°19'53"	122°19'53"	122°19'49"	122°19'49"
	<b>Percent</b>							
Fe <sub>2</sub> O <sub>3</sub>	63.90	25.00	24.90	1.54	1.60	1.06	1.04	0.90
	<b>Parts per million</b>							
Au	0.04	0.04	0.04	0.04	0.04	0.03	0.04	0.04
Ag	10	13	13	<5	<5	<5	<5	<5
As	<4	<4	<4	<4	<4	<4	<4	<4
Ba	254	140	49	19	59	27	<11	54
Bi	25	<4	<4	<4	<4	<4	<4	<4
Cd	<5	<5	<5	<5	<5	<5	<5	<5
Ce	18	<6	<6	<6	<6	<6	<6	54
Co	nd	nd	nd	nd	nd	nd	nd	nd
Cr	113	11	12	10	90	29	12	24
Cu	76	<4	<4	<4	<4	<4	<4	<4
Ga	8	<3	<3	<3	<3	<3	<3	<3
Ge	<3	<3	<3	<3	<3	<3	<3	<3
La	29	<5	<5	<5	<5	<5	<5	146
Li	nd	nd	nd	nd	nd	nd	nd	nd
Mn	nd	nd	nd	nd	nd	nd	nd	nd
Mo	<6	<6	6	<6	<6	<6	<6	<6
Nb	<7	<7	<7	<7	<7	<7	<7	<7
Ni	33	36	52	4	37	14	5	6
Pb	13	<4	<4	<4	<4	15	<4	18
Rb	<2	<2	<2	<2	24	<2	<2	<2
Sb	<4	<4	<4	<4	<4	<4	<4	<4
Sc	nd	nd	nd	nd	nd	nd	nd	nd
Sn	<4	<4	<4	<4	<4	<4	<4	<4
Sr	110	5	2	<2	<2	2	<2	15
Ta	<5	<5	<5	<5	<5	<5	<5	<5
Te	<6	<6	<6	<6	<6	<6	<6	<6
Th	6	2	<2	<2	2	<2	<2	<2
U	3	<2	<2	<2	<2	<2	<2	<2
V	789	31	12	3	12	5	<3	<3
W	nd	nd	nd	nd	nd	nd	nd	nd
Y	9	2	3	<2	<2	<2	<2	16
Zn	52	42	28	<3	6	5	<3	<3
Zr	73	25	<5	<5	7	<5	<5	<5

## Appendix 1 (continued)

GSWA no.	<i>Trace element analysis only</i>							
	112479	112480	112481	112482	112483	112484	112485	112486B
Rock type	quartz vein	quartz vein	quartz vein	quartz vein	quartz vein	quartz vein	quartz vein	calc silicate
Latitude	22°34'07"	22°34'07"	22°34'07"	22°34'07"	22°34'07"	22°34'07"	22°34'07"	22°34'00"
Longitude	122°19'49"	122°19'49"	122°19'49"	122°19'49"	122°19'40"	122°19'46"	122°19'46"	122°19'55"
	<b>Percent</b>							
Fe <sub>2</sub> O <sub>3</sub>	3.70	1.24	1.39	1.83	0.96	1.02	1.19	1.76
	<b>Parts per million</b>							
Au	0.04	0.03	0.04	0.04	0.04	0.03	0.04	0.05
Ag	<5	<5	<5	<5	<5	<5	<5	6
As	<4	<4	<4	<4	<4	<4	<4	<4
Ba	237	29	33	27	47	93	120	95
Bi	<4	<4	<4	<4	<4	<4	<4	<4
Cd	<5	<5	<5	<5	<5	<5	<5	<5
Ce	53	17	46	54	6	11	82	47
Co	nd	nd	nd	nd	nd	nd	nd	nd
Cr	27	25	20	44	29	12	10	131
Cu	11	<4	<4	5	<4	<4	<4	<4
Ga	<3	<3	<3	<3	<3	<3	3	11
Ge	<3	<3	<3	<3	<3	<3	<3	<3
La	108	24	49	<5	5	5	41	26
Li	nd	nd	nd	nd	nd	nd	nd	nd
Mn	nd	nd	nd	nd	nd	nd	nd	nd
Mo	<6	<6	<6	<6	<6	<6	<6	<6
Nb	<7	<7	<7	<7	<7	<7	<7	21
Ni	31	8	9	16	5	6	8	106
Pb	50	9	20	<4	<4	<4	11	25
Rb	<2	2	3	<2	<2	7	15	7
Sb	<4	<4	<4	<4	<4	<4	<4	<4
Sc	nd	nd	nd	nd	nd	nd	nd	nd
Sn	<4	<4	<4	<4	<4	<4	<4	<4
Sr	26	6	10	<2	3	5	19	1 189
Ta	<5	<5	<5	<5	<5	<5	<5	<5
Te	<6	<6	<6	<6	<6	<6	<6	<6
Th	<2	<2	2	<2	<2	<2	17	13
U	2	<2	<2	<2	<2	<2	<2	<2
V	9	<3	3	<3	8	6	8	43
W	nd	nd	nd	nd	nd	nd	nd	nd
Y	7	4	5	5	<2	2	4	7
Zn	22	<3	<3	4	<3	3	4	15
Zr	9	<5	7	<5	<5	7	45	463

## Appendix 1 (continued)

GSWA no.	<i>Trace element analysis only</i>							
	112487	112488	112489	112490	112491	112492	112493	112494
Rock type	quartz vein	quartz vein	quartz vein	quartz vein	quartz vein	quartz vein	quartz vein	quartz vein
Latitude	22°34'00"	22°34'00"	22°34'00"	22°34'00"	22°34'00"	22°34'00"	22°34'08"	22°34'08"
Longitude	122°19'55"	122°19'55"	122°19'55"	122°19'55"	122°19'55"	122°19'55"	122°19'54"	122°19'54"
	<b>Percent</b>							
Fe <sub>2</sub> O <sub>3</sub>	2.18	0.86	1.03	1.27	0.76	1.02	2.65	0.94
	<b>Parts per million</b>							
Au	0.03	0.02	0.02	0.02	0.02	0.01	0.01	0.02
Ag	<5	<5	<5	<5	<5	<5	<5	<5
As	<4	<4	<4	<4	<4	<4	<4	<4
Ba	95	17	<11	30	<11	<11	56	32
Bi	<4	<4	<4	<4	<4	<4	<4	<4
Cd	<5	<5	<5	<5	<5	<5	<5	<5
Ce	18	<6	<6	<6	<6	<6	23	12
Co	nd	nd	nd	nd	nd	nd	nd	nd
Cr	57	17	12	29	8	27	37	19
Cu	<4	<4	90	<4	<4	<4	5	<4
Ga	4	<3	<3	<3	<3	<3	<3	<3
Ge	<3	<3	<3	<3	<3	<3	<3	<3
La	8	<5	<5	<5	<5	<5	<5	7
Li	nd	nd	nd	nd	nd	nd	nd	nd
Mn	nd	nd	nd	nd	nd	nd	nd	nd
Mo	<6	<6	166	<6	<6	<6	<6	<6
Nb	<7	<7	<7	<7	<7	<7	<7	<7
Ni	36	8	7	9	5	9	11	7
Pb	5	8	<4	43	<4	<4	<4	<4
Rb	37	<2	<2	2	<2	<2	5	<2
Sb	<4	<4	<4	<4	<4	<4	<4	<4
Sc	nd	nd	nd	nd	nd	nd	nd	nd
Sn	<4	<4	<4	<4	<4	<4	<4	<4
Sr	21	4	2	6	<2	<2	14	8
Ta	<5	<5	<5	<5	<5	<5	<5	<5
Te	<6	<6	<6	<6	<6	<6	<6	<6
Th	5	<2	<2	<2	<2	<2	4	2
U	<2	<2	<2	<2	<2	<2	<2	<2
V	28	4	<3	3	<3	<3	14	<3
W	nd	nd	nd	nd	nd	nd	nd	nd
Y	6	<2	<2	<2	<2	<2	3	<2
Zn	11	18	4	10	<3	<3	5	<3
Zr	51	<5	<5	<5	<5	<5	26	8

## Appendix 1 (continued)

GSWA no.	<i>Trace element analysis only</i>							
	112495	112496	112497	112498A	112498B	112498C	112499A	112499B
Rock type	quartz vein	quartz vein	quartz vein	quartz vein	quartz vein	quartz vein	gossan	gossan
Latitude	22°34'08"	22°34'08"	22°34'08"	22°34'08"	22°34'08"	22°34'08"	22°34'14"	22°34'14"
Longitude	122°19'54"	122°19'54"	122°19'54"	122°19'54"	122°19'54"	122°19'54"	122°19'55"	122°19'55"
	<b>Percent</b>							
Fe <sub>2</sub> O <sub>3</sub>	1.02	1.12	0.92	1.30	1.34	0.87	68.20	74.10
	<b>Parts per million</b>							
Au	0.01	0.01	<0.01	0.01	0.02	0.02	0.02	0.02
Ag	<5	<5	<5	<5	<5	<5	7	8
As	<4	<4	<4	<4	<4	<4	8	7
Ba	28	112	11	21	35	<11	1 117	502
Bi	<4	<4	<4	<4	<4	<4	<4	<4
Cd	<5	<5	<5	<5	<5	<5	<5	<5
Ce	13	21	<6	13	15	11	70	12
Co	nd	nd	nd	nd	nd	nd	nd	nd
Cr	13	30	25	25	18	20	94	92
Cu	<4	<4	<4	<4	<4	<4	20	43
Ga	<3	<3	<3	<3	<3	<3	<3	<3
Ge	<3	<3	<3	<3	<3	<3	3	<3
La	6	11	<5	<5	6	<5	47	23
Li	nd	nd	nd	nd	nd	nd	nd	nd
Mn	nd	nd	nd	nd	nd	nd	nd	nd
Mo	<6	<6	<6	<6	<6	<6	<6	<6
Nb	<7	<7	<7	<7	<7	<7	<7	<7
Ni	5	10	8	6	10	6	4 105	4 572
Pb	<4	4	4	<4	<4	<4	<4	4
Rb	<2	<2	<2	<2	2	<2	<2	<2
Sb	<4	<4	<4	<4	<4	<4	<4	<4
Sc	nd	nd	nd	nd	nd	nd	nd	nd
Sn	<4	<4	<4	<4	<4	<4	<4	<4
Sr	8	2	<2	5	2	<2	88	42
Ta	<5	<5	<5	<5	<5	<5	<5	<5
Te	<6	<6	<6	<6	<6	<6	<6	<6
Th	2	<2	<2	2	2	<2	<2	<2
U	<2	<2	<2	<2	<2	<2	3	2
V	<3	3	4	7	7	<3	443	455
W	nd	nd	nd	nd	nd	nd	nd	nd
Y	<2	3	<2	2	5	<2	86	48
Zn	<3	<3	<3	<3	4	<3	344	248
Zr	<5	<5	<5	8	<5	<5	16	<5

## Appendix 1 (continued)

GSWA no.				Trace element analysis only				
	112499C	112499D	112499E	112499F	112499G	112500A	112500B	112500C
Rock type	gossan	quartz vein	gossan	quartz vein	gossan	gossan	ferruginous quartz vein	quartz vein
Latitude	22°34'14"	22°34'14"	22°34'14"	22°34'14"	22°34'14"	22°34'17"	22°34'17"	22°34'17"
Longitude	122°19'55"	122°19'55"	122°19'55"	122°19'55"	122°19'55"	122°19'52"	122°19'52"	122°19'52"
	<b>Percent</b>							
Fe <sub>2</sub> O <sub>3</sub>	63.5	1.54	64.50	1.02	4.22	25.00	11.00	2.12
	<b>Parts per million</b>							
Au	0.04	0.02	0.03	0.01	0.01	0.02	0.02	0.02
Ag	5	<5	<5	<5	<5	12	6	<5
As	<4	<4	<4	<4	<4	4	<4	<4
Ba	112	18	244	<11	31	135	180	71
Bi	<4	<4	<4	<4	<4	<4	<4	<4
Cd	10	<5	<5	<5	15	<5	<5	<5
Ce	961	6	15	7	1 920	17	33	<6
Co	nd	nd	nd	nd	nd	nd	nd	nd
Cr	34	21	252	16	34	1 682	78	19
Cu	90	<4	312	<4	8	136	15	<4
Ga	<3	<3	7	<3	<3	3	<3	<3
Ge	<3	<3	<3	<3	<3	<3	<3	<3
La	143	<5	6	<5	246	13	8	<5
Li	nd	nd	nd	nd	nd	nd	nd	nd
Mn	nd	nd	nd	nd	nd	nd	nd	nd
Mo	<6	<6	<6	<6	<6	<6	7	<6
Nb	<7	<7	<7	<7	<7	<7	<7	<7
Ni	732	26	673	12	44	502	176	26
Pb	124	<4	50	<4	143	27	32	<4
Rb	<2	<2	<2	<2	<2	<2	<2	<2
Sb	<4	<4	<4	<4	<4	<4	<4	<4
Sc	nd	nd	nd	nd	nd	nd	nd	nd
Sn	<4	<4	5	<4	<4	<4	<4	<4
Sr	5	<2	16	<2	5	6	18	8
Ta	<5	<5	<5	<5	<5	<5	<5	<5
Te	7	<6	<6	<6	<6	<6	<6	<6
Th	<2	<2	12	<2	<2	8	2	<2
U	9	<2	10	<2	29	9	4	<2
V	20	<3	188	4	8	185	33	21
W	nd	nd	nd	nd	nd	nd	nd	nd
Y	79	<2	32	<2	92	26	46	4
Zn	146	3	223	<3	7	63	21	5
Zr	17	<5	46	<5	<5	111	12	<5



## Appendix 1 (continued)

GSWA no.	<i>Trace element analysis only</i>							
	112500D	112906	112911	112953	112956	112962	112967	113101
Rock type	quartz vein	gossan	gossan	tourmalinite	ironstone	meta-BIF	gossan	quartz vein
Latitude	22°34'17"	22°40'35"	22°39'25"	22°45'26"	22°47'47"	22°47'43"	22°51'07"	22°33'58"
Longitude	122°19'52"	122°27'29"	122°28'49"	122°26'20"	122°29'44"	122°28'35"	122°22'48"	122°19'47"
	<b>Percent</b>							
Fe <sub>2</sub> O <sub>3</sub>	0.94	nd	nd	nd	nd	nd	nd	0.94
	<b>Parts per million</b>							
Au	0.02	0.05	0.05	0.02	0.03	0.02	0.04	0.03
Ag	<5	nd	nd	5	6	15	13	<5
As	<4	4	<4	<4	<4	<4	<4	<4
Ba	11	467	1 217	240	765	193	188	19
Bi	<4	<4	<4	8	<4	<4	<4	<4
Cd	<5	<5	<5	<5	<5	<5	<5	<5
Ce	<6	23	10	100	71	<6	<6	7
Co	nd	nd	nd	18	16	<3	<3	nd
Cr	18	87	8	109	22	51	4	14
Cu	<4	31	462	30	151	119	10	<4
Ga	<3	5	<3	24	4	10	15	<3
Ge	<3	<3	4	<3	3	3	3	<3
La	<5	12	7	51	25	<5	<5	<5
Li	nd	<6	<6	nd	nd	nd	nd	nd
Mn	nd	nd	nd	nd	nd	nd	nd	nd
Mo	<6	<6	<6	54	<6	14	106	<6
Nb	<7	<7	<7	17	<7	<7	<7	<7
Ni	8	131	69	36	48	56	5	6
Pb	13	9	174	499	11	64	<4	<4
Rb	<2	<2	16	20	25	2	<2	8
Sb	<4	<4	<4	<4	<4	<4	4	<4
Sc	nd	21	28	nd	nd	nd	nd	nd
Sn	<4	8	<4	<4	<4	4	37	<4
Sr	4	27	13	66	35	11	6	<2
Ta	<5	<5	<5	8	<5	<5	<5	<5
Te	<6	<6	<6	<6	<6	<6	<6	<6
Th	<2	5	<2	18	3	4	<2	5
U	<2	2	7	4	5	5	<2	<2
V	<3	227	15	113	45	494	9	<3
W	nd	nd	nd	6	10	10	5	nd
Y	<2	39	38	30	34	11	<2	<2
Zn	4	150	329	234	182	107	<3	<3
Zr	<5	74	<5	158	43	34	5	<5

## Appendix 1 (continued)

GSWA no. Rock type	<i>Trace element analysis only</i>							
	113102 quartz vein	113103 quartz vein	113104 quartz vein	113105 quartz vein	113106 quartz vein	113107 barite	113108 gossan	113109 gossan
Latitude	22°33'58"	22°33'58"	22°33'58"	22°33'56"	22°33'55"	22°31'21"	22°31'21"	22°31'21"
Longitude	122°19'47"	122°19'47"	122°19'47"	122°19'45"	122°19'45"	122°02'13"	122°02'13"	122°02'13"
	<b>Percent</b>							
Fe <sub>2</sub> O <sub>3</sub>	1.46	4.10	1.26	0.84	1.39	11.00	45.00	33.00
	<b>Parts per million</b>							
Au	0.04	0.02	0.02	0.05	0.19	<0.01	<0.01	<0.01
Ag	<5	<5	<5	<5	<5	<2	<2	<2
As	<4	<4	<4	<4	<4	<4	8	11
Ba	<11	<11	108	13	20	476 000	49 660	64 420
Bi	<4	<4	<4	<4	<4	4	<4	<4
Cd	<5	<5	<5	<5	<5	<5	<5	<5
Ce	<6	<6	<6	9	<6	222	17	21
Co	nd	nd	nd	nd	nd	nd	nd	nd
Cr	19	20	17	11	17	27	<4	<4
Cu	<4	<4	<4	<4	56	145	22	37
Ga	<3	3	<3	<3	<3	<3	<3	<3
Ge	<3	<3	<3	<3	<3	<3	4	6
La	<5	<5	<5	<5	<5	<5	11	8
Li	nd	nd	nd	nd	nd	nd	nd	nd
Mn	nd	nd	nd	nd	nd	38	<5	<5
Mo	<6	<6	<6	<6	<6	5	10	19
Nb	<7	<7	<7	<7	<7	<7	<7	10
Ni	6	6	6	5	6	28	4	13
Pb	4	<4	4	<4	<4	6	5	4
Rb	<2	<2	2	<2	<2	12	3	<2
Sb	<4	4	<4	<4	<4	4	5	<4
Sc	nd	nd	nd	nd	nd	nd	nd	nd
Sn	<4	<4	<4	<4	<4	<4	<4	<4
Sr	4	<2	7	<2	<2	8 474	851	861
Ta	<5	<5	<5	<5	<5	<5	5	<5
Te	<6	<6	<6	<6	<6	<6	<6	<6
Th	2	<2	2	2	<2	<2	<2	<2
U	<2	<2	<2	<2	<2	<2	7	2
V	<3	62	<3	<3	4	165	201	7
W	nd	nd	nd	nd	nd	nd	nd	nd
Y	<2	<2	<2	<2	<2	17	5	12
Zn	<3	<3	<3	<3	<3	14	<3	<3
Zr	<5	<5	<5	<5	<5	<5	<5	<5

## Appendix 1 (continued)

GSWA no. Rock type	<i>Trace element analysis only</i>							
	113110 barite	113111A chert	113112 barite	113113 quartz vein	113114A barite	113115 gossan	113116 barite	113117 gossan
Latitude	22°31'21"	22°31'21"	22°31'21"	22°31'21"	22°31'21"	22°31'10"	22°31'10"	22°31'10"
Longitude	122°02'13"	122°02'13"	122°02'13"	122°02'13"	122°02'13"	122°02'00"	122°02'00"	122°02'00"
	<b>Percent</b>							
Fe <sub>2</sub> O <sub>3</sub>	13.00	4.00	5.00	2.00	12.00	15.00	5.00	18.20
	<b>Parts per million</b>							
Au	0.01	0.01	0.01	0.01	0.01	<0.01	0.01	0.01
Ag	<2	<2	<2	<2	<2	<2	<2	<2
As	16	<4	8	<4	4	4	<4	4
Ba	216 300	34 750	176 400	10 250	231 300	142 000	470 400	129 800
Bi	4	<4	<4	<4	5	<4	12	<4
Cd	<5	<5	<5	<5	<5	<5	<5	<5
Ce	100	124	70	12	124	27	212	30
Co	nd	nd	nd	nd	nd	nd	nd	nd
Cr	13	11	10	6	10	<4	18	<4
Cu	66	8	49	<4	69	138	125	119
Ga	<3	<3	<3	<3	<3	<3	<3	<3
Ge	<3	<3	<3	<3	<3	3	<3	3
La	5	52	<5	5	15	7	<5	<5
Li	nd	nd	nd	nd	nd	nd	nd	nd
Mn	14	25	<5	17	67	129	<5	52
Mo	5	<2	3	<2	5	50	2	20
Nb	<7	<7	<7	<7	9	<7	<7	<7
Ni	17	8	14	5	20	15	25	15
Pb	7	4	<4	<4	17	<4	10	<4
Rb	3	55	<2	5	91	<2	<2	<2
Sb	4	<4	4	<4	<4	<4	7	<4
Sc	nd	nd	nd	nd	nd	nd	nd	nd
Sn	<4	<4	<4	<4	<4	<4	<4	<4
Sr	3 007	567	2 803	198	4 285	1 625	8 137	1 327
Ta	<5	<5	<5	<5	<5	<5	<5	<5
Te	<6	<6	<6	<6	<6	<6	<6	<6
Th	<2	5	<2	<2	10	<2	<2	<2
U	6	3	<2	<2	2	2	<2	3
V	53	17	37	8	44	114	117	128
W	nd	nd	nd	nd	nd	nd	nd	nd
Y	12	28	3	<2	53	6	6	3
Zn	6	5	7	<3	10	<3	10	<3
Zr	<5	<5	<5	<5	<5	<5	<5	<5

## Appendix 1 (continued)

GSWA no.	<i>Trace element analysis only</i>							
	113118 quartz vein	113119 ferruginous chert	113120 quartz vein	113121 quartz vein	113123 gossan	113124 quartz vein	113125 quartz vein	113126 gossan
Latitude	22°31'40"	22°31'48"	22°31'25"	22°31'25"	22°31'19"	22°31'19"	22°32'38"	22°32'38"
Longitude	122°01'50"	122°01'57"	122°01'48"	122°01'48"	122°01'55"	122°01'55"	122°02'01"	122°02'01"
	<b>Percent</b>							
Fe <sub>2</sub> O <sub>3</sub>	<0.07	31.00	<0.07	1.00	76.90	1.00	6.99	11.00
	<b>Parts per million</b>							
Au	0.02	0.03	0.02	0.02	0.02	0.01	0.02	0.02
Ag	<2	<2	<2	<2	<2	<2	<2	<2
As	<4	<4	<4	<4	18	<4	10	<4
Ba	409	396	55	76	895	304	96	645
Bi	<4	<4	<4	<4	<4	<4	<4	<4
Cd	<5	<5	<5	<5	<5	<5	<5	<5
Ce	<6	<6	<6	<6	15	<6	<6	<6
Co	nd	nd	nd	nd	nd	nd	nd	nd
Cr	8	37	5	10	14	5	5	16
Cu	<4	13	8	8	49	<4	87	14
Ga	<3	5	<3	<3	4	<3	6	6
Ge	<3	3	<3	<3	3	<3	<3	<3
La	<5	<5	<5	<5	<5	<5	<5	<5
Li	nd	nd	nd	nd	nd	nd	nd	nd
Mn	12	<5	<5	<5	336	<5	94	50
Mo	<2	<2	<2	<2	80	<2	5	<2
Nb	<7	13	<7	<7	<7	<7	<7	<7
Ni	5	20	4	6	107	5	29	11
Pb	<4	12	<4	<4	29	<4	3 041	9
Rb	<2	<2	<2	<2	5	5	2	6
Sb	<4	<4	<4	4	<4	<4	<4	<4
Sc	nd	nd	nd	nd	nd	nd	nd	nd
Sn	<4	<4	<4	<4	5	<4	<4	<4
Sr	13	8	2	3	51	16	5	34
Ta	<5	<5	<5	<5	<5	<5	<5	<5
Te	<6	<6	<6	<6	<6	<6	<6	<6
Th	<2	<2	<2	<2	2	<2	<2	2
U	<2	<2	<2	<2	9	<2	<2	<2
V	<3	323	<3	14	80	3	157	84
W	nd	nd	nd	nd	nd	nd	nd	nd
Y	<2	2	<2	2	18	<2	<2	5
Zn	<3	10	<3	<3	128	<3	135	6
Zr	<5	<5	<5	<5	62	6	26	25

## Appendix 1 (continued)

GSWA no.	<i>Trace element analysis only</i>							
	113127 quartz vein	113128 pelite	113129 shale	113130 conglomerate	113131 conglomerate	113132 conglomerate	113133 gossan	113134 gossan
Latitude	22°32'38"	22°33'32"	22°33'34"	22°33'34"	22°33'34"	22°33'34"	22°35'48"	22°35'48"
Longitude	122°02'01"	122°02'25"	122°02'43"	122°02'43"	122°02'43"	122°02'43"	122°02'36"	122°02'36"
	<b>Percent</b>							
Fe <sub>2</sub> O <sub>3</sub>	4.00	6.99	13.00	5.99	10.00	16.00	83.90	54.10
	<b>Parts per million</b>							
Au	0.02	0.02	0.02	0.02	0.02	0.01	<0.01	0.02
Ag	<2	<2	<2	<2	<2	<2	2	<2
As	7	<4	8	<4	4	7	20	12
Ba	299	837	1 111	888	689	943	867	708
Bi	<4	<4	<4	<4	<4	<4	<4	<4
Cd	<5	<5	<5	<5	<5	<5	<5	<5
Ce	<6	94	110	154	237	345	46	278
Co	nd	nd	nd	nd	nd	nd	nd	nd
Cr	5	128	50	21	39	13	<4	10
Cu	42	<4	<4	<4	<4	<4	<4	397
Ga	3	24	16	7	10	10	4	8
Ge	<3	<3	<3	<3	<3	<3	13	4
La	<5	47	70	87	121	182	18	17
Li	nd	nd	nd	nd	nd	nd	nd	nd
Mn	17	486	107	142	120	69	159	251
Mo	<2	<2	<2	<2	<2	2	25	7
Nb	<7	17	14	10	18	7	<7	21
Ni	9	46	17	11	16	10	<3	94
Pb	121	13	15	8	14	13	<4	<4
Rb	<2	144	212	63	121	48	<2	4
Sb	<4	<4	<4	<4	4	<4	<4	<4
Sc	nd	nd	nd	nd	nd	nd	nd	nd
Sn	<4	5	7	<4	<4	<4	<4	<4
Sr	8	68	26	27	39	28	7	24
Ta	<5	<5	<5	<5	<5	<5	<5	<5
Te	6	<6	<6	<6	<6	<6	<6	<6
Th	<2	21	28	42	99	18	<2	4
U	<2	2	8	3	10	4	2	11
V	45	123	116	59	115	119	11	54
W	nd	nd	nd	nd	nd	nd	nd	nd
Y	<2	27	61	25	99	33	13	63
Zn	14	40	20	7	15	6	<3	126
Zr	6	179	287	485	2 059	205	<5	30

## Appendix 1 (continued)

GSWA no. Rock type	<i>Trace element analysis only</i>							
	113135 gossan	113136 sandstone	113137 alluvium	113138 quartz vein	113139 quartz vein	113140 chert	113141 quartz vein	113142 quartz vein
Latitude	22°34'23"	22°34'00"	22°34'00"	22°33'34"	22°33'37"	22°35'14"	22°35'15"	22°35'05"
Longitude	122°01'54"	122°0'05"	122°0'05"	122°0'23"	122°0'08"	122°02'44"	122°02'31"	122°01'46"
	<b>Percent</b>							
Fe <sub>2</sub> O <sub>3</sub>	35.00	5.00	5.00	1.00	2.00	5.00	4.00	3.00
	<b>Parts per million</b>							
Au	0.01	0.01	<0.01	0.01	0.01	0.01	0.02	0.01
Ag	<2	<2	<2	<2	<2	<2	<2	<2
As	11	<4	<4	<4	<4	<4	<4	<4
Ba	213	158	172	16	165	1440	112	491
Bi	<4	<4	<4	<4	<4	<4	<4	<4
Cd	<5	<5	<5	<5	<5	<5	<5	<5
Ce	37	310	370	<6	<6	143	26	23
Co	nd	nd D	nd	nd	nd	nd	nd	nd
Cr	32	24	24	11	18	5	6	20
Cu	<4	<4	<4	166	26	<4	<4	<4
Ga	<3	6	4	<3	<3	11	<3	8
Ge	<3	<3	<3	<3	<3	<3	<3	<3
La	16	178	156	<5	<5	83	6	17
Li	nd	nd	nd	nd	nd	nd	nd	nd
Mn	235	24	23	12	5	42	<5	132
Mo	4	<2	<2	<2	9	<2	<2	<2
Nb	17	7	7	<7	<7	10	<7	<7
Ni	131	11	10	5	6	10	6	9
Pb	19	11	8	66	<4	16	<4	9
Rb	9	63	33	<2	<2	184	<2	56
Sb	4	4	<4	<4	<4	<4	<4	<4
Sc	nd	nd	nd	nd	nd	nd	nd	nd
Sn	<4	<4	<4	<4	<4	<4	<4	<4
Sr	26	15	15	2	9	91	3	23
Ta	<5	<5	<5	<5	<5	<5	<5	<5
Te	<6	<6	<6	<6	<6	<6	<6	<6
Th	2	29	19	2	<2	34	<2	8
U	3	6	5	<2	<2	4	<2	2
V	48	65	60	<3	13	37	11	33
W	nd	nd	nd	nd	nd	nd	nd	nd
Y	130	209	149	2	<2	34	<2	26
Zn	132	7	6	27	<3	10	<3	8
Zr	14	394	293	5	<5	294	<5	96

## Appendix 1 (continued)

GSWA no.				Trace element analysis only				
	113143	113144	113145	113146	113147	113148	113149	113150
Rock type	quartz vein	schist	gossan	quartz vein	quartz vein	gossan	quartz vein	quartz vein
Latitude	22°34'57"	22°34'57"	22°34'17"	22°34'17"	22°34'17"	22°34'17"	22°34'17"	22°34'20"
Longitude	122°01'42"	122°01'42"	122°03'26"	122°03'26"	122°03'26"	122°03'26"	122°03'26"	122°03'25"
	<b>Percent</b>							
Fe <sub>2</sub> O <sub>3</sub>	<0.07	6.99	83.90	3.00	5.99	17.00	1.00	3.00
	<b>Parts per million</b>							
Au	0.01	0.01	0.01	0.01	0.01	0.02	0.01	<0.01
Ag	<2	<2	<2	<2	<2	<2	<2	<2
As	<4	<4	22	<4	<4	5	<4	<4
Ba	213	1 386	745	476	924	1 024	290	46
Bi	<4	<4	<4	<4	<4	<4	<4	<4
Cd	<5	<5	<5	<5	<5	<5	<5	<5
Ce	24	212	33	12	46	25	17	21
Co	nd	nd	nd	nd	nd	nd	nd	nd
Cr	9	165	10	4	5	8	<4	6
Cu	<4	<4	6	<4	<4	<4	<4	<4
Ga	<3	14	<3	<3	13	13	<3	<3
Ge	<3	<3	7	<3	<3	<3	<3	<3
La	12	62	17	7	22	16	8	10
Li	nd	nd	nd	nd	nd	nd	nd	nd
Mn	37	622	188	8	76	85	20	51
Mo	<2	<2	21	<2	<2	<2	<2	<2
Nb	<7	8	<7	<7	<7	<7	<7	<7
Ni	6	65	8	5	7	8	5	9
Pb	<4	4	7	<4	8	12	<4	5
Rb	11	269	2	2	125	147	<2	<2
Sb	<4	<4	<4	<4	<4	<4	<4	<4
Sc	nd	nd	nd	nd	nd	nd	nd	nd
Sn	<4	<4	<4	<4	<4	<4	<4	<4
Sr	5	25	20	9	12	21	6	9
Ta	<5	<5	<5	<5	<5	<5	<5	<5
Te	<6	<6	<6	<6	<6	<6	<6	<6
Th	<2	11	4	<2	11	11	<2	2
U	<2	2	3	<2	6	7	<2	<2
V	4	118	299	3	68	156	<3	24
W	nd	nd	nd	nd	nd	nd	nd	nd
Y	9	50	28	3	51	66	23	10
Zn	6	124	8	3	11	13	<3	<3
Zr	<5	133	5	<5	52	63	<5	<5

## Appendix 1 (continued)

GSWA no. Rock type	<i>Trace element analysis only</i>							
	113151 mylonite	113152 quartz vein	113153 gossan	113154 quartz vein	113155 conglomerate	113156 gossan	113157 shale	113158 shale
Latitude	22°35'34"	22°36'15"	22°36'15"	22°36'15"	22°35'52"	22°35'47"	22°35'47"	22°35'47"
Longitude	122°04'04"	122°05'21"	122°05'21"	122°05'21"	122°05'35"	122°05'38"	122°05'38"	122°05'38"
	<b>Percent</b>							
Fe <sub>2</sub> O <sub>3</sub>	2.00	2.00	67.90	3.00	4.00	54.90	15.00	4.00
	<b>Parts per million</b>							
Au	0.01	0.01	<0.01	0.01	0.01	0.01	0.01	0.01
Ag	<2	<2	<2	<2	<2	<2	<2	<2
As	<4	<4	10	<4	<4	26	<4	<4
Ba	129	325	1 004	407	455	327	195	439
Bi	<4	<4	5	<4	<4	<4	<4	<4
Cd	<5	<5	<5	<5	<5	<5	<5	<5
Ce	60	<6	<6	<6	31	23	61	46
Co	nd	nd	nd	nd	nd	nd	nd	nd
Cr	7	5	7	<4	29	24	60	42
Cu	58	<4	2 718	25	<4	<4	114	<4
Ga	6	<3	<3	<3	6	5	22	10
Ge	<3	<3	3	<3	<3	<3	<3	<3
La	25	<5	<5	<5	17	18	34	24
Li	nd	nd	nd	nd	nd	nd	nd	nd
Mn	14	16	59	23	62	3 671	899	373
Mo	<2	2	6	6	<2	4	<2	<2
Nb	<7	<7	<7	<7	<7	22	22	<7
Ni	6	6	748	6	18	139	62	31
Pb	11	84	7	110	5	<4	4	7
Rb	66	<2	<2	<2	91	43	52	123
Sb	<4	<4	<4	<4	<4	<4	<4	<4
Sc	nd	nd	nd	nd	nd	nd	nd	nd
Sn	5	<4	<4	<4	<4	<4	<4	4
Sr	8	13	55	12	29	94	17	13
Ta	<5	<5	<5	<5	<5	<5	<5	<5
Te	<6	<6	8	<6	<6	<6	<6	<6
Th	5	<2	<2	<2	16	7	8	13
U	3	<2	5	<2	4	9	2	3
V	27	10	257	24	44	183	452	62
W	nd	nd	nd	nd	nd	nd	nd	nd
Y	19	<2	14	2	17	20	25	21
Zn	7	14	8	16	12	250	156	16
Zr	86	10	<5	6	115	73	283	98



## Appendix 1 (continued)

GSWA no.	<i>Trace element analysis only</i>							
	113159	113160	113161	113162	113163	113164	113165	113166
Rock type	quartz vein	hematite	gossan	breccia	sandstone	ferruginous sandstone	shale	quartz vein
Latitude	22°35'28"	22°35'15"	22°35'05"	22°34'57"	22°36'33"	22°36'33"	22°36'27"	22°36'14"
Longitude	122°04'51"	122°04'57"	122°05'10"	122°04'47"	122°06'10"	122°06'10"	122°06'11"	122°06'39"
	<b>Percent</b>							
Fe <sub>2</sub> O <sub>3</sub>	7.99	80.90	10.00	1.00	51.90	51.90	4.00	1.00
	<b>Parts per million</b>							
Au	0.01	0.01	<0.01	<0.01	<0.01	<0.01	<0.01	0.01
Ag	<2	<2	<2	<2	<2	<2	<2	<2
As	7	<4	4	<4	16	22	<4	<4
Ba	235	956	454	649	478	288	166	127
Bi	<4	<4	5	<4	<4	<4	<4	<4
Cd	<5	<5	<5	<5	<5	<5	<5	<5
Ce	<6	8	22	<6	66	10	10	<6
Co	nd	nd	nd	nd	nd	nd	nd	nd
Cr	<4	<4	8	5	47	41	19	9
Cu	98	<4	7	<4	<4	<4	<4	<4
Ga	<3	<3	<3	4	9	7	<3	<3
Ge	<3	3	<3	<3	<3	<3	<3	<3
La	<5	6	12	<5	49	7	5	<5
Li	nd	nd	nd	nd	nd	nd	nd	nd
Mn	106	75	5 642	20	48	104	26	7
Mo	25	<2	12	<2	3	<2	<2	<2
Nb	<7	<7	<7	<7	22	<7	<7	<7
Ni	9	6	23	7	5	9	18	6
Pb	36	16	19	<4	7	8	5	<4
Rb	<2	<2	17	108	30	35	8	<2
Sb	<4	4	<4	<4	<4	<4	<4	<4
Sc	nd	nd	nd	nd	nd	nd	nd	nd
Sn	<4	<4	<4	<4	<4	<4	<4	<4
Sr	9	62	36	6	27	16	55	4
Ta	<5	<5	<5	<5	<5	<5	<5	<5
Te	9	<6	<6	<6	<6	<6	<6	<6
Th	<2	2	6	2	5	6	3	<2
U	<2	<2	12	<2	9	7	<2	<2
V	16	43	21	6	329	404	18	<3
W	nd	nd	nd	nd	nd	nd	nd	nd
Y	3	5	15	4	337	4	9	<2
Zn	4	<3	17	4	<3	4	6	<3
Zr	<5	13	41	6	42	44	30	<5

## Appendix 1 (continued)

GSWA no.	<i>Trace element analysis only</i>							
	113167	113168	113169	113170	113171	113172	113173	113174
Rock type	quartz vein	ferruginous quartz vein	ferruginous quartz vein	gossan	gossan	ferricrete	gossan	ferruginous quartz vein
Latitude	22°36'17"	22°36'18"	22°36'13"	22°36'13"	22°36'13"	22°36'13"	22°36'10"	22°36'10"
Longitude	122°06'39"	122°06'39"	122°06'39"	122°06'39"	122°06'39"	122°06'39"	122°06'41"	122°06'41"
	<b>Percent</b>							
Fe <sub>2</sub> O <sub>3</sub>	2.00	8.99	5.99	15.00	11.00	72.90	13.00	5.00
	<b>Parts per million</b>							
Au	0.01	<0.01	<0.01	0.01	0.02	0.01	0.01	<0.01
Ag	<2	<2	<2	<2	<2	<2	<2	4
As	<4	4	6	6	16	9	4	<4
Ba	136	95	271	195	574	1 049	309	827
Bi	<4	<4	<4	<4	<4	<4	<4	<4
Cd	<5	<5	<5	<5	<5	<5	<5	<5
Ce	<6	<6	19	7	<6	63	<6	15
Co	nd	nd	nd	nd	nd	nd	nd	nd
Cr	5	11	9	13	13	26	9	10
Cu	<4	<4	5	<4	4	25	18	<4
Ga	<3	3	<3	<3	<3	3	<3	<3
Ge	<3	<3	<3	<3	<3	<3	3	<3
La	<5	<5	22	5	<5	38	<5	6
Li	nd	nd	nd	nd	nd	nd	nd	nd
Mn	42	7	192	93	155	11 300	583	2 318
Mo	<2	19	<2	6	3	7	2	2
Nb	<7	<7	<7	<7	<7	<7	<7	<7
Ni	4	8	8	12	8	59	9	10
Pb	<4	<4	7	26	7	4	29	7
Rb	12	10	2	<2	<2	4	<2	3
Sb	<4	<4	<4	<4	<4	5	<4	<4
Sc	nd	nd	nd	nd	nd	nd	nd	nd
Sn	<4	<4	<4	<4	<4	<4	<4	<4
Sr	4	2	12	20	34	72	13	26
Ta	<5	<5	<5	<5	<5	<5	<5	<5
Te	<6	<6	<6	<6	<6	<6	<6	<6
Th	2	3	2	2	2	<2	<2	2
U	<2	2	<2	14	2	5	<2	3
V	15	36	14	53	31	312	11	32
W	nd	nd	nd	nd	nd	nd	nd	nd
Y	<2	<2	6	7	2	22	2	4
Zn	<3	<3	7	67	7	30	6	9
Zr	9	<5	12	13	10	37	6	14

## Appendix 1 (continued)

GSWA no.	<i>Trace element analysis only</i>							
	113175	113176	113177	113178	113179	113180	113181	113182
Rock type	<i>gossan</i>	<i>calc silicate</i>	<i>calc silicate</i>	<i>gabbro</i>	<i>ferruginous sandstone</i>	<i>ferruginous sandstone</i>	<i>ferruginous conglomerate</i>	<i>dolerite</i>
Latitude	22°35'42"	22°35'14"	22°35'14"	22°34'59"	22°38'08"	22°38'08"	22°38'08"	22°37'27"
Longitude	122°06'46"	122°07'36"	122°07'36"	122°07'50"	122°07'29"	122°07'29"	122°07'29"	122°07'50"
	<b>Percent</b>							
Fe <sub>2</sub> O <sub>3</sub>	12.00	1.00	4.00	5.00	54.10	64.90	23.00	16.00
	<b>Parts per million</b>							
Au	0.01	<0.01	0.01	0.01	<0.01	<0.01	<0.01	0.01
Ag	<2	<2	<2	<2	<2	<2	<2	<2
As	15	<4	<4	<4	19	29	5	<4
Ba	223	375	215	433	1790	1054	922	767
Bi	16	<4	<4	<4	<4	<4	<4	<4
Cd	<5	<5	<5	<5	<5	<5	<5	<5
Ce	<6	18	<6	9	38	35	69	79
Co	nd	nd	nd	nd	nd	nd	nd	nd
Cr	10	7	196	348	34	27	93	51
Cu	652	<4	172	7	<4	<4	<4	200
Ga	3	13	13	12	7	5	9	25
Ge	<3	<3	<3	<3	<3	3	3	<3
La	5	8	7	5	31	29	39	36
Li	nd	nd	nd	nd	nd	nd	nd	nd
Mn	180	119	689	944	7	12	<5	1440
Mo	5	<2	<2	<2	16	25	5	<2
Nb	<7	<7	<7	<7	<7	<7	16	19
Ni	16	7	100	96	8	8	<3	53
Pb	31	9	39	16	4	4	12	11
Rb	<2	35	48	83	38	22	89	36
Sb	<4	<4	<4	<4	<4	<4	<4	<4
Sc	nd	nd	nd	nd	nd	nd	nd	nd
Sn	<4	<4	<4	<4	<4	4	<4	5
Sr	35	108	267	227	155	79	24	250
Ta	<5	<5	<5	<5	<5	<5	<5	<5
Te	8	<6	<6	<6	<6	<6	<6	<6
Th	3	4	2	3	7	4	12	8
U	4	2	<2	<2	4	4	5	<2
V	127	9	44	95	243	342	274	448
W	nd	nd	nd	nd	nd	nd	nd	nd
Y	5	14	7	9	119	113	4	45
Zn	9	15	48	50	<3	<3	4	143
Zr	12	66	70	85	67	30	69	319

## Appendix 1 (continued)

GSWA no.	<i>Trace element analysis only</i>							
	113183	113184	113185	113186	113187	113188	113189	113190
Rock type	gossan	quartz vein	quartz vein	quartz vein	gossan	meta-BIF	meta-BIF	gossan
Latitude	22°36'50"	22°36'50"	22°36'47"	22°36'47"	22°36'47"	22°36'37"	22°36'37"	22°36'37"
Longitude	122°12'00"	122°12'00"	122°12'04"	122°12'04"	122°12'04"	122°11'51"	122°11'51"	122°11'51"
	<b>Percent</b>							
Fe <sub>2</sub> O <sub>3</sub>	72.90	<0.07	1.00	2.00	40.00	54.90	62.90	56.90
	<b>Parts per million</b>							
Au	0.01	0.01	<0.01	<0.01	0.01	<0.01	0.01	<0.01
Ag	<2	<2	<2	<2	<2	<2	<2	<2
As	<4	<4	<4	<4	<4	<4	<4	<4
Ba	106	19	12	19	219	45	69	292
Bi	<4	<4	<4	<4	<4	<4	<4	<4
Cd	<5	<5	<5	<5	<5	<5	<5	<5
Ce	37	<6	13	6	133	8	19	34
Co	nd	nd	nd	nd	nd	nd	nd	nd
Cr	13	21	<4	20	49	20	34	118
Cu	525	<4	<4	10	256	32	37	1413
Ga	3	<3	<3	<3	4	<3	4	6
Ge	3	<3	<3	<3	3	4	3	<3
La	11	<5	5	<5	54	6	11	15
Li	nd	nd	nd	nd	nd	nd	nd	nd
Mn	171	46	19	10	107	385	552	566
Mo	<2	<2	<2	<2	<2	<2	<2	3
Nb	<7	<7	<7	<7	18	14	<7	<7
Ni	169	6	6	9	151	64	92	293
Pb	23	<4	<4	<4	28	<4	4	76
Rb	2	2	<2	<2	2	<2	<2	15
Sb	<4	<4	<4	<4	<4	<4	<4	<4
Sc	nd	nd	nd	nd	nd	nd	nd	nd
Sn	<4	<4	<4	<4	<4	<4	<4	<4
Sr	5	<2	<2	2	17	18	<2	7
Ta	<5	<5	<5	<5	<5	<5	<5	<5
Te	<6	<6	<6	<6	<6	<6	<6	<6
Th	3	<2	<2	2	6	<2	4	8
U	9	<2	<2	<2	12	<2	3	27
V	14	<3	<3	5	80	54	66	578
W	nd	nd	nd	nd	nd	nd	nd	nd
Y	45	<2	4	2	39	9	11	42
Zn	236	3	4	7	91	81	122	254
Zr	20	<5	<5	8	100	6	8	76

## Appendix 1 (continued)

GSWA no.	<i>Trace element analysis only</i>							
	113191	113192	113193	113194	113195	113196	113197	113198
Rock type	<i>gossan</i>	<i>ferruginous quartz vein</i>	<i>pelite</i>	<i>schist</i>	<i>gossan</i>	<i>gossan</i>	<i>gossan</i>	<i>gossan</i>
Latitude	22°36'32"	22°34'32"	22°34'32"	22°37'14"	22°41'13"	22°41'13"	22°41'13"	22°41'13"
Longitude	122°11'51"	122°06'12"	122°06'12"	122°05'39"	122°07'28"	122°07'28"	122°07'28"	122°07'28"
	<b>Percent</b>							
Fe <sub>2</sub> O <sub>3</sub>	73.90	10.00	5.99	2.00	27.00	64.90	69.90	46.90
	<b>Parts per million</b>							
Au	0.01	0.01	<0.01	0.01	0.01	0.01	0.01	0.01
Ag	<2	<2	<2	<2	<2	3	<2	<2
As	<4	<4	<4	<4	18	76	88	97
Ba	375	321	271	2 407	3 298	3 897	2 041	5 904
Bi	<4	<4	<4	<4	<4	<4	<4	<4
Cd	7	<5	<5	<5	<5	<5	<5	<5
Ce	535	10	12	65	56	23	36	23
Co	nd	nd	nd	nd	nd	nd	nd	nd
Cr	<4	4	12	7	46	6	6	<4
Cu	7	183	19	<4	<4	182	234	537
Ga	<3	<3	11	12	8	<3	3	6
Ge	<3	<3	<3	<3	4	3	<3	3
La	278	7	7	33	35	12	19	23
Li	nd	nd	nd	nd	nd	nd	nd	nd
Mn	96	152	540	130	30	3 065	2 560	371
Mo	2	<2	<2	<2	2	<2	5	3
Nb	<7	<7	<7	11	23	<7	<7	20
Ni	35	30	27	10	<3	171	89	171
Pb	27	15	6	18	15	7	31	9
Rb	4	16	34	135	107	6	11	44
Sb	<4	<4	<4	<4	<4	<4	<4	<4
Sc	nd	nd	nd	nd	nd	nd	nd	nd
Sn	<4	<4	<4	<4	7	<4	<4	6
Sr	23	97	9	141	98	53	40	50
Ta	<5	<5	<5	<5	<5	<5	<5	<5
Te	<6	12	<6	<6	<6	<6	<6	<6
Th	3	2	6	14	18	6	2	7
U	<2	<2	<2	<2	4	10	4	5
V	10	36	106	39	122	98	52	70
W	nd	nd	nd	nd	nd	nd	nd	nd
Y	16	4	7	15	25	31	34	20
Zn	66	6	31	17	6	233	83	238
Zr	25	25	65	147	141	27	30	31

## Appendix 1 (continued)

GSWA no.	<i>Trace element analysis only</i>							
	113199	113200	114201	114202	114203	114204	114206	114207
Rock type	<i>gossan</i>	<i>ferruginous quartz vein</i>	<i>gossan</i>	<i>quartz vein</i>	<i>gossan</i>	<i>gossan</i>	<i>gossan</i>	<i>gossan</i>
Latitude	22°41'13"	22°42'00"	22°43'44"	22°43'44"	22°42'43"	22°55'14"	22°55'14"	22°58'10"
Longitude	122°07'28"	122°09'33"	122°08'15"	122°08'15"	122°07'00"	122°25'33"	122°25'33"	122°23'40"
	<b>Percent</b>							
Fe <sub>2</sub> O <sub>3</sub>	43.00	8.99	54.10	1.00	56.90	76.90	70.90	36.00
	<b>Parts per million</b>							
Au	0.01	<0.01	0.01	0.01	<0.01	0.01	<0.01	0.01
Ag	<2	<2	<2	<2	3	3	3	2
As	91	10	18	<4	29	12	55	51
Ba	629	392	875	162	1 378	750	2 348	1 451
Bi	<4	<4	<4	<4	<4	<4	<4	<4
Cd	<5	<5	<5	<5	<5	<5	<5	<5
Ce	37	74	185	<6	23	9	10	107
Co	nd	nd	nd	nd	nd	nd	nd	nd
Cr	42	5	24	12	78	8	<4	54
Cu	301	179	36	<4	<4	60	<4	69
Ga	5	<3	6	<3	6	3	<3	9
Ge	3	<3	<3	<3	4	<3	<3	4
La	21	9	66	5	8	<5	<5	62
Li	nd	nd	nd	nd	nd	nd	nd	nd
Mn	226	402	291	102	146	1 856	2 009	422
Mo	4	2	2	<2	<2	5	16	<2
Nb	19	<7	<7	<7	<7	<7	<7	28
Ni	99	13	103	5	5	58	33	26
Pb	47	21	15	<4	14	<4	<4	11
Rb	3	<2	58	<2	22	4	15	54
Sb	6	<4	<4	4	<4	<4	<4	<4
Sc	nd	nd	nd	nd	nd	nd	nd	nd
Sn	<4	<4	7	<4	7	<4	<4	16
Sr	34	48	60	8	38	43	39	95
Ta	<5	<5	<5	<5	<5	<5	<5	<5
Te	<6	<6	<6	<6	<6	<6	<6	<6
Th	4	2	8	<2	5	3	5	48
U	17	<2	3	<2	2	<2	2	7
V	138	77	58	<3	129	39	32	169
W	nd	nd	nd	nd	nd	nd	nd	nd
Y	3	23	33	2	5	12	11	46
Zn	166	6	108	<3	9	64	33	33
Zr	10	12	46	<5	24	21	19	1 091

## Appendix 1 (continued)

GSWA no.	Trace element analysis only								
	114208	114209	114210	114211	114212	114213	114214	114215	114216
Rock type	gossan	gossan	gossan	gossan	gossan	carbonate	quartz vein	hematite	sandstone
Latitude	22°58'10"	22°58'10"	22°59'53"	22°56'45"	22°57'12"	22°56'48"	22°56'38"	22°56'38"	22°56'33"
Longitude	122°23'40"	122°23'40"	122°23'21"	122°22'39"	122°23'20"	122°27'34"	122°28'00"	122°28'00"	122°28'42"
	<b>Percent</b>								
Fe <sub>2</sub> O <sub>3</sub>	38.00	40.00	42.00	24.00	68.90	26.00	3.00	78.90	4.00
	<b>Parts per million</b>								
Au	0.01	0.01	<0.01	0.01	0.01	<0.01	0.01	0.01	0.01
Ag	3	2	<2	<2	4	2	<2	3	<2
As	58	12	6	5	14	4	<4	28	16
Ba	2 220	1 572	1 121	1 766	344	204	28	1 387	73
Bi	<4	<4	<4	<4	<4	<4	<4	<4	<4
Cd	<5	<5	<5	<5	<5	<5	<5	<5	<5
Ce	138	29	41	23	31	9	<6	<6	15
Co	nd	nd	nd	nd	nd	nd	nd	nd	nd
Cr	65	45	13	<4	17	4	13	4	19
Cu	275	22	17	68	<4	86	<4	546	<4
Ga	14	5	3	<3	3	<3	<3	<3	3
Ge	4	4	3	3	<3	<3	<3	4	<3
La	90	21	38	25	12	10	<5	<5	8
Li	nd	nd	nd	nd	nd	nd	nd	nd	nd
Mn	7 514	176	55 540	13 510	7 863	8 083	88	961	26
Mo	3	<2	<2	2	2	7	<2	8	<2
Nb	24	20	15	17	<7	14	<7	<7	<7
Ni	38	19	354	77	188	38	30	40	7
Pb	7	<4	9	<4	11	<4	7	<4	11
Rb	70	53	39	24	24	5	5	3	44
Sb	<4	<4	<4	<4	<4	<4	<4	<4	<4
Sc	nd	nd	nd	nd	nd	nd	nd	nd	nd
Sn	22	<4	4	27	7	41	<4	<4	<4
Sr	107	101	20	182	70	140	17	26	11
Ta	<5	5	<5	<5	<5	<5	<5	<5	<5
Te	<6	<6	<6	<6	<6	<6	<6	<6	<6
Th	20	8	4	<2	5	<2	<2	4	7
U	9	2	14	<2	11	7	<2	2	2
V	191	122	76	105	154	37	9	36	32
W	nd	nd	nd	nd	nd	nd	nd	nd	nd
Y	31	18	25	19	34	30	2	9	7
Zn	103	40	318	8	274	6	20	33	7
Zr	122	63	31	83	41	28	5	8	78

## Appendix 1 (continued)

GSWA no.	Trace element analysis only								
	114217	114218	114219	114220	114221	114222	114223	114224	114225
Rock type	sandstone	sandstone	ferruginous sandstone	gossan	ferruginous siltstone	quartz vein	alluvium	ferruginous shale	ferruginous siltstone
Latitude	22°56'33"	22°56'33"	22°56'40"	22°57'14"	22°57'02"	22°57'02"	22°57'05"	22°55'21"	22°48'48"
Longitude	122°28'42"	122°28'42"	122°29'10"	122°28'52"	122°28'55"	122°28'55"	122°10'10"	122°09'11"	122°0'27"
	<b>Percent</b>								
Fe <sub>2</sub> O <sub>3</sub>	2.00	3.00	47.90	16.00	17.00	3.00	37.00	28.00	40.00
	<b>Parts per million</b>								
Au	<0.01	0.01	<0.01	0.01	<0.01	0.01	0.01	<0.01	<0.01
Ag	<2	<2	<2	<2	<2	<2	<2	<2	<2
As	<4	7	16	10	<4	10	8	<4	<4
Ba	327	365	2 592	852	1 240	4 697	66	457	645
Bi	<4	<4	<4	5	<4	<4	<4	<4	<4
Cd	<5	<5	<5	<5	<5	<5	<5	<5	<5
Ce	19	71	43	8	7	14	19	6	11
Co	nd	nd	nd	nd	nd	nd	nd	nd	nd
Cr	16	26	<4	6	11	12	203	114	16
Cu	<4	<4	<4	17	<4	<4	25	<4	18
Ga	<3	3	<3	<3	4	<3	5	4	6
Ge	<3	<3	3	<3	<3	<3	<3	4	<3
La	7	32	24	<5	5	6	15	<5	11
Li	nd	nd	nd	nd	nd	nd	nd	nd	nd
Mn	16	72	27	16 180	50	851	78	<5	102
Mo	<2	<2	2	<2	<2	<2	<2	<2	<2
Nb	<7	<7	17	<7	<7	<7	17	16	17
Ni	7	6	4	190	12	17	21	9	81
Pb	10	18	11	34	14	12	25	10	7
Rb	68	28	19	8	83	20	2	<2	41
Sb	<4	<4	<4	6	<4	<4	<4	<4	<4
Sc	nd	nd	nd	nd	nd	nd	nd	nd	nd
Sn	<4	<4	<4	<4	<4	<4	<4	<4	<4
Sr	20	35	21	143	53	57	6	19	39
Ta	<5	<5	<5	<5	<5	<5	<5	5	<5
Te	<6	<6	<6	<6	<6	<6	<6	<6	<6
Th	5	8	2	2	6	3	4	6	2
U	2	2	<2	4	4	2	2	4	2
V	19	20	9	59	126	29	475	97	77
W	nd	nd	nd	nd	nd	nd	nd	nd	nd
Y	12	10	14	19	11	15	14	3	17
Zn	8	5	11	17	9	52	47	3	76
Zr	100	81	28	53	93	25	65	34	110